Charles University in Prague

Faculty of Science

Study program: Biology

Field of study: Cell and Developmental Biology

Bc. Petr Daněk

Molekulární mechanismus účasti proteinů rodiny CSL v odpovědi na oxidativní stress u *Schizosaccharomyces pombe*

The molecular mechanism of CSL protein participation in oxidative stress response in *Schizosaccharomyces pombe*

Diploma thesis

Supervisor: RNDr. Martin Převorovský, Ph.D.

PRAGUE 2015

Prohlášení

Prohlašuji, že jsem závěrečnou práci zpracoval samostatně a že jsem uvedl všechny použité informační zdroje a literaturu. Tato práce ani její podstatná část nebyla předložena k získání jiného nebo stejného akademického titulu.

V Praze, 13.8.2015

Petr Daněk

Acknowledgement

I would like to express my sincere thanks to RNDr. Martin Převorovský, Ph.D. for his support, valued comments, suggestions, and engagement I received during the learning process of this thesis. I am also grateful to Doc. Petr Folk, Csc., the head of the Laboratory of Gene Expression Regulation, and Mgr. Jarmila Tvarůžková for useful comments and productive discussions. Furthermore, my thanks goes to all other lab members for making kind, helpful, and always friendly working atmosphere.

Abstrakt

Pro správné fungování organismu je nezbytné udržovat v jeho buňkách vyvážený redoxní stav, neboť zatímco relativně nízká koncentrace volných kyslíkových radikálů je třeba pro adekvátní transdukci signálů, vyšší koncentrace těchto molekul (oxidativní stres) má prokazatelně škodlivé účinky a je spojena s řadou patologických stavů a onemocnění. Z tohoto důvodu se v buňkách během evoluce vyvinula široká škála vysoce konzervovaných antioxidačních mechanismů. Byly zevrubně popsány rozsáhlé a složité interakční vztahy mezi signálními proteiny a drahami regulujícími odpověď na oxidativní stres, nicméně naše znalost odpovědi na oxidativní stres ještě není kompletní a stále jsou objevovány nové regulační proteiny a mechanismy. Výsledky několika současných vědeckých prací ukazují, že se transkripční faktory patřící do proteinové rodiny CSL, které jsou nezbytné zejména pro embryonální vývoj metazoí jako efektory signální dráhy Notch, mohou na regulaci odpovědi na oxidativní stres také podílet. Poltivá kvasinka *Schizosaccharomyces pombe,* hojně používaný a pro studium buněčných odpovědí na stresové podněty dobře etablovaný modelový organismus, obsahuje dva paralogy transkripčních faktorů CSL, nazvané Cbf11 a Cbf12. Naše laboratoř ukázala, že buňky s delecí genu *cbf11* jsou vysoce rezistentní vůči peroxidu vodíku. Tato rezistence se zdá být způsobena zvýšenou aktivitou některých genů stresové odpovědi včetně *ctt1, gst2, pyp2* a *atf1*. Cbf11 je patrně negativním regulátorem těchto genů a jejich Cbf11-dependentní represe je nejspíše zprostředkována modulací signálních drah řídících buněčnou reakci na oxidativní stres. Odhalili jsme funkční propojení proteinu Cbf11 s drahami Sty1/Atf1 a Pap1. Naše výsledky prokázaly, že delece genu *cbf11* skutečně způsobuje navýšení aktivity transkripčního faktoru Pap1, detailně prostudovaného aktivátoru genů *ctt1* a *gst2*. Navíc jsme v buňkách *cbf11Δ* detekovali podstatné změny dynamiky signální transdukce v dráze Sty1/Atf1. Vliv transkripčního faktoru Cbf12 na hladinu transkriptu genů *ctt1, gst2, pyp2* a *atf1* byl naopak zanedbatelný. Naše výsledky identifikovaly nový protein, který se významně podílí na regulaci odpovědi poltivé kvasinky vůči oxidativnímu stresu, determinovaly signální dráhy, které jsou proteinem Cbf11 ovlivněny, a mohou sloužit jako podklad pro budoucí studie a vytvoření přesného mechanistického modelu působení proteinu Cbf11. Tato práce může zároveň přispět k pochopení funkcí transkripčních faktorů CSL nezávislých na Notch, z nichž některé již byly popsány v odborné literatuře.

Abstract

Redox homeostasis maintenance is important for proper organism and cell function, for while relatively low amount of reactive oxygen (and nitrogen) species contributes to the fine tuning of signal transduction, excessive concentration of ROS (oxidative stress) has demonstrably harmful effects and is tightly connected to many pathological states. Cells therefore evolved broad palette of antioxidant mechanisms that express striking level of conservation among different species. Large, intricate stress response signaling networks have been already described; nonetheless, novel molecules employed in stress-related signaling are still being discovered. Several studies recently suggested transcription factors CSL, proteins essential for regulation of metazoan development as effectors of Notch signaling, are also involved in response to oxidative stress. The fission yeast *Schizosaccharomyces pombe*, well established model of response to various stresses, comprises two paralogs of CSL proteins – Cbf11 and Cbf12. We have found cells depleted of *cbf11* are highly resistant to hydrogen peroxide. This resistance appears to be caused by upregulation of important stress responsive genes including *ctt1*, *gst2*, *pyp2*, and *atf1*. Cbf11 is therefore negative regulator of these genes, which suppresses their expression probably indirectly through modulation of stress-response signaling. We have found Cbf11 is functionally connected with both Sty1/Atf1 and Pap1 pathways. Indeed, loss of Cbf11 resulted in increased activity of Pap1, which is known regulator of *ctt1* and *gst2*, and in remarkable alterations in Sty1/Atf1 signaling dynamics. The role of Cbf12 in regulation of *ctt1*, *gst2*, *pyp2*, and *atf1* transcript level was negligible. Our results identified new protein that participates in oxidative stress response regulation in fission yeast, determined signaling pathways that are influenced by Cbf11, provided foundation for upcoming research that should reveal exact mechanistic model of Cbf11 action, and might contribute to our knowledge of Notch independent CSL functions in metazoa, some of which have been already described in the scientific literature.

List of Abbreviations

4-HNE	4-hydroxynonenal
AA/BIS	acrylamide/bis-acrylamide solution
ADAM	a disintegrin and metalloproteinase domain-containing protein
ANK	ankyrin repeats
ATP	adenosine triphosphate
BSA	bovine serum albumin
BTD	β-treefold domain
bZIP	basic leucine zipper domain
CBP	CREB-binding protein
cDNA	complementary DNA
CESR	core environmental stress response
CIR	CBF1-interacting co-repressor
CRE	cAMP-response element
CREB	cAMP response element-binding protein
CSL	CBF1, Su(H), LAG-1
CTD	C-terminal domain
DEPC	diethylpyrocarbonate
DMSO	dimethyl sulfoxide
dNTPs	deoxynucleotides
DSL	Delta, Serrate, LAG-2
DTT	dithiothreitol
EBD	EGF-motif binding domain
EDTA	ethylenediaminetetraacetic acid
EGF	epidermal growth factor
ELRs	epidermal growth factor-like repeats
EMM	Edinburgh minimal medium
GAPDH	glyceraldehyde-3-phosphate dehydrogenase
gDNA	genomic DNA
HEPES	4-(2-hydroxyethyl)-1-piperazineethanesulfonic acid
HIF-1α	hypoxia-inducible factor 1α
HRP	horseradish peroxidase
ChIP	chromatin immunoprecipitation

ChIP-seq	chromatin immunoprecipitation followed by sequencing
IAA	iodoacetamide
IgG	immunoglobulin G
LB	lysogeny-broth medium
LD	loading dye
LiAc	lithium acetate
LNG	Lin-12, Notch, Glp1
MAML1	mastermind-like protein 1
MAPK	mitogen activated protein kinase
MAPKK	mitogen activated protein kinase kinase
MAPKKK	mitogen activated protein kinase kinase kinase
MDA	malondialdehyde
NADPH	nicotineamide adenine dinucleotide phosphate
NES	nuclear exporting signal
NEXT	Notch extracllular truncation
NF-κB	nuclear factor kappaB
NLS	nuclear localizing signal
NotchEC	extracellular Notch domain
NotchIC	intracellular Notch domain
NotchR	Notch receptor
NRT	no-reverse transcriptase
NTC	no-template control
NTD	N-terminal domain
ONPG	o-nitrophenyl-D-galactopyranoside
ORF	open reading frame
PAC	motif C-terminal to PAS motif
PAGE	polyacrylamide gel electrophoresis
PAS	Per, Arnt, Sim
PCR	polymerase chain reaction
PDGF	platelet-derived growth factor
PEG	polyethylene glycol
PEST	proline, glutamic acid, serine, and threonine
PTEN	phosphatase and tensin homolog
PTP	tyrosine phosphatase

qPCR	quantitative PCR
RAM	RBP-jκ associated molecule
RBP-Jκ	recombination signal binding protein for immunoglobulin kappa J
RHR-C	C-terminal rel homology region
RHR-N	N-terminal rel homology region
RNAi	RNA interference
ROS	reactive oxygen species
rpm	rotations per minute
RT-qPCR	real-time quantitative PCR
SAPK	stress activated protein kinase
SD	standard deviation
SDS	sodium dodecyl sulfate
SKIP	SKI-interacting protein
SMRT	silencing mediator for retinoid or thyroid-hormone receptors
TAE	TRIS-acetate buffer
TAP	tandem affinity purification
TBS	TRIS-buffered saline
TBST	TRIS-buffered saline with tween
TCA	trichloroacetic acid
TD	transmembrane domain
TE	TRIS-EDTA
TRIS	2-amino-2-hydroxymethyl-propane-1,3-diol
UTR	untranslated region
VEGF	vascular endothelial growth factor
WT	wild type
YES	yeast extract with supplements

Table of Contents

1. INTRODUCTION

Our knowledge of the reactive oxygen species (ROS) and their role in cellular physiology is still growing and depending on their concentration, both harmful and beneficial effects of ROS have been described. Oxidative stress (when the concentration of ROS exceeds steady state) is known to be connected with many physiological and pathological processes like aging, apoptosis, cancer, diabetes, and cardiovascular or neurodegenerative diseases [1]. Thus, cells evolved large field of regulatory mechanisms to accurately maintain cellular redox homeostasis. In fission yeast *Schizosaccharomyces pombe*, transcription factor Pap1 and SAPK (Stress-activated Protein Kinase) Sty1 cooperate in activation of oxidative stress response when cells are exposed to excessive ROS amount [2]. Our preliminary data strongly suggest that two homologs of CSL (CBF1, Su(H), LAG-1), the family of transcription factors employed in metazoan embryonic development via Notch signaling, presented in *S. pombe* - Cbf11 and Cbf12 - are involved in regulation of stress signaling. Indeed, there is some indirect evidence pointing to the connection between CSL transcription factors and resistance to oxidative stress in humans. First, oxidative stress induced by treatment with LD_{50}-equivalent concentration of H_2O_2 or menadione activates Notch signaling in human neuroblastoma cells [3]. Second, attenuation of Notch signaling by vaccarin pretreatment enhances intracellular level of superoxide dismutase and protects human endothelial cells from H_2O_2-induced damage [4].

2. THESIS OBJECTIVES

The purpose of this work is to investigate the role of CSL transcription factors in oxidative stress response signaling in fission yeast *Schizosaccharomyces pombe*. We will explore the influence of CSL proteins on the basal and stress-induced expression of important stress responsive genes, SAPK (Sty1/Atf1) pathway components, and determine the DNA binding dynamics of CSL proteins to the promoters of these genes before or after the induction of oxidative stress. Because Sty1/Atf1 pathway is not sole inductor of stress response, the influence of the CSL proteins on the activity of Pap1 will be elucidated as well.

3. LITERATURE REVIEW

3.1. Oxidative stress

A term reactive oxygen species (ROS) is used for designating partially reduced forms of molecular oxygen O_2 that are potent oxidizing agents. This category of chemical compounds includes superoxide anion radical $O_2^{\bullet-}$, hydrogen peroxide H_2O_2, and hydroxyl radical $OH^{\bullet}$. The most prominent endogenous source of ROS are probably mitochondria which convert approximately 1-2 % of cellular oxygen into $O_2^{\bullet-}$ [5]. Superoxide anion radical is produced mostly by unspecific and erroneous one-electron reduction of O_2 mediated by protein (complex I-IV) and non-protein (coenzyme Q) components of the electron transport chain [6], or by catalytic activity of NADPH oxidases [7]. Different superoxide dismutases further faciliate reduction and disproportionation of $O_2^{\bullet-}$, consequently producing hydrogen peroxide H_2O_2 [8]. Additionally, mitochondria contains many proteins with coordinated metal cofactors that might react with H_2O_2 and produce extremely reactive and damaging hydroxyl radical $OH^{\bullet}$ via Fenton reaction [9].

3.2. The importance of oxidative stress

3.2.1. The role of ROS in defense against pathogens

Previous research pointed out that organisms are able to utilize ROS, originally considered as exclusively harmful by-products of metabolism, in several processes [1]. First, increase in the level of ROS is tightly connected with mammalian immunity. Stimulated macrophages produce ROS primarily by NADPH oxidases. Subsequent change in redox homeostasis towards the pro-oxidative state participates in the activation of NF-κB (Nuclear Factor kappaB) [10, 11], a key pro-inflammatory signaling pathway, which regulates expression of many cytokines, adhesion molecules, chemokines, immunoreceptors, and transcription factors [12, 13]. Moreover, augmented ROS production is used for pathogen killing in neutrophils, where phagosomal myeloperoxidase converts H_2O_2 to microbicidal hypochlorous acid HOCl [14]. Additionally, plants generate ROS for the protection against diseases as well. Levine *et al.* showed that the infection of plants is followed by oxidative burst which results in H_2O_2-dependent death of affected cells and activation of protective genes in cells that are adjacent to the damaged site [15]. However, serious body of evidence indicates remarkable regulatory role of ROS also in physiological processes.

3.2.2. The role of ROS in cellular signaling

Hydrogen peroxide promotes growth factor signaling (for instance responses to Epidermal Growth Factor EGF, Platelet-derived Growth Factor PDGF, and Vascular Epidermal Growth Factor VEGF), MAPK (Mitogen Activated Protein Kinase) signaling, PI3K (Phophoinositide-3-kinase) pathway, DNA damage response, and other signaling pathways [16]. Moreover, PDGF binding to its receptor results in elevated production of H_2O_2, suggesting the existence of positive redox feedback loop that could probably enforce a signal transduction in stimulated cells [17]. The most robust signal-supporting effect of H_2O_2 is attributed to the inhibition of tyrosine phosphatases (PTPs), including important regulator PTEN (Phosphatase and Tensin Homolog), via oxidation of its active cysteines [18–20].

3.2.3. The relevance of cysteine oxidation

Cysteine thiol groups (SH) with relatively low pKa that are at physiological cytoplasmic pH present in deprotonated thiolate anion form (S^-), were determined as a plausible target for H_2O_2 mediated oxidation [21]. There are three gradual states of oxidized cysteine. Firstly, thiolate anion is oxidized to sulfenic acid (SO^-), which can be (when the concentration of H_2O_2 is sufficiently high) subsequently oxidized to sulfinic acid (SO_2^-). Third form, sulfonic acid (SO_3^-), is formed when the second state, sulfinic acid is oxidized again (Fig. 1). This modification is irreversible and affected proteins are usually permanently damaged. Cysteine in sulfenic form exhibits also the ability to create intra- and intermolecular disulfide bonds that might seriously bias the tertiary and quaternary structure of proteins [22]. However, direct oxidation of cysteines is not probable, because reactivity of cysteines of common proteins with H_2O_2 is too low and reaction is therefore unfavorable. Hence, the role of H_2O_2 scavenging proteins such as peroxiredoxins is anticipated. Active cysteines of peroxiredoxins have very low pKa and consequently higher affinity for H_2O_2. Present model assumes that oxidized peroxiredoxins pose the ability to interact with other proteins and specifically oxidize their cysteines [21].

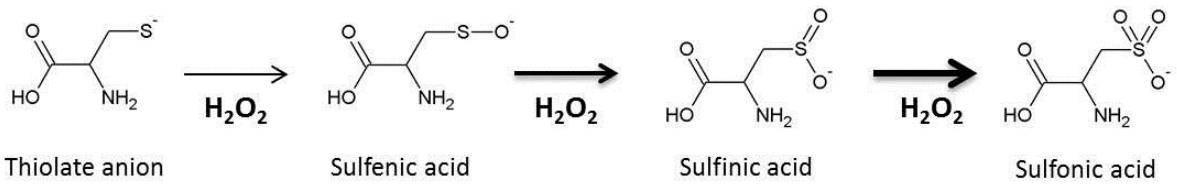

Fig. 1 – Scheme of gradual cysteine oxidation: Cysteine naturally present in thiolate anion form can be gradually oxidized to sulfenic acid (SO^-), sulfinic acid (SO_2^-), and irreversibly to sulfonic acid (SO_3^-) in the presence of hydrogen peroxide or other ROS.

Intriguingly, increase in tyrosine phosphorylation due to PTPs inactivation is not the only signal-regulating effect of hydrogen peroxide. Elevated concentrations of H_2O_2 have been reported to modulate activity of some proteases (e.g. caspase 3), adaptor proteins and chaperones (e.g. Hsp33, Hsp70), and transcription factors (e.g. NF-κB, AP-1, p53, HIF-1α) via cysteine oxidation as well [23]. Altogether, hydrogen peroxide affects important cellular signaling pathways at different levels with obvious biological relevance and is probably responsible for context-dependent tuning of cellular signaling, activation of inflammation, and other physiological processes [1].

3.2.4. ROS as harmful agents

The excessive amounts of ROS might be generated both endogenously (through activation of NADPH oxidases, malfunction of oxidative phosphorylation, heavy metal poisoning, UV radiation, etc.) or exogenously (e.g. by immune system during inflammation). Steady state-exceeding enlargement of ROS pool results in nonspecific dose-dependent damage to the cellular structures and signaling deregulation. This set of harmful events is commonly referred as oxidative stress. Pleiotropic consequences of this state are very serious and can be even lethal [1]. Despite the fact that causality has not been proved yet, oxidative stress is associated with many pathological states [24] like cancer [25], diabetes [26], neurodegenerative diseases [27], or cardiovascular diseases [28].

3.2.4.1. ROS-mediated DNA damage

Moreover, ROS were reported as serious DNA damaging agents. During oxidative stress, ROS react with both sugar moiety and bases of nucleotides, producing wide range of nucleotide modifications that might consequently cause base mispairing, deletions, tandem base lesions, abasic sites, DNA replication block, single and double strand breaks,

mutations generated by error-prone DNA reparation processes, DNA strand crosslinks, and even DNA-protein crosslinks [29, 30].

3.2.4.2. The ROS-mediated protein damage

The ability of ROS to modulate protein structure and function has been discussed above. But, with the rising concentration of ROS, the selectivity and specificity of protein modifications decreases [21] and multiple oxidation of various amino acids occurs. Among them, aromatic and sulfur-containing amino acids are the most susceptible to oxidation. Amino acid modifications can also impair structure, catalytic activity or binding properties of proteins. Furthermore, ROS may induce also oxidation and even fragmentation of the polypeptide backbone [31]. Cells usually comprise a wide range of protein-repairing mechanisms, for example Thioredoxin/Thioredoxin-Reductase system or Glutaredoxin/Glutathione/Glutathione-Reductase system that mediate reduction of oxidized amino acids. The very principle of these systems is quite simple. Oxygen adduct is transferred from damaged protein to the active cysteine of scavenging protein (e.g. thioredoxin) which is subsequently regenerated by specific reductase in ATP-dependent manner. Despite of the efficiency of such protective system, serious damage caused by high concentration of ROS cannot be easily repaired [32]. Intense oxidative stress is typically linked to irreversible amino acid oxidation, which is especially exerted by terminal oxidation of cysteine thiol to sulfonic acid [22] and amino acid side chain hydroxylation [31]. Hence, irreversibly damaged proteins must be degraded. Interestingly, dysfunctions of proteolytic machinery or distinct alterations of protein structure that prevent protein cleavage might result in aggregation of cross-linked proteins, [32] whose connection to neurodegenerative diseases is well documented elsewhere [33].

3.2.4.3. The ROS-mediated lipid damage

Beside DNA and proteins, cellular lipids were also reported to be readily modified by reactive oxygen forms [34]. ROS (mainly hypochlorous acid and hydroxyl radical) usually abstract hydrogen from fatty acids carbons that are connected by double bond, converting it into the lipid radical ($L^{\bullet}$). Ongoing reaction with molecular oxygen produces a peroxyl radical form of the fatty acid ($LOO^{\bullet}$). Intriguingly, this peroxyl radical can further abstract hydrogen from the adjacent fatty acid, generating lipid hydroperoxide (LOOH) and another lipid radical ($L^{\bullet}$). This reaction represents the initiation step of the chain reaction through which the oxidative damage is propagated across the lipid

membrane [35]. Lipid hydroperoxides are created from various lipid substrates like free fatty acids, sterols, unsaturated glycolipids, and phospholipids [36] and exert relatively high stability compared to ROS, which allows them to diffuse through the cytoplasm and/or membranes and oxidize other distant biomolecules (e.g. membrane proteins). Spontaneous as well as catalyzed decomposition of lipid hydroperoxide (LOOH) into various lipid aldehydes might occur. Among them, malondialdehyde (MDA) and 4-hydroxynonenal (4-HNE) are considered as the most harmful chemicals that can covalently bind DNA and variety of proteins. Protein damage caused by lipid aldehydes is manifested by either inactivation or constitutive activation of proteins. Thus, the activity of membrane transporters, enzymes, receptors, transcription factors, translation factors or antioxidant proteins might be altered [37]. Additionally, studies performed with artificial membrane models showed alterations in structure, shape, fluidity, and permeability of lipid bilayer following photo-induced oxidative stress [38, 39] and even disintegration of the membrane after serious oxidative damage was observed [40].

3.3. Oxidative stress response in *S. pombe*

Cells need accurate regulation of ROS concentration for proper signaling and homeostasis maintanance. For this purpose, cells contain wide range of evolutionarily conserved, tightly regulated anti-oxidative molecules and enzymes. Despite intensive scrutiny, the complicated signaling network is still not completely unraveled. The fission yeast *Schizosaccharomyces pombe* seems to be optimal model for studying stress-related signaling. First, important proteins employed in regulation of stress response in *S. pombe* are homologous to mammalian stress-response regulators [2]. Second, simple and powerful tools for genetic manipulations have been developed for studies with *S. pombe*, allowing us to describe gene functions on the basis of observed phenotypes of different mutants [41].

Oxidative stress in *S. pombe* triggers very complex transcription change [42] that substantially affects physiology of the cell [43, 44]. Chen *et al.* characterized Core Environmental Stress Response (CESR) genes whose expression is changed in various stress conditions. Changes of the expression of CESR genes involve upregulation of about 140 genes and downregulation of nearly 100 genes during stress conditions. Stress-induced CESR genes encode proteins participating in carbohydrate and lipid metabolism, transcription, signaling regulation, and DNA repair. As expected, genes for chaperones,

heat-shock proteins, and antioxidants have been also identified as CESR genes. Interestingly, induction of CESR genes is accompanied by expression changes of diverse gene clusters that appear to be stressor specific. Hydrogen peroxide treatment resulted in upregulation of 56 stressor specific and 140 CESR genes, including catalase, thioredoxin, thioredoxin peroxidase, thioredoxin reductase, and glutathione-S-transferase [42]. These enzymes belong to the group of major macromolecular antioxidants in the cells [45].

3.3.1. Antioxidant enzymes

3.3.1.1. Superoxide dismutase

To defend themselves against $O_2^{\bullet-}$ (which is frequent byproduct of oxidative phosphorylation [5]), fission yeast harbors two superoxide dismutases encoded by *sod1* and *sod2* genes, which are induced during oxidative stress and disproportionate $O_2^{\bullet-}$ to H_2O_2 and O_2 [46, 47]. Protein product of *sod1* is a metalloenzyme that has Cu or Zn ion within its active site and is commonly localized in cytoplasm [46], whereas *sod2* produces Mn-containing form of enzyme which is located predominantly in mitochondria [47]. Evidence suggests that both Sod1 and Sod2 are important for *S. pombe* resistance to oxidative stress [46, 47]. Moreover, a series of oxidatively damaged organ tissues observed in *Sod1*$^{-/-}$ mice exemplifies the importance of superoxide dismutases for eukaryots [48]. Despite that superoxide dismutases seem to be prominent antioxidants, cells must also prevent oxidative damage caused by a product of $O_2^{\bullet-}$ disproportionation, hydrogen peroxide.

3.3.1.2. Catalase

Catalase, the heme-containing homotetrameric enzyme ubiquitously present in prokaryotic and eukaryotic organisms, catalyzes rapid disproportionation of hydrogen peroxide to H_2O and O_2. It has been evaluated that catalase can metabolize even 1540.8 μmol of H_2O_2 per minute per mg of rat liver tissue protein [49, 50]. Catalase (Ctt1) is a product of *ctt1* gene and is important H_2O_2 scavenger in fission yeast [51]. Logically, *ctt1* deletion mutants are very sensitive to H_2O_2, but catalase is obviously not essential for cells in physiological conditions [52]. This is supported by the observation that catalase null mice exert wild type phenotype, but are susceptible to brain mitochondria damage [50]. Large body of evidence shown that only negligible amount of catalase is present in

unstressed cells but it is rapidly upregulated when cells are exposed to hydrogen peroxide [42, 49].

3.3.1.3. Thioredoxins

Thioredoxins are small thiol oxidoreductases involved in cellular redox state regulation. Their intricate interactions are partially summarized in Fig. 2. Genome of *S. pombe* contains two genes for thioredoxins – *trx1* which encodes transcript of cytosolic thioredoxin Trx1 and *trx2* whose functional product is mitochondrial thioredoxin Trx2 [53]. While Trx1 is necessary for fission yeast's adaptation to oxidative stress, Trx2 probably does not play any important role in resistance to this condition [54]. According to different study, Trx2 rather protects mitochondrial Fe-S containing enzymes from being oxidized [55]. Cytoplasmic thioredoxins contain two reduced cysteines with low redox potential that serve as electron donors for reduction of intra- and intermolecular disulfide bonds in oxidatively damaged proteins. Reduction of thioredoxin's substrate is accompanied by concomitant creation of S-S bond (oxidation) between both thioredoxin's active cysteines [56]. Thioredoxins might also reduce enzymes that form intramolecular S-S bonds during their catalytic cycle and reactivate them in this manner [57]. In both cases, oxidized thioredoxin (S-S) undergoes NADPH dependent reduction mediated by thioredoxin reductase Trr1 [58]. Additionally, Trx1 donates electrons to glutathion peroxidase Gpx1, a H_2O_2 metabolizing enzyme, and lipid hydroperoxides [59]. Thus, Trx1-Trr1 system is important regulator of cellular redox state, diverse enzymatic reactions, and proteome-wide thiol oxidation. Indeed, deletion of Trx1 or Trr1 resulted in increase of thiol oxidation in whole proteome [60]. One of the proteins with oxidized thiols observed in *Δtrx1* cells was peroxiredoxin Tpx1 [61].

3.3.1.4. Peroxiredoxins

Peroxiredoxins are abundant enzymes that metabolize various peroxide substrates, producing water (in case of H_2O_2) or alcohol. Beside cellular redox regulation, peroxiredoxins affect broad scale of physiological processes in the cell as well. They might regulate cell signaling, function like chaperons, or even phospholipase A2. Importance of these enzymes is confirmed by many pathological phenotypes of peroxiredoxin mutants, including hemolytic anemia, predispositions to tumor development, abnormal erythrocyte morphology, and others. Peroxiredoxins are divided into three groups according to their catalytic activity. *S. pombe* contains only one peroxiredoxin - Tpx1 that belongs to the

group known as 2-Cys peroxiredoxins [62]. Cysteines in active sites of peroxiredoxins are the most susceptible thiol groups for oxidation among all tested proteins due to their low pKa [21] that is decreased by surrounding amino acids (arginine, threonine, and proline). The catalytic cycle of 2-Cys peroxiredoxins consists of three steps. At first, thiolate anion (S^-) attacks H_2O_2, generating H_2O and sulfenic acid (SO^-) which is subsequently attacked by thiolate anion from the active site of the second subunit of peroxiredoxin. Formation of intersubunit S-S bond with concomitant release of the second H_2O molecule follows. To restore enzymatic activity of peroxiredoxin, the disulfide bond must be reduced [63]. This reduction is faciliated by (already described) thioredoxin Trx1 [61]. When high concentration of H_2O_2 is applied, SO^- intermediate is oxidized to sulfinic acid SO_2^-. Overoxidation of active cysteine stops catalytic cycle by prevention of intersubunit S-S bond formation and inactivates Tpx1 in this manner. Intriguingly, it seems that Tpx1 is a prominent substrate for thioredoxin Trx1, which reduces Tpx1 and concomitantly oxidizes itself. Thus, the absence of Tpx1 in its S-S form (due to its overoxidation to SO_2^-) during intense oxidative stress results in accumulation of reduced Trx1 that is subsequently available for reduction of other oxidatively damaged proteins. It has been hypothesized that this phenomenon contributes to the fine-tuning of oxidative stress response in dependence on the stress intensity [61, 64]. Several publications provide convincing evidence that catalytically active form of Tpx1 is essential for activation of stress response to minor oxidative stress which is mediated by transcription factor Pap1 in *S. pombe*. In contrast, overoxidation of Tpx1 inhibits Pap1 and allows activation of stress response to intense oxidative stress via Sty1-dependent manner. Thus, Tpx1 functions as a molecular switch between two distinct transcriptional programs [61, 65, 66]. However, inhibited Pap1 might be reactivated during prolonged oxidative stress by Sty1-regulated sulfiredoxin Srx1, which reverts overoxidation of Tpx1 [65].

3.3.1.5. Glutathione-S-transferases

Other enzymes that significantly contribute to the redox homeostasis maintenance are glutathione-S-transferases. Glutathione-S-transferases are evolutionarily conserved proteins involved in detoxification of the organism. They typically conjugate tripeptide glutathione with electrophilic xenobiotic substrate and thereby increase its polarity and solubility [67]. *S. pombe* possesses three glutathione-S-transferases with different functions – Gst1, Gst2, and Gst3. Gst1 and Gst2 proteins are localized throughout the cell and display 79% identity. This two enzymes show specific activity to xenobiotic agent

1-chloro-2,4-dinitrobenzen. However, Gst1 alone is probably not important for resistance to oxidative stress, while Gst2 appears to have a role in cellular adaptation to tetra-butylhydroperoxide. Interestingly, dissimilar Gst3 is less active towards 1-chloro-2,4-dinitrobenzen but exerts striking peroxidase activity towards cumene hydroperoxide. Consistently, Gst3 is necessary for the adaptation of fission yeast to both tetra-butylhydroperoxide and H_2O_2. Thus, unlike Gst1, Gst2 and Gst3 are important antioxidants in fission yeast [68].

3.3.2. Oxidative stress response signaling

Two major signaling pathways regulating response to oxidative stress have been identified in *S. pombe*. The first pathway employs transcription factor Pap1 and is responsible for reaction to low levels of ROS, whereas the second pathway is represented by Mitogen Activated Protein Kinase (MAPK) Sty1, which activates transcription factor Atf1 and regulates response to high ROS concentration and to large variety of cellular stresses [69].

3.3.2.1. Pap1 pathway

Pap1 is 61.5 kDa protein that binds DNA via N-terminal leucine zipper motif followed by conserved basic domain (bZIP) which exerts approximately 40% identity to mammalian AP-1 transcription factors (c-Jun and c-Fos) [70]. AP-1 transcription factors usually form heterodimers that bind AP-1 consensus binding sequence 5'-TGAGTCA-3' [71]. Indeed, Pap1 homodimerizes and binds this sequence *in vitro* as well [70].

Pap1 is localized in unstressed cells predominantly within the cytoplasm. This cellular distribution is maintained by nuclear exportin Crm1 that interacts with Nuclear Exporting Signal (NES) at the C terminus of Pap1 and mediates its nuclear export [72]. Low concentration (0.2mM) of H_2O_2 activates Pap1 which subsequently undergoes rapid nuclear translocation [73]. Originally, it has been assumed that direct oxidation of cysteines in Pap1 by H_2O_2 might result in conformational change and activation of this transcription factor [74]. However, peroxiredoxin Tpx1 was identified as the upstream regulator of Pap1. Vivancos *et al.* showed that low concentration of hydrogen peroxide oxidizes active cysteine in Tpx1 to sulfenic acid (SO^-), from where the oxygen adduct is directly transferred to the redox sensitive Cys278 or Cys501 in Pap1 [65, 66]. Disulfide bond that forms between these two cysteines upon thiol oxidation subsequently causes

change of the protein tertiary structure. Data suggests that this conformational change probably makes NES inaccessible for nuclear exporter Crm1. Thus, nuclear export of Pap1 is abrogated and Pap1 accumulates in the nucleus where it can bind DNA and modulate gene transcription [72, 74]. Overall model of Pap1 signaling is illustrated in Fig. 2.

Nuclear localization and activity of Pap1 was reported to be impaired when higher concentration (1mM) of H_2O_2 was applied [73]. Because Tpx1 is easily inhibited by overoxidation to sulfinic acid (SO_2^-) [61], it has been hypothesized that Tpx1 might have a role in both activation and inactivation of Pap1. Indeed, overoxidation of Tpx1 abolished Pap1 activation. Sulfinic acid blocks intersubunit S-S bond formation during catalytic cycle of Tpx1 and consequent inhibition of Cys278 and Cys501 oxidation in Pap1 is also likely [65, 66].

Additionally, thioredoxin Trx1 seems to be the Tpx1-dependent upstream regulator of Pap1 for several reasons. First, reduced Trx1 is responsible for reduction of disulfide bonds [56] which are essential for Pap1 activation [74]. Second, accumulation of oxidized Trx1 caused by mutation in thioredoxin reductase Trr1 resulted in nuclear translocation of Pap1 [73]. Third, Tpx1 with intersubunit S-S bond appears to be a prominent substrate for Trx1. Sulfinic acid (SO_2^-) in overoxidized Tpx1 prevents intersubunit S-S formation. Therefore, reduced Trx1 accumulates and is available for reduction of S-S bond in transcription factor Pap1 that is inhibited in this manner [61]. These observations suggest Trx1 can serve as either activator or inhibitor of Pap1, depending on its Tpx1-regulated redox state.

Contrary to depicted regulatory mechanism, the activation and nuclear translocation of Pap1 has been observed 30 to 60 min after the 1mM H_2O_2 treatment (intense oxidative stress) [73]. This reactivation was dependent on Sty1/Atf1 pathway [65], which is triggered in cells for example by intense oxidative stress [69]. Pap1 reactivation is in these conditions mediated by Sty1/Atf1-induced sulfiredoxin Srx1 that reduces sulfinic acid (SO_2^-) in Tpx1 to sulfenic acid (SO^-) [65, 66].

This signaling crosstalk has obvious striking functional purpose. Analysis of the fission yeast transcriptome revealed that transcription factor Pap1 is responsible for induction of relatively small subset of genes comprising mainly antioxidants (such as catalase *ctt1*, thioredoxins *trx1, trx2*, or thioredoxin reductase *trr1* [42, 69]) and genes involved in multidrug resistance (glutathion-S-transferases *gst1, gst2*) [75, 76], while

expression of CESR genes remains unchanged during minor oxidative stress. Expression of Pap1-dependent genes allows cells to cope with the mild redox imbalance and restore cellular homeostasis without any serious impact on its physiological state. Some pieces of evidence suggest Pap1 might be antagonistic towards Sty1/Atf1 pathway, because CESR genes whose expression is regulated by Atf1 are repressed during cellular response to minor oxidative stress [69]. Consistently, high concentration of ROS, besides triggering Sty1/Atf1 pathway, inactivates Pap1 in Tpx1-dependent manner, enabling full induction of CESR genes [65, 69]. Expression of CESR genes seriously impacts life of the cell with intention to protect it – cell cycle arrest and inhibition of proteosynthesis for example might occur. Hence, it is advantageous to deal with minor oxidative stress via Pap1 pathway without such a "drawback".

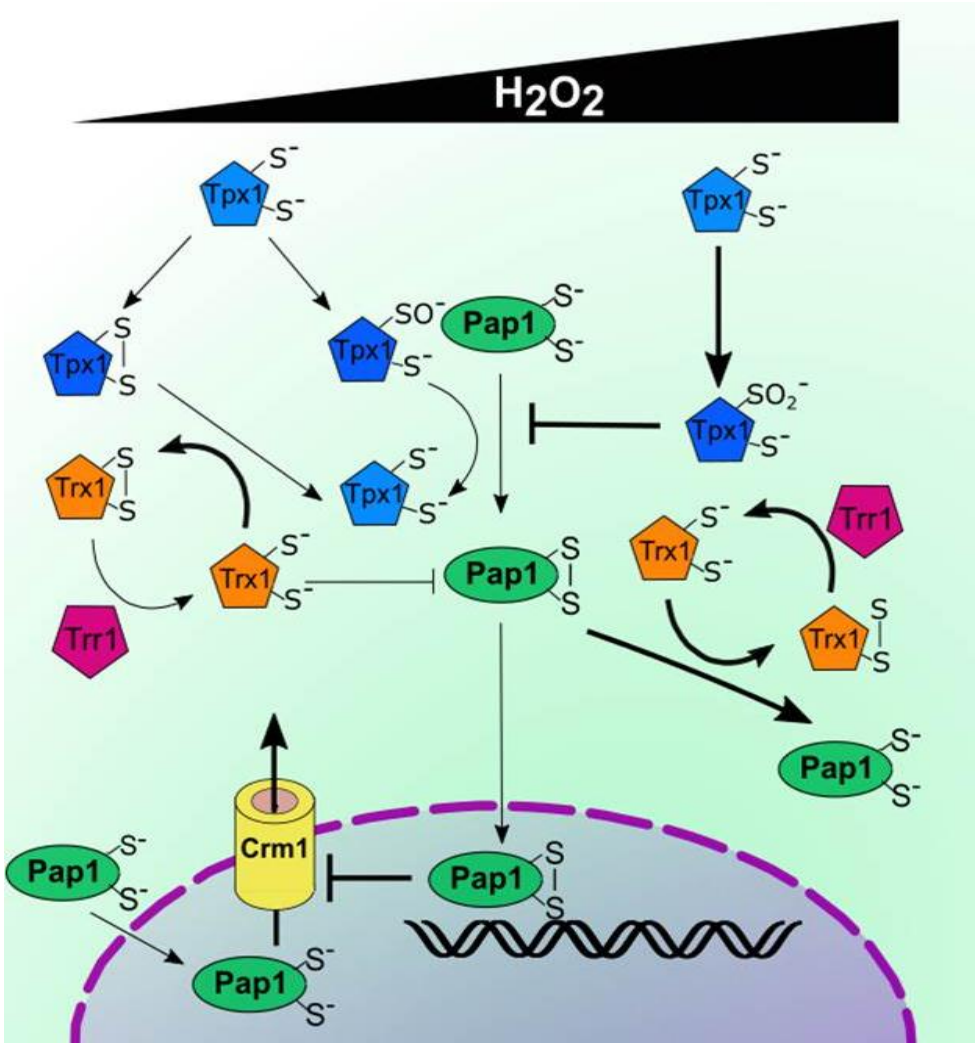

Fig. 2 – Schematic model of Pap1 signaling during minor and intense oxidative stress. Nuclear exporter Crm1 excludes reduced Pap1 from the nucleus, maintaining its cytoplasmic localization in normal conditions. Peroxiredoxin Tpx1 contains oxidative-sensitive cysteine that is converted to sulfenic acid (SO^-) by low concentrations of hydrogen peroxide. Tpx1-SO^- subsequently oxidizes transcription factor Pap1 which forms an intramolecular disulfide bond that changes its tertiary structure. Resulting masking of NES abolishes Crm1-Pap1 interaction and Pap1 accumulates in the nucleus. Oxidized Tpx1 also forms intersubunit disulfide bond that stops its catalytic cycle, until it is reduced by thioredoxin Trx1. Trx1, in general, reduces disulfide bonds in various proteins including Pap1. Trx1-mediated reduction of Pap1 results in its inactivation. However, Trx1 is depleted by interaction with its major substrate Tpx1, enabling full activation of Pap1 in this manner. Concentrated hydrogen peroxide over-oxidizes sensitive cysteine of Tpx1 to sulfinic acid (SO_2^-) that impairs interaction and oxidation of Pap1. Furthermore, sulfinic acid also inhibits catalytic cycle of Tpx1 that consequently cannot form a disulfide bond. Reduced thioredoxin Trx1 is therefore unable to restore catalytic activity of Tpx1, accumulates in the cell and reduces all persistent oxidized Pap1, enhancing the inhibitory effect of high concentration of H_2O_2 on Pap1 signaling. The picture was created on the basis of literature cited in this chapter.

3.3.2.2. Sty1/Atf1 pathway

While Pap1 induces expression of antioxidant genes in response to minor oxidative stress, Sty1/Atf1 signaling remodels the cellular transcriptome towards the adaptation to various types of intense stresses including oxidative stress, heat stress, osmotic stress, or heavy metal poisoning [42].

Sty1 is a 40.2 kDa tyrosine MAPK employed in the transduction of external and internal signals to given effector molecules. Active MAPKKK transfers phosphate to the specific MAPKK which provides activating phosphorylation of MAPK Sty1. When activated, Sty1 translocates to the nucleus where it predominantly phosphorylates transcription factor Atf1. This pathway is conserved in various fungal species and to a certain extent even in mammals. Moreover, Sty1 is homologous to mammalian kinase p38 that is also required for the triggering of stress response [2]. The importance of p38 for organism is declared for example by the fact that its deregulation is associated with many cancer types [77]. Major effector of Sty1 kinase – bZIP (basic leucine zipper) transcription factor Atf1 is a member of ATF/CREB subfamily of transcription factors that are also present in mammals [78]. Thus, Sty1/Atf1 signaling is conserved pathway that regulates stress response across phylogeny.

Sty1 functions as a signaling hub which integrates different environmental and internal signals (for which can be referred as SAPK – Stress-activated Protein Kinase). Histidine kinases Mak2 and Mak3 which transmit signal via His-to-Asp phosphorelay system were identified as prominent and specific activators of Sty1/Atf1 pathway in the response to H_2O_2. These kinases contain C-terminal histidine kinase domain with adjacent heme harboring PAS/PAC domain that is commonly found in redox and oxygen sensors in prokaryotic organisms [79]. Heme in PAS/PAC domain is thought to initiate alterations in the tertiary structure of the protein in dependence on oxygen availability. According to the proposed model, H_2O_2-induced conformational change of Mak2 and Mak3 results in kinase auto-activation and consequent phosphorylation of their substrate Mpr1 (Histidine-containing response regulator phosphotransferase) on His221 [79, 80]. Mpr1 is associated with its substrate Mcs4 (Mitotic catastrophe suppressor) via glycolytic enzyme glyceraldehyde-3-phosphate dehydrogenase GAPDH which is encoded by *tdh1* gene. This interaction probably increases efficiency of the phosphorelay, enabling rapid cellular reaction to stress condition. Consistently, oxidation of Cys152 of GAPDH has been shown

to enhance the Mpr1 association with Mcs4 [81]. Phosphorylation allows Mpr1 to directly transmit phosphate to Asp412 residue of Mcs4 that consequently binds [79, 80] and activates MAPKKK Wis4 [82]. However, more recent studies suggest Mcs4 rather (additionally to activation of Wis4) permanently stabilizes interaction between two related MAPKKK Wis4 and Win1. Unimpaired integrity of Mcs4-Wis4-Win1 complex seems to be essential for the proper signal transduction [83]. Signal from Wis4-Win1 complex is further propagated to MAPKK Wis1 through phosphorylation of its Ser469 and Thr473 residues [84]. Interestingly, it has been shown that Wis1 is associated with intact Mcs4-Wis4-Win1 complex in unstressed cells and dissociates when the stress response pathway is triggered, regardless of Wis4 and Win1 kinase activities [83]. Subsequently, MAPKK Wis1 activates MAPK Sty1 via phosphorylation of its Thr171 and Tyr173 [85-87]. When activated, Sty1 translocates to the nucleus where it associates with and phosphorylates transcription factor Atf1 [88–90], that is essential for the basal expression and induction of almost 70 % of CESR genes during intense oxidative, heat and osmotic stress [42]. Scheme illustrating Sty1/Atf1 is depicted in Fig. 3.

Two tyrosine phosphatases Pyp1 and Pyp2 were identified as negative regulators of Sty1 kinase. Despite the fact that both phosphatases are able to dephosphorylate Sty1, their different expression profiles suggest Pyp1 and Pyp2 have distinct functions in Sty1 regulation. Transient Sty1-dependent accumulation of *pyp2* mRNA was observed in diverse stress conditions while expression of *pyp1* is stable, constitutive and stress-independent. Nevertheless, only double deletion mutants *pyp1Δ pyp2Δ* had lethal phenotype, indicating there is certain level functional redundancy between these two phosphatases [85, 86]. Cells with introduced deletion of *pyp1* had hyperactivated Sty1 and similar morphology aso cells with constitutively active MAPKK Wis1 [91]. Furthermore, inhibition of Pyp1 during glucose limitation and cadmium toxicity [92], or inhibition of Pyp1-Sty1 interaction during heat shock [87] resulted in MAPKK-independent activation of Sty1. Taken together, the low activity of Sty1 in unstressed cells is sustained predominantly via ubiquitously expressed phosphatase Pyp1.

In contrast, expression of Pyp2 elevates 5 min after the activation of Sty1, culminates 30 min upon the treatment with stressor and led to the decreased level of Tyr173-phosphorylated Sty1 [86]. Additionally to the increased transcript level, stabilization of the protein contributed to upregulation of Pyp2 during oxidative stress. Unlike Pyp1, Pyp2 comprises approximately 270 amino acid long linker region (between

N-terminal MAPK binding domain and C-terminal phosphatase domain) which is responsible for the Pyp2 destabilization. Activated Sty1 has been shown to interact with Pyp2 and phosphorylate its linker region on Ser234 and Thr279, hindering Pyp2 degradation in this manner [93]. Thus, Pyp2 is critical protein in Sty1 negative feedback loop that is important for proper termination of the stress response when the stress conditions are diminished.

Atf1 is a ~60 kDa bZIP transcription factor highly similar to mammalian transcription factors ATF2 and ATFa. The most conserved part of the protein, its C terminus, contains DNA binding basic region followed by leucine zipper that enables Atf1 to dimerize. As its mammalian homologs, Atf1 binds ATF/CRE consensus binding sequence 5'-TGACGTCA-3' [78]. Both Pap1 and Atf1 are members of bZIP transcription factor family but unlike Pap1, Atf1 is constitutively localized in the nucleus [88], where it associates with promoters of target genes in both stress and non-stress conditions [94]. Atf1 can act as a homodimer or heterodimer with bZIP transcription factor Pcr1 [95]. It is still unclear, which processes are regulated by Atf1 alone or by Atf1-Pcr1 heterodimer. However, ChIP-on-chip analysis revealed that Sty1 is recruited to promotes predominantly in the form of heterodimer Atf1-Pcr1 in cells treated with 0.5mM H_2O_2. Deletion of each of these two biding partners resulted in significantly decreased association with Sty1, suggesting the importance of Atf1-Pcr1 heterodimer in stress response. To describe cellular situation in extended complexity, it is necessary to admit that genes controlled solely by Atf1 or Pcr1 homodimers were detected as well [94]. Consistently, both Atf1 and Pcr1 have been shown to be important for cellular resistance to stress in exponentially growing culture [95]. Additionally, Lawrence *et al.* provided evidence that interaction between Atf1 and Pcr1 enhances the stability of these proteins respectively. It has been hypothesized that this mechanism of mutual stabilization might be responsible for control and co-regulation of Atf1 and Pcr1 protein pools [96]. Atf1-Pcr1 heterodimer regulates for instance expression of *ctt1*, *pyp2*, and *atf1* genes [42, 94]. Thus, Atf1 triggers positive feedback loop by increasing its own levels and negative feedback loop as well. Negative feedback is in this case executed by Atf1-dependent augmentation of phosphatase Pyp2 level and consequent termination of Sty1 signaling.

It has been thought that Atf1 is activated by phosphorylation, however, weak upregulation of Atf1-dependent genes was observed in unphosphorable Atf1 mutant (*atf1-11M*) cells compared to *atf1Δ* strain upon stress stimuli. Moreover, *atf1-11M* cells are

resistant to diverse stresses while *atf1Δ* cells are not. The important observation that half-life of Atf1-11M is remarkably lower than the half-life of its wild type variant finally led to the conclusion that the environmental stress-dependent hyperphosphorylation of Atf1 leads rather to the stabilization of the protein [96]. More recent study consistently discovered that elimination of Atf1 upstream activators does not abandon its activity completely [97].

Besides the prominent role in initiation of transcription of stress responsive genes, several papers described other mechanisms through which gene expression might be regulated by transcription factor Atf1. It has been postulated that DNA-bound Atf1 associates with nucleoporin Nup85. After the stress-dependent induction of Atf1-bound genes, the proximity to the nuclear pore enables rapid transport of their novel transcript into cytoplasm. Intriguingly, Atf1 also recruits components of RNAi (RNA interference) that are responsible for the silencing of target genes. Proposed model indicates that phosphorylation of Atf1 is followed by cytoplasmic translocation of RNAi components, enabling full activation of target gene in this manner [98]. Others suggest that active heterodimer Atf1-Pcr1 might be involved in specific mRNA destabilization [99]. There is relatively small subset of genes in *S. pombe* whose expression is repressed by active Atf1 [42] via unknown mechanism that has never been sufficiently explained. The role of epigenetic modulation might be therefore promising subject for further research. Additionally, Atf1 regulates nucleosome positioning in stress responsive genes, depletes histones from promoters of these genes, and suppress their cryptic transcription [100].

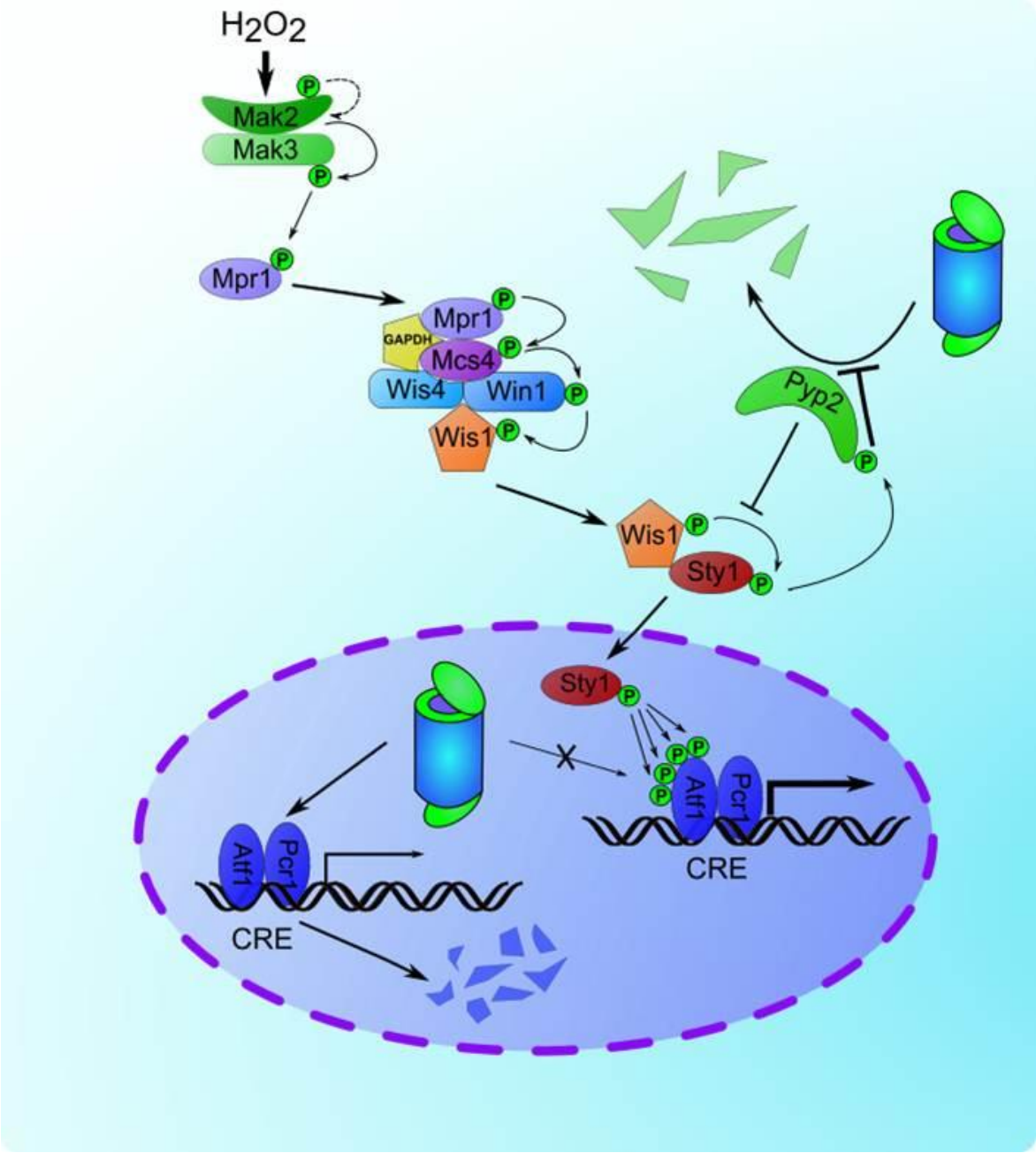

Fig. 3 – Schematic model of Sty1/Atf1 signaling during oxidative stress. H_2O_2 specific sensors Mak2 and Mak3 undergo auto-activation in the presence of hydrogen peroxide and transfer phosphate group to the protein Mpr1 which subsequently associates via GAPDH with complex of Mcs4, MAPKKK, and MAPKK.. Mpr1 directly phosphorylates Mcs4 that activates first kinases in MAPK module – Wis4 and Win1 by phosphate transfer. These two kinases provide activatory phosphorylation to MAPKK Wis1. When activated, Wis1 dissociates from the protein complex, associates with MAPK Sty1 and phosphorylates it. Sty1 translocates to the nucleus where it is responsible for hyperphosphorylation of transcription factor Atf1. Hyperphosphorylated Atf1 is stabilized, accumulates in the nucleus and transcription rate of Atf1-bound genes increases. Sty1-mediated phosphorylation also stabilizes its negative regulator phosphatase Pyp2, triggering negative feedback loop in this manner. The picture was created on the basis of literature cited in this chapter.

3.4. CSL transcription factors

CSL (CBF1, Su(H), LAG-1) family of transcription factors encompasses number of highly identical and evolutionarily conserved proteins present in all metazoans and several other species. These proteins were studied mainly in *Drosophila melanogaster* (where the CSL is termed Supressor of Hairless Su(H)), *Caenorhabditis elegans* (Lin-12 and Glp-1 phenotype - LAG-1), *Xenopus laevis* (X-Su(H)), *Mus musculus* (Recombination Signal Binding Protein for Immunoglobulin kappa J - RBP-Jκ), and *Homo sapiens* (C-promoter Binding Factor 1 - CBF1) [101, 102]. Members of CSL protein family are crucial transcription factors for the differentiation of cells and the key effectors of the Notch signaling pathway, which is a prominent regulator of the metazoan development [102-106].

3.4.1. Notch signaling

Notch signaling is, in general, responsible for regulation of cell-fate decision, differentiation, and organogenesis, where a key determining factor is a type and character of cell-to-cell contact [107]. In human, functional Notch pathway is important for proper development of kidneys, liver, cardio-vascular system, skeleton, eye, genitals, and other systems. Diverse mutations of Notch components have been reported to cause serious inherited or acquired malformations and malfunctions of organs [108]. Aberrant Notch signaling is also connected with the cell transformation and cancer in adults [109]. Furthermore, Notch pathway is important for regulation of human embryonic stem cells differentiation to motor neuron [110]. However, Notch signaling is the best studied in *D. melanogaster* [111], where it regulates for example eye [112], wing [113], and neuron development [114].

The Notch signaling is triggered by proteolytic cleavage of transmembrane Notch receptor (NotchR) that follows binding of NotchR specific ligand. NotchR is composed of three distinct domains. The relatively subtile transmembrane domain (TD) anchors NotchR to the cytoplasmic membrane with the N-terminal part of the protein exhibited at the cell surface and cytoplasmic C terminus. The extracellular domain (NotchEC) comprises 10-36 Epidermal Growth Factor-like Repeats (ELRs) distal to TD, followed by 3 cysteine-containing LNG (Lin-12, Notch, Glp1) repeats and Lys/Arg rich proteolytic cleavage site that is adjacent to the TD. C-terminal intracellular domain of Notch (NotchIC) consists of TD-proximal Nuclear Localisation Signal NLS and RAM domain

(RBP-jκ Associated Molecule) followed by two NLS with subsequent six consecutive ankyrin repeats (ANK) and destabilizing PEST motif at the C terminus of the protein. Prominent is also intracellular cleavage site of the NotchR represented by conserved Val residue contiguous to the TD [115].

NotchEC is regulatory part of the protein that mediates intercellular contact via direct interaction with its ligands - DSL (Delta, Serrate, LAG-2) molecules. DSL are transmembrane proteins, whose EGF-motif binding domain (EBD) is exposed at the surface of adjoining cells. Properly glycosylated NotchR recognizes EBD of DSL protein and subsequent receptor-ligand association induces conformational change of NotchR [116] that uncovers extracellular NotchR cleavage site for ADAM (A Disintegrin And Metalloprotease) protease. When the NotchEC is removed, the NotchR is converted into intracellular intermediate NEXT (Notch Extracellular Truncation) that is susceptible for proteolytic cleavage mediated by γ-secretase. This protease releases free form of NotchIC into cytoplasm. Subsequently, NotchIC translocates to the nucleus where it directly associates with transcription factor CSL and induces appropriate transcriptional activation (Fig. 4) [101]. Induced expression changes are tissue- and cell type-specific and this plasticity is particularly mediated via ELRs number variability [115].

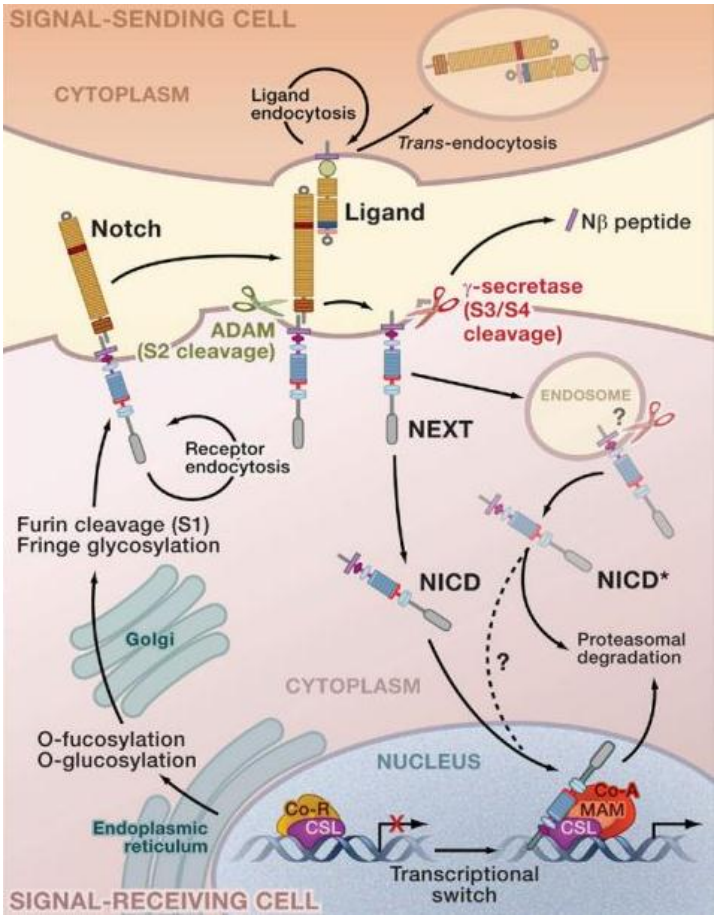

Fig. 4 – Schematic model of Notch signaling. The picture was taken from [101]. Interaction between Notch receptor and its ligand results in conformational change of receptor that is subsequently cleaved by ADAM protease. First proteolysis generates second, intracellular cleavage site that is occupied and cleaved by γ-secretase, releasing intracellular domain of Notch receptor (NotchIC/NICD). Free form of NotchIC translocates to the nucleus where it associates with CSL transcription factor, causing the displacement of co-repressor complex and recruitment of CSL co-activators which enable activation of target gene.

3.4.2. The structure of CSL transcription factors

Among various organisms, CSL proteins might include variable N- and C- terminal extensions; however, the core of the protein is strikingly conserved. For instance, there is 72% identity between *D. melanogaster* and *H. sapiens* CSL core [102]. Additionally, Kaspar and Klein showed human CBF1 expressed in *D. melanogaster* could effectively substitute Su(H) function, indicating that CSL transcription factors from one organism are, supposedly due to their high identity, functionally compatible with other species [113].

The core of CSL proteins is generally folded into three distinct domains, connected together by β-strand C4 which stabilizes overall protein structure. Despite the lack of sequence identity, the tertiary structure of N-terminal domain (NTD) and C-terminal domain (CTD) is closely related to the RHR-N and RHR-C domains of Rel transcription factors (sandwich of seven β-sheets conformed into immunoglobulin-like fold). The amino acid sequences of NTD and CTD are separated by β-trefoil domain (BTD) (Fig. 5). Regardless of structural similarity to Rel proteins, CSL transcription factors, however, bind DNA as monomers [117]. The DNA binding domain of CSL proteins, which recognizes and mediates specific interaction with the sequence 5'-CGTGGGAA-3' [118], is formed by both NTD and BTD, while CTD does not interact with DNA and rather stabilizes overall protein fold [117].

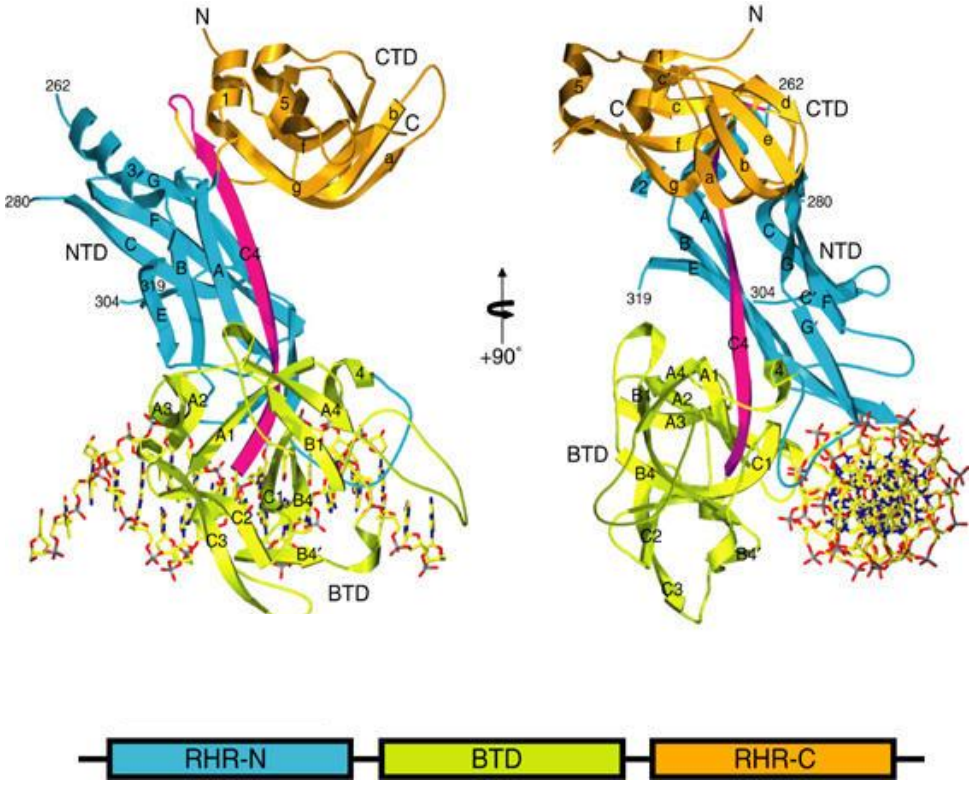

Fig. 5 – Structure of DNA-bound LAG-1 CSL family member from *C. elegans*. The picture was taken from [117] and adjusted. Figure illustrates positions and orchestration of NTD (RHR-N), BTD, and CTD (RHR-C) of inactive, DNA-associated CSL transcription factor LAG-1, as well as position of these domains in primary protein structure.

3.4.3. Notch-dependent activation of CSL

When bound to a promoter region, CSL transcription factors suppress transcription of target genes in metazoa [104, 113, 119, 120] through recruitment and establishment of co-repressor complex. In vertebrates, assembly of co-repressor complex requires an adaptor Ski-interacting Protein SKIP, which directly interacts with CSL transcription factor and recruits other co-repressors [121], predominantly Silencing Mediator for Retinoid and Thyroid Receptor SMRT, CBF-interacting Repressor CIR, and histone deacetylases HDAC1 and HDAC2 [102, 122].

As briefly described earlier, interaction with NotchIC switches the function of CSL factors from transcriptional repressor to activator. NotchIC binding results in the displacement of the co-repressor complex and subsequent recruitment of co-activators to CSL-NotchIC complex. BTD and NotchIC that comprises RAM domain and six ankyrin repeats (ANK) play a fundamental role in this process. RAM docks to the hydrophobic pocket of BTD, while electrostatic interactions mediate interaction between ANK and CTD. Subsequently, a transcription co-activator MAML1 (Mastermind-like protein 1) interacts with the second ankyrin repeat of NotchIC, and with both CTD and NTD of CSL. NotchIC and MAML1 binding causes substantial conformational changes of CTD and BTD that probably result in modulation of binding properties of SKIP. Its previously low affinity for NotchIC rises, while affinity towards co-repressor SMRT is decreased. Therefore, SKIP directly associate with fourth ANK of NotchIC with concomitant dissociation of SMRT and CIR co-repressors, enabling assembly of transcription initiation complex [121, 123] that includes for example profoundly known histone acetylase CBP/p300 [124].

3.4.4. CSL transcription factors in fungi

Generally accepted model of CSL function (depicted in Fig. 4) is based on convincing and large body of evidence. According to this concept, CSL transcription factors are essential for the development of multicellular animals, but are unimportant for single cells in the culture [125]. However, discovery of two paralogs of CSL proteins in unicellular fission yeast *S. pombe* seems to compromise CSL factors as metazoan hallmarks [122]. Despite the absence of Notch components in the genome of fission yeast, deletion of the *S. pombe* CSL paralog *cbf11* causes broad palette of phenotypes, while phenotypes of *cbf12Δ* were rather mild [126], suggesting that these transcription factors

(especially Cbf11) might regulate gene expression even in the organism that lacks Notch pathway completely.

Computational analyses have revealed thirty three CSL sequences in various fungal species. More than one copy of CSL-coding genes per genome was found in the most of analyzed fungi [127]. Putative amino acid sequences of fungal CSL are remarkably more divergent than their metazoan relatives. However, a high degree of identity has been observed among NTDs and BTDs, and amino acid sequences of DNA binding domains have been shown to be completely conserved. It is therefore possible that fungal (*S. pombe*) CSL proteins can bind CSL consensus binding sequence as their metazoan counterparts [128]. In contrast, fungal CSL proteins display increased variability in hydrophobic region that organizes NotchIC-binding pocket and binding sites of its co-factors in metazoa. Despite the fact that the predicted CTD sequences showed high divergence among analyzed fungal CSL proteins, preserved β-strand C4 suggests that metazoan-like architecture of the protein, especially mutual fold and position of NTD and BTD, might be conserved and maintained through evolution (Fig. 5). It has been interestingly hypothesized that CSL proteins originated in the common ancestor of fungi and metazoans by insertion of BTD into the middle part of Rel proteins. Subsequently, these proteins were lost in some clades or underwent genome duplication, and were adopted by Notch pathway in metazoa. It is proper to make a note that, hypothetically, ancient Notch-independent properties of CSL transcription factors might be retained from fungi to mammals, affecting the physiology of given organisms [127, 129]. Indeed, some of the Notch-independent activities of CSL proteins have been already described in detail [130–133].

3.4.4.1. CSL transcription factors in *S. pombe*

Among recently known CSL-containing fungal species, two paralogs (called Cbf11 and Cbf12) of CSL transcription factors have been discovered in the fission yeast *S. pombe*, well-studied and established model organism in biology [127, 129]. Hence, presence of accessible and standardized protocols, powerful genetic tools, thoroughly annotated genome and its relatively high similarity to mammalian cells makes the fission yeast *S. pombe* optimal model for investigation of primal functions of CSL family members. A typical feature of fungal CSL proteins is intrinsically disordered N-terminal extension that can occupy up to 34 % of the whole protein length. Significant enrichment

of phosphorylation sites and PEST domains in N-terminal extensions of fungal CSL raises a question, whether these sequences are employed in CSL regulation in fungi. The observations that N-terminal extension impairs DNA binding activity of Cbf12 [127] and that the extension is required for the nuclear localization of both Cbf11 and Cbf12 [128], subsequently confirmed its regulatory role.

Because CSL transcription factors in fungi were not subjected to molecular and biochemical examination before and all contemporary insight was based rather on similarities, assumptions and computational predictions, clear and explicit determination of fungal CSL properties demanded convincing scientific evidence. Thus, previously predicted ability of Cbf11 to bind CSL consensus binding sequence and activate transcription of target genes was confirmed *in vitro* and *in vivo*. It has been shown that Cbf12 can trigger transcription of target genes but its binding to DNA was not proved [128].

The level of *cbf11* mRNA exceeds *cbf12* transcript level during logarithmic growth phase. On the other hand, *cbf12* transcript level increases during stationary growth phase and during sexual differentiation even exceeds expression of *cbf11*, indicating its regulatory role in these physiological events. Cbf11 seems to be involved in many aspects of the physiology of the fission yeast. Strain deficient in *cbf11* gene exerts growth rate retardation, altered colony morphology, cold-sensitivity, enhanced cell-cell adhesion, increased frequency of nuclear division defects (cut phenotype) and impaired genome integrity. It has been shown that overexpression of *cbf12* results in similar phenotypes suggesting that fungal CSL paralogs have antagonistic functions [126].

3.4.4.2. The role of fungal CSL transcription factors in oxidative stress response

Dr. Převorovský has further found that *S. pombe* cells with deletion of genes coding CSL transcription factors (*cbf11* and *cbf12*) are resistant to extreme concentrations of hydrogen peroxide. According to Fig. 6, *cbf11Δ* cells treated with 100mM H_2O_2 showed similar viability as untreated *cbf11Δ* cells, while growth and survival of wild type was seriously affected by the treatment. Deletion of *cbf12* has lesser, but still remarkable protective effect.

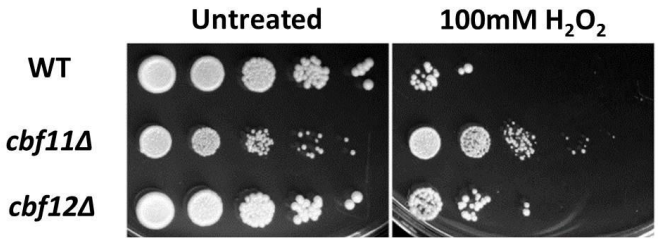

Fig. 6 – Resistance of CSL knock-out cells to H_2O_2: Cells were washed in 100mM H_2O_2 for 100 min then the culture was 5-times 10-fold diluted, and cultivated on agar plates. Experiment was performed by Dr. Převorovský

Subsequent high-throughput experiments performed by Dr. Převorovský found putative binding of CSL proteins to the promoters of *atf1*, and *pyp2* genes which encode important components of Sty1/Atf1 signaling (Fig. 8), and that mRNA levels of antioxidant enzymes in *cbf11Δ* cells are increased (Fig. 7). These results suggest CSL proteins are connected to SAPK pathway in *S. pombe* and might be employed in the regulation of the stress response. Thus, the molecular mechanism of Cbf11-dependent modulation of stress response in *S. pombe* will be investigated in this project.

4. MATERIALS AND METHODS

4.1. Antibodies and enzymes

Antibodies used for protein analysis by western blotting and chromatin immunoprecipitation are listed in Table 1. Table 2 comprises all enzymes that were used in this study.

Table 1 – The list of used antibodies

Antibody	Source	Cat. number	Dilution
Mouse anti HA-tag	Covance	MMS-101P-500	1:1000
Mouse anti V5-tag	Serotec	SV5-Pk1	1:1000
Rabbit anti Phospho p38	Cell Signal. Tech.	9211S	1:1000
Mouse anti PSTAIR	Sigma	P7962	1:10 000
Goat anti mouse IgG-HRP	Santa Cruz	sc-2031	1:5000
Goat anti rabbit IgG-HRP	Santa Cruz	sc-2030	1:2000

Table 2 –The list of used enzymes

Enzyme	Source	Application
BglII endonuclease	Thermo Scientific	*cbf11* deletion
DNase I	Epicentre	RNA purification
Fast AP phosphatase	Thermo Scientific	Construction of pMP127
HindIII endonuclease	Thermo Scientific	Construction of pMP127
HpaI endonuclease	Thermo Scientific	Construction of pMP127
Proteinase K	Epicentre	RNA purification
Proteinase K	Roche Diagnostics	ChIP
M-MuLV reverse transcriptase	Thermo Scientific	cDNA synthesis
Taq polymerase	Thermo Scientific	PCR, colony PCR
XbaI endonuclease	Thermo Scientific	*cbf11* deletion
XhoI endonuclease	Thermo Scientific	*cbf11* deletion

4.2. Oligonucleotides

Primers for qPCR analysis (LightCycler® 450 Real-Time PCR System, Roche) were designed following manufacturer's instructions, using IDT PrimerQuest (https://eu.idtdna.com/PrimerQuest/Home/Index) and IDT Oligo Analyzer (http://eu.idtdna.com/calc/analyzer) online software.

Primer requirements for Roche LightCycler 450

- Amplicon size: 50-150 bp
- Melting temperature: 59-61 °C
- GC content: 30-80 %
- Oligonucleotide size 20-22 bp

Oligonucleotides for verification of Nat MX6 integration into *cbf11* locus (Table 4) were taken from the laboratory stock. Sequences of interest were downloaded from the database at www.pombase.org [53] and processed via DNA-Protein Sequence Cleaner available www.cellbiol.com. Primers for gene expression analysis were designed into the open reading frame (ORF) of target genes (Table 3), while the coordinates of Cbf11 binding sites (for evaluation of chromatin immunoprecipitation – ChIP) in the promoter regions of target genes (Table 5) were determined on the base of ChIP-seq data (obtained from Dr. Převorovský). Putative Pap1 binding sites (Table 5) in the promoter regions of *ctt1*, *gst2*, *pyp2*, and *sty1* for ChIP were acquired from literature [76], [134] or predicted by on-line computational analyses.

4.2.1. Prediction of Pap1 binding sites

Genomatix MatInspector (https://www.genomatix.de/matinspector.html; used 6.2.2015), TRANSFAC (http://www.biobase-international.com/product/transcription-factor-binding-sites#resources; used 6.2.2015), and ALGGEN-PROMO version 8.3 (http://alggen.lsi.upc.es/cgi-bin/promo_v3/promo/promoinit.cgi?dirDB=TF_8.3) were used. Sequences 1 kb (and 1.5 kb in case of *pyp2* promoter) upstream of transcription start site of *ctt1*, *gst2*, *pyp2*, and *sty1* were downloaded from www.pombase.org [53] in fasta format, uploaded to the software mentioned above and searched for AP-1 (*Homo sapiens*), YAP1 (*Saccharomyces cerevisiae*) and Pap1 (*S. pombe*) binding sites with default settings. All mentioned transcription factors have very similar DNA binding properties [135].

Table 3 – The list of used oligonucleotides for RT-qPCR

ORF	Primer	Sequence	Source
act1	**MP137**	5‘ TCCTCATGCTATCATGCGTCTT 3‘	Převorovský
	MP138	5‘ CCACGCTCCATGAGAATCTTC 3‘	
atf1	**MaP173**	5‘ CCGACCCTTCATTAACATTAC 3‘	Oravcová
	MaP174	5‘ CCGTTGGCATATCAGAATTAG 3‘	
cbf11	**MaP175**	5‘ AACCCATCAGCGAAGAATA 3‘	Oravcová
	MaP176	5‘ CCAGAGAAAGCCGTAAGT 3‘	
cbf12	**MaP177**	5‘ CAAAGTGTTGTGCTCCAATA 3‘	Oravcová
	MaP178	5‘ CCTTCCAATTATCGTGCTTC 3‘	
ctt1	**PD01**	5‘ CCGACGACATTACCAAGTA 3‘	Daněk
	PD02	5‘ ACGAGCAGTATCAGGAGTA 3‘	
gst2	**MaP146**	5‘ TGGAAGAGTACCTACTTTAGTT 3‘	Oravcová
	MaP147	5‘ CAGGGTCATCAAAGGATAATG 3‘	
pyp2	**PD05**	5‘ TGCCTTCTTATCCCTCCT 3‘	Daněk
	PD06	5‘ ACGACGTTGCTGGATTTA 3‘	
rho1	**MP169**	5‘ GGTCTATGTTCCCACTGTTT 3‘	Převorovský
	MP170	5‘ CTTCTTGTCCAGCCGTA 3‘	

Table 4 – The list of used oligonucleotides for genotyping of *S. pombe* strains

Primer	Sequence	Application	Source
MP150	5‘ AGGGATCGAAAGACATCCGC 3‘	Upstream integration site of Nat MX6 to *cbf11*	Převorovský
MP44	5‘ GTCGTTAGAACGCGGCTACA 3‘		
MP151	5‘ GCTTGTACACACGGCCTTCAA 3‘	Downstream integration site of Nat MX6 to *cbf11*	Převorovský
MP33	5‘ GCGCACGTCAAGACTGTC 3‘		

Table 5 – The list of used oligonucleotides for ChIP evaluation

Cbf11-TAP ChIP			
Primer	**Gene**	**Sequence**	**Amplicon coordinates**
MaP90	*atf1*	5‘ GTATCGTCTTGCTCGGTT 3‘	Ch II: 1546066-1546198
MaP91		5‘ CCACACTTCCACCTGTTT 3‘	
PD03	*ctt1*	5‘ GAATTACCAACGTCATATTTGC 3‘	Ch III: 58878-59019
PD04		5‘ ACTACGATAGGCTGTAGAAGA 3‘	
MaP96	*cut6*	5‘ TTGCTACAGGAAGAGGAAG 3‘	Ch I: 1253522-1253603
MaP97		5‘ TAGAAAAGTTGGATGCGTG 3‘	
MaP134	*gst2*	5‘ CGTATTACTGAGTGCTTATGT 3‘	Ch III: 2296128-2296304
MaP135		5‘ TGATTCACTGTAAAAACCCAC 3‘	
PD07	*pyp2*	5‘ GCGTCACTCGTCACATTA 3‘	Ch I: 5201545-5201639
PD08		5‘ TGCTAAGCGACCGTTTATT 3‘	
MP88	Intergenic	5‘ AGCTGCTAGACACCTTCAAA 3‘	Ch I: 1928359-1928274
MP89	locus P4	5‘ CCTACGGTCAAGAGAAAACT 3‘	
Pap1-3Pk ChIP			
Primer	**Gene**	**Sequence**	**Amplicon coordinates**
MaP78	Intergenic	5‘ CGGTAAATTGATACGCCC 3‘	Ch I: 499187-499310
MaP79	locus M40	5‘ GACATCCCGACAATACATC 3‘	
MP137	*act1* ORF	5‘ TCCTCATGCTATCATGCGTCTT 3‘	Ch II: 1476764-1476687
MP138		5‘ CCACGCTCCATGAGAATCTTC 3‘	
PD13	*ctt1* (CP1)	5‘ AAGTATTCTAATTTCAGTAACCTCC 3‘	Ch III: 59614-59700
PD14		5‘ GCTTCCCGTAGAGGTATAA 3‘	
PD15	*ctt1* (CP2)	5‘ GTCAGCGTCTGTGTCTA 3‘	Ch III: 59057-59168
PD16		5‘ CTCATACCGTTACTTGGC 3‘	
PD17	*ctt1* (CP3)	5‘ GATGCTCTTTGGCTCACT A 3‘	Ch III: 58873-58966
PD18		5‘ GTGTAGAATTACCAACGTCATA 3‘	
PD21	*gst2* (GP3)	5‘ GAGAAAGCGGGTCGAATA 3‘	Ch III: 2296763-
PD22		5‘ GTGTCTTACACGCAGAGT 3‘	2296874
PD23	*gst2* (GP2)	5‘ AATGGGTGCTGACTAACAA 3‘	Ch III: 2296132-
PD24		5‘ AACTAGAACGAGGATGCC 3‘	2296221
PD25	*pyp2* (PP1)	5‘ GCATAGTGCTACACAGTACAA 3‘	Ch I: 5201409-5201597
PD26		5‘ GACGAGTGACGCTTAGAG 3‘	
PD27	*pyp2* (PP2)	5‘ GCATGGAAGCCCTATTCT 3‘	Ch I: 5202060-5202179
PD28		5‘ GTGGCGCTGGGATATAAA 3‘	
PD29	*sty1* (SP1)	5‘ GACTTGTTGCACCTAATTATCC 3‘	Ch I: 208595-208752
PD30		5‘ GTAGTTAATTTGCTTGTTTGCC 3‘	

MaP primers were designed by Dr. Oravcová; MP primers by Dr. Převorovský; PD primers by Bc. Daněk

4.3. Plasmids

Plasmids used in this study for *cbf11* deletion and for construction of reporter vector for β-galactosidase assay are listed in Table 6.

Table 6 – The list of used plasmids

Plasmid	Application	Source
pMP91	*cbf11* deletion	M. Převorovský
pMP120	Reporter vector pREPORT-U with Pap1 binding sites	M. Převorovský
pMP121	Reporter vector pREPORT-L [136]	M. Převorovský
pMP127	Reporter vector pREPORT-L with Pap1 binding sites	P. Daněk

4.4. Commercially available kits

Several procedures were performed using commercial kits that are listed in Table 7.

Table 7 – The list of applied commercially available kits

Product	Source	Application
MasterPure™ Yeast RNA Purification	Epicentre	RNA purification
Nucleospin® Gel and PCR Clean-up	Macherey-Nagel	pMP127 construction
Nucleospin® Plasmid	Macherey-Nagel	pMP127 construction
RevertAid™ First Strand cDNA Synthesis	Thermo Scientific	Reverse transcription
DC™ Protein Assay	Bio-Rad	Western blotting

4.5. *Schizosaccharomyces pombe* strains

Diverse *S. pombe* strains, involved in experiments described in following chapter, are listed in Table 8.

Table 8 – The list of applied strains of *Schizosaccharomyces pombe*

Strain	Genotype	Source
JB32	*h+s*	lab. stock
JB146	*h- Δatf1::ura4 ura4-D18*	lab. stock
JB147	*h- Δpap1::ura4 ura4-D18*	lab. stock
JB149	*h- Δsty1::ura4 ura4-D18*	lab. stock
JB725	*h- Δpka1::KanMX6*	lab. stock
JB1062	*h+ ura4-D18 leu1-32*	lab. stock
MP19	*h+cbf11-ctap4::natR*	lab. stock
MP21	*h+Δcbf12::natR*	lab. stock
MP25	*h+Δcbf11::kanR, Δcbf12::natR*	lab. stock
MP44	*h+Δcbf11::kanR*	lab. stock
MP84	*h- ura4-D18 leu1-32 Δcbf11::natR*	lab. stock
MP350	*h+ Δcbf11::natR Δpka1::kanMX6*	J. Tvarůžková
MP367	*h- ura4-D18 Δatf1::ura4 Δcbf11::natR*	J. Tvarůžková
MP368	*h- ura4-D18 Δpap1::ura4 Δcbf11::natR*	J. Tvarůžková
MP382	*h- Δsty1::ura4 ura4-D18 Δcbf11::natR*	J. Tvarůžková
MP403	*h+ atf1-2HA6his::leu2 leu1-32*	lab. stock
MP404	*h- sty1-HA6H::ura4 ura4D*	lab. stock
MP427	*h+ atf1-2HA6his::leu2 leu1-32 Δcbf11::natR*	P. Daněk
MP428	*h- sty1-HA6H::ura4 ura4D Δcbf11::natR*	P. Daněk
MP430	*h– ade6-M216 pap1+(3Pk)::ura4+ his7-366 leu1-32 ura4-D18*	E. Veal [66]
MP479	*h– ade6-M216 pap1+(3Pk)::ura4+ his7-366 leu1-32 ura4-D18 Δcbf11::natR*	P. Daněk
MP494	*Δpap1::ura4 ura4-D18 leu1-32*	P. Daněk

4.6. Microorganism culture

4.6.1. *Schizosaccharomyces pombe*

The media components (Table 9) were dissolved in deionized water which was prepared with Rovapur 100 (Watrex) and Ultrapur (Watrex) filtres. The solution was subsequently sterilized (autoclave Tuttnauer 2540EK) in 121 °C for 20 minutes.

Cells were taken from the glycerol stocks stored in -80 °C, plated on YES agar plates (Table 9) in Petri dishes and incubated in 32 °C for 3 days. If necessary, cells might be further stored in 25 °C. Then the appropriate amount of biomass was transferred into Erlenmayer flasks (100 ml) with 10 ml of liquid YES medium (Table 9) inside, cultivated, and shaked with frequency 180 rpm (rotation per minute) in 32 °C for 12 hours (Ecotron, Infors HT). Optical density (OD_{600}) of the culture was measured with CO8000 Cell Density Meter (WPA Biowave) against water as a blank (OD_{600} usually reached values from 0.3 to 0.6). Subsequent calculation revealed which OD_{600} should 50 ml of prepared culture have to reach OD_{600} = 0.5 within approximately 12 hours. Afterward, adequate volume of cell cultures was withdrew, transferred to sterile Erlenmayer flask (250 ml) and YES medium was added up to 50ml. Cells were cultured (32 °C; 180 rpm) to mid-log phase of growth, treated, and harvested according to the given protocol. Logarithmic phase of growth is indicated by OD_{600} = 0.5.

Table 9 – Composition of media

Liquid YES medium	
Yeast Exctract Powder (Formedium)	0.5%
Glucose (Sigma)	3%
SP Supplements PSU0101 (Formedium)	0.025%
YES Agar plates	
Yeast Exctract Powder (Formedium)	0.5%
Glucose (Sigma)	3%
SP Supplements (Formedium)	0.025%
Agar (Sigma)	2%
Liquid EMM	
EMM broth without dextrose (Formedium)	1.23%
Glucose	2%
Adenine	0.02%
Leucine	0.02%
Uracil	0.02%
Thiamine	0.02%
EMM agar plates	
EMM broth without dextrose (Formedium)	1.23%
Agar (Sigma)	3%
Glucose	2%
Adenine	0.02%
Leucine	0.02%
Uracil	0.02%
Thiamine	0.02%

4.6.1.1. Glycerol stock preparation

5 ml of microorganism culture were incubated for 2 days in YES medium in 32 °C, shaked witch frequency 180 rpm (Ecotron, Infors HT). Then 600 µl of culture were transferred to sterile 2ml plastic tube with the screw cap and properly mixed with 600 µl of 60% sterile glycerol solution. Cells were afterward incubated for 20 min on ice and stored in -80 °C.

4.6.1.2. Lithium-acetate transformation of *S. pombe*

All procedures were performed in sterile environment. Cells (10 ml of liquid culture) were cultivated to OD_{600} = 0.5, poured to the falcon tube (15 ml) and centrifuged (1000 g; 3 min; 20 °C). Supernatant was discarded, sediment resuspended in 1 ml of sterile deionized H_2O, transferred to clean micro test tube (1.5 ml), and centrifuged again (1000 g; 3 min; 20 °C). Sediment was washed with 1 ml of LiAc/TE solution, spun (1000 g; 3 min; 20 °C), and resulting pellet was resuspended in 100 µl LiAc/TE, mixed with 2 µl of denatured (95 °C; 10 min; 20 °C) salmon sperm DNA (Sigma) and with 10 µl of transforming DNA (linearized plasmid), and incubated for 10 min in room temperature. 260 µl of newly prepared solution of 40% PEG (polyethylene glycol)/LiAc/TE were subsequently added and whole cell suspension was incubated in 30 °C for 60 min. Then 43 µl of DMSO (dimethyl sulfoxide) were added, sample was transferred to 42 °C, and incubated there for 5 min. Cells were further centrifuged (1000 g; 3 min; 20 °C), supernatant discarded, leaving approximately 100 µl, in which the sediment was resuspended and subsequently plated on solid YES agar plates (Table 9); overnight incubation in 32 °C followed. Cells were afterwards transferred to solid YES plates with suitable selection agent (100 µg/ml nourseothricine for selection of cells transformed with Nat MX6. Cells transformed with whole plasmid carrying auxotrophic selection (pMP127) were pleated directly to solid EMM depleted of leucine (in case of selection with *LEU2*).

Buffers and solutions:

LiAc	1 mol/l lithium acetate; pH = 7.5
TE buffer	0.1 mol/l TRIS-HCl; 10 mmol/l EDTA; pH = 7.5
LiAc/TE	1 ml LiAc; 1 ml TE buffer; 8 ml H_2O
40% PEG/LiAc/TE	960 µl 50% PEG; 120 µl LiAc; 120 µl TE buffer

4.6.2. *Escherichia coli*

The media components (Table 10) were dissolved in deionized water that was prepared with Rovapur 100 (Watrex) and Ultrapur (Watrex) filtres. The solution was subsequently sterilized (autoclave Tuttnauer 2540EK) in 121 °C for 20 minutes.

Bacteria were taken from the glycerol stocks stored in -80 °C, plated on LB agar plates (Table 10) with ampicillin (bacteria contained plasmid with the gene for ampicilin resistance (*ampR*), thus ampicilin was added to media to make a selection pressure for the plasmid maintenance) in Petri dishes and incubated in 37 °C. After 24 hours of incubation an appropriate amount of biomass was transferred with a wooden toothpick into Erlenmayer flask (250 ml) with 50 ml of LB medium inside (Table 10). Cells were incubated overnight in 37 °C and shaked with frequency 180 rpm.

Table 10 – Composition of LB medium

Liquid medium	
Universal pepton M66 (Merck)	1%
Yeast extract powder (Formedium)	0.5%
NaCl (Sigma)	0.5%
Ampicilin	100 µg/ml
Agar plates	
Universal pepton M66 (Merck)	1%
Yeast extract powder (Formedium)	0.5%
NaCl (Sigma)	0.5%
Agar bacteriological (Oxoid)	2%
Ampicilin (Biotica)	100 µg/ml

4.6.2.1. Electroporation of *E. coli*

Competent *E. coli* (DH5α; Stratagene) cells were slowly de-frosted on ice and 40 µl of cell suspension were transferred into chilled electroporation cuvette (Cell Projects) in sterile conditions. Then 3 µl of plasmid DNA was added to the cuvette and cells were electropored (2500 V; 200 Ω; 25 µF) by GenePulser Xcell (Bio-Rad). *E. coli* cells were resuspended in 1 ml of LB medium (Table 10) containing 0.5% glucose, cultivated in 37 °C for 30 min immediately after the electroporation, and subsequently plated on LB agar plates (Table 10) with suitable selection agent (ampicilin).

4.7. Nucleic acid manipulation techniques

4.7.1. Agarose gel electrophoresis

The agarose gel (1% or 2%) was prepared by boiling 1 g or 2 g of agarose SeaKem® (Lonza) in 100 ml of TAE (TRIS-acetic acid-EDTA) buffer until agarose was completely melted. Melted agarose was poured into gel tray equipped with comb (each well 4-15×1 mm) to the maximal thickness 5 mm and slowly cooled at room temperature. Solid agarose gel was transferred to the electrophoretic chamber BlueMarine™ 100 (7×10 cm large gel; electrode separation 18 cm; 14-140 V per cm, maximum voltage 300 V) or BlueMarine™ 200 (15×15 cm large gel; electrode separation 28.5 cm; 20-200 V per cm; maximum voltage 500 V) and poured over with TAE buffer.

After the comb removal, 5-30 µl of DNA samples were mixed with one fifth of the sample volume of 6× LD (Loading Dye, Thermo Scientific) and loaded to wells. 6 µl of marker of nucleic acid molecular weight were also loaded. For analysis of large DNA molecules GeneRuler™ 1 kb DNA Ladder (Thermo Scientific) and for distinction of smaller DNA fragments GeneRuler™ DNA Ladder Mix (Thermo Scientific) or GeneRuler™ 50 bp DNA Ladder (Thermo Scientific) were used.

Loaded DNA samples were separated usually by operating voltage set between 60-120 V, depending on the size of the gel. Agarose gel was stained with ethidium bromide-water solution (0.5 µg/ml) for 10 minutes when the electrophoretic separation of DNA fragments was finished. The gel was subsequently washed in distilled water and DNA visualized using UV-transiluminator Foto UV/21 (Fotodyne). Gels were photographed with Panasonic DMC-F27 camera equipped with red/UV filter. The exposition time was set to 1-3.5 s.

Buffers and solutions:

TAE buffer 40mM TRIS; 20mM glacial acetic acid; 2mM Na_2EDTA; pH = 8.5

4.7.2. DNA extraction from agarose gel

DNA fragments generated by restriction cleavage (see section 4.7.5.) were separated by electrophoresis (see section 4.7.1.) in 1% agarose gel (65 V; 2 h). Piece of agarose gel containing DNA fragment of interest was cut out with lancet, transferred to the clean micro test tube (1.5 ml), and processed with Nucleospin® Gel and PCR Clean-up kit following manufacturer's instructions. Extraction yielded 28 µl of purified DNA.

4.7.3. Chromosomal DNA purification

Either biomass from single colony or sedimented cells (1000 g; 3 min; 20 °C) from 100 µl of liquid cell culture (OD_{600} = 0.5) were resuspended in 100 µl of 200mM lithium acetate containing 1% SDS (sodium dodecyl sulfate), vortexed and incubated for 5 min in 70 °C. After cooling down, 300 µl of 96% ethanol were added to each sample, briefly stired by vortexing and centrifuged (20 000 g; 3 min; 20 °C). Supernatant was discarded, sediment (containing precipitated nucleic acids) washed with 500 µl of 70% ethanol, and centrifuged again (20 000 g; 3 min; 20 °C). Pellet was dissolved in 100 µl of deionized H_2O. Cellular debris was sedimented by centrifugation (20 000 g; 1 min; 20 °C) and supernatant containing dissolved nucleic acids was transferred to clean micro test tube. DNA concentration was determined with spectrophotometer NanoDrop 2000 (Thermo Scientific).

4.7.4. Plasmid DNA purification

Bacteria *E. coli* carrying plasmid of interest were inoculated the day before DNA purification into 10 ml of liquid LB medium (Table 10) and incubated overnight in 37 °C shaking (180 rpm). Culture was transferred to falcon test tube (15 ml), sedimented (3000 g; 10 min; 4 °C), and pellet was resuspended in 2 ml of pre-cooled solution I. Test tube was subsequently removed from ice and its content was mixed with 4 ml of warm (room temperature) solution II, stired, and incubated in room temperature. After 5 minutes of incubation, sample was placed on ice and 3 ml of pre-cooled solution III were added. Sample was stired and incubated for 15 min on ice.

White coagulate occurred during the incubation. Sample (with coagulate) was transferred to polypropylene centrifugation tubes and sedimented (20 000 g; 15 min; 20 °C). Supernatant was transferred to clean falcon test tube, perfectly mixed with isopropanol whose amount was equal to 0.6 of supernatant volume, and immediately

centrifuged (2500 g; 6 min; 4 °C). Sediment was air dried, dissolved in 300 µl of deionized H_2O, and transferred to the clean micro test tube.

Volume of dissolved sediment-H_2O solution was established and the same volume of 10M LiCl was added. The final solution was perfectly homogenized and incubation in -80 °C for at least 30 min followed. Sample was subsequently centrifuged (20 000 g; 5 min; 4 °C) and supernatant transferred to the clean micro test tube. DNA was precipitated by addition of 750 µl of 96% ethanol and subsequent incubation in -80 °C for 30 min. Provided precipitate was spun (20 000 g; 5 min; 4 °C), washed in 1 ml of 70% ethanol, spun again (20 000 g; 5 min; 4 °C), air dried, and dissolved in 100 µl of deionized H_2O.

Buffers and solutions:

Solution I	20mM TRIS-HCl – pH = 8; 10mM EDTA-NaOH; 1% glucose
Solution II	1% SDS; 0.2M NaOH
Solution III	3M potassium acetate; 2M acetic acid; pH = 5

4.7.5. Restriction cleavage of DNA

Concentration of plasmid DNA that was isolated according to protocol 4.7.4. could not be measured because DNA isolate contained contaminating RNA. DNA amount added to each reaction was therefore estimated from electrophoretogram. Ten times diluted plasmid DNA sample (purified according to 4.7.4. protocol) was mixed with restriction endonuclease (Table 2) and suitable buffer. Reaction mixture was prepared according to Table 11. If a sample was subjected to digestion by more than one restriction endonuclease simultaneously, the type, amount of buffers, and quantity of each enzyme were determined with on-line software Double Digest Calculator (Thermo Scientific; https://www.lifetechnologies.com). DNA was cleaved for 4 hours in 37 °C. Then, restriction endonucleases were inactivated by incubation in 75 °C for 10 min or by addition of the proper volume of 6× LD (Loading Dye – Thermo Scientific).

Table 11 – Reaction mixture for restriction cleavage of DNA

Reagents	Volume (total = 30 µl)
DNA	1 µl
Reaction buffer (10×)	3 µl
Enzyme	0.5 µl
Deionized H_2O	up to 30 µl (25.5 µl)

4.7.6. Phosphatase treatment of DNA fragments

DNA fragment (plasmid backbone) was dephosphorylated by FastAP phosphatase (Thermo Scientific) to prevent self-ligation of its free ends. Reaction mixture was prepared according to Table 12; the volume of DNA solution added to phosphatase reaction was estimated from electrophoretogram. Samples were incubated for 10 min in 37 °C. Phosphatase was inactivated by 5 min incubation in 75 °C.

Table 12 – Reaction mixture for dephosphorylation of DNA fragments

Reagents	Volume (total = 28 µl)
DNA	24 µl
FastAP buffer (10×)	3 µl
FastAP phospatase	1 µl

4.7.7. Ligation of DNA fragments

This procedure was used for the construction of reporter vector pMP127. Dephosphorylated (see 4.7.6.), linearized vector backbone from pMP120 depleted of DNA fragment containing selection marker *ura4* (see section 4.7.5.) was mixed with marker gene *LEU2*. For *LEU2* marker insertion, DNA was mixed with T4 DNA ligase buffer (Thermo Scientific) and T4 DNA ligase according to Table 13 and incubated in room temperature for 30 min. The volume of DNA solutions added to ligation reaction was estimated from electrophoretogram. Subsequently, samples were incubated overnight in water bath placed in the refrigerator (4 °C).

Table 13 – Reaction mixture for ligation of two DNA fragments

Reagents	Volume
Dephosphorylated vector backbone	9 µl
LEU2 marker gene	9 µl
T4 buffer (10×)	2 µl
DNA ligase T4	0.2 µl

4.7.8. RNA purification

Cells were grown in 50 ml of YES medium (see Table 9) in Erlenmayer's flask (250 ml) in 32 °C to OD_{600} = 0.5. Then 2 ml of cell culture were transferred to micro test tube (2 ml) and spun (1000 g; 2 min; 20 °C). Supernatant was discarded and pellet frozen in liquid nitrogen.

Total RNA fraction was purified from the frozen (-80 °C) pelleted cells using MasterPure™ Yeast RNA Purification Kit (Epicentre) precisely following manufacturer's instructions and protocol. Contaminating DNA was removed from the samples also according to the protocol. RNA yield was established using spectrophotometer NanoDrop 2000 (Thermo Scientific), measuring absorbance of UV ligh (wave length 260 nm).

4.7.9. Reverse transcription

Reverse transcription has been performed using commercial kit RevertAid™ First Strand cDNA Synthesis Kit (Thermo Scientific). All water used in this protocol was treated with DEPC (diethylpyrocarbonate). 1 ml of DEPC per 1 l of H_2O was incubated overnight in the fume hood and deactivated by autoclaving. The mixture of deoxyriboucleotides (dNTPs) has been prepared by mixing appropriate amounts of each deoxyribonucleotide stock (Thermo Scientific) to provide 10mM dNTPs solution in DEPC-treated water.

Right volume of each RNA sample containing 2 µg of purified RNA was transferred to micro test tube (0.5 ml), mixed with 1 µl (0.2 µg/µl) of random hexamer primer (Thermo Scientific) and bring with DEPC-treated water to total volume 12.5 µl. Samples were subsequently vortexed, briefly centrifuged, and incubated for 5 min in 65 °C. After the incubation all samples were cooled on ice and briefly centrifuged. The reaction mixture was assembled according to Table 14, gently mixed using automatic

pipette, and briefly centrifuged again. One NRT (No Reverse Transcriptase) control was prepared for qPCR analysis, consisting of the very same reagents except M-MuLV reverse transcriptase that was replaced with 1 µl of DEPC-treated water, and of the sample with the highest RNA yield. C_P values (result of qPCR) of NRT controls reveal quantity of contaminating DNA that was not degraded by DNase I during RNA purification.

All samples were subjected to short pre-incubation (5 min in 25 °C) and then incubated in 42 °C for 60 min. M-MuLV reverse transcriptase was inactivated by 5 min long incubation in 70 °C.

Table 14 – Reaction mixture for cDNA synthesis

Reagents	Volume (total = 20 µl)
RNA sample with primers	12.5 µl
Reaction buffer (5×)	4 µl
RiboLock™ RNase Inhibitor (40 u/µl)	0.5 µl
dNTPs (10 mM)	2 µl
RevertAid™ M-MuLV (200 u/ µl)	1 µl

4.8. Polymerase chain reaction (PCR)

4.8.1. Standard PCR

Standard PCR was used for genotyping of *S. pombe* strains and for verification of specificity of designed oligonucleotides. Reagents were bought from Thermo Scientific. Reaction mixtures were prepared on ice. NTC (No Template Control) for each reaction mixture containing distinct pair of primers has been prepared by replacing given volume of dissolved DNA with deionized water. The presence of PCR product in NTC suggests DNA contamination of reagents and should not occur. PCR products were analyzed by agarose gel electrophoresis (see 4.7.1.).

The composition of PCR reaction mixture and program used for genotyping of *S. pombe* is described in Table 15. The duration of amplification phase (*) is variable and can be adjusted according to the amplicon size and Taq polymerase processivity (~1 kb/min). Reaction mixtures were prepared in micro test tubes (0.2 ml) and PCR was performed in Applied Biosystems® Veriti® Thermal Cycler (Life Technologies).

Table 15 – Reaction mixture and program for *S. pombe* genotyping by PCR

Reaction mixture per one PCR (V = 20 µl)		**PCR program**	
dNTPs (2.5mM each)	1.6 µl		
Primer 1 (10µM)	1 µl	95 °C, 3 min	
Primer 2 (10µM)	1 µl	35 cycles	94 °C, 30 s
10x Taq buffer -	2 µl		54 °C, 30 s
$MgCl_2$ (25mM)	2.8 µl		72 °C, 1 min*
gDNA (100 ng/µl)	5 µl	72 °C, 5 min	
H_2O	6.5 µl		
Taq polymerase	0.1 µl		

***** The duration of amplification phase (*), might be changed according to the amplicon size and Taq polymerase processivity (~1 kb/min)

4.8.1.1. Validation of oligonucleotides by PCR

The ability of PCR mixture containing designed primers to amplify product of specific size was tested by ordinary PCR with 100 ng/µl concentrated gDNA (genomic DNA) as a template (Table 16). PCR was performed in Applied Biosystems® Veriti® Thermal Cycler (Life Technologies) and products of reaction were separated by 2% agarose gel electrophoresis, and their molecular size corresponded with the expected length of designed amplicons.

Table 16 - Program and reaction mixture per one PCR (total volume 10 µl)

Reagents (total volume = 10 µl)		**PCR program**	
dNTPs (2.5mM each)	0.8 µl		
Primer 1 (10µM)	0.3 µl	95 °C, 1 min	
Primer 2 (10µM)	0.3 µl	35 cycles	95 °C, 15
10x Taq buffer -	1 µl		60 °C, 30
$MgCl_2$ (25mM)	1.6 µl		72 °C, 20
gDNA (100 ng/µl)	1 µl	72 °C, 2 min	
H_2O	5 µl		
Taq	0.05 µl		

4.8.2. Colony PCR

Colony PCR was used for genotyping of *S. pombe* colonies growing on the selection plates after the transformation process. Reaction mixture was prepared according to Table 17. Very small amount of biomass was taken from each colony with a sterile toothpick and added to the reaction mixture as a template.

Table 17 - Reaction mixture and program for *S. pombe* genotyping by colony PCR

Reaction mixture per one PCR (V = 20 µl)		**PCR program**	
dNTPs (2.5mM each)	1.6 µl		
Primer 1 (10µM)	1 µl	95 °C, 5 min	
Primer 2 (10µM)	1 µl	35 cycles	94 °C, 30 s
10× Taq buffer -	2 µl		54 °C, 30 s
$MgCl_2$ (25mM)	2.8 µl		72 °C, 1 min
H_2O	6.5 µl	72 °C, 5 min	
Taq polymerase	0,1 µl		

4.8.3. Quantitative PCR (qPCR)

qPCR was used for primers specificity and reaction efficiency determination, analysis of ChIP, and for relative quantification of cDNA (complementary DNA) prepared according to the protocol 4.7.9. (RT-qPCR – Reverse Transcription quantitative PCR). All applications were performed using LightCycler® 480 Real-Time PCR System (Roche).

Preparation of reaction mixture and qPCR program was very similar for all three applications. Samples and reagents were kept on ice. Suitable amount MESA GREEN qPCR MasterMix Plus for SYBR® (Eurogentec), stored in 1ml aliquots in -20 °C, was slowly melted. Each qPCR reaction (total volume 10 µl) contained 5 µl of qPCR MasterMix, 0.6 µl of 10µM primers (0.3 µl each), proper amount of DNA template and deionized water. PCR premix was prepared for all reactions performed with the identical pair of primers at once (Table 18). This mixture was vortexed, shortly spun, and 5.6 µl of mixture per reaction were transferred to LightCycler® Multiwell Plate 384 (Roche). Each sample was analyzed in triplicate (three qPCR reactions per sample and one pair of primers). One NTC was prepared for each reaction mixture.

For expression analysis (RT-qPCR) 4.4 µl of 100× diluted cDNA were added to each well, while 4.4 µl of DNA diluted to concentration 4.5 ng/µl (19.8 ng of DNA per

reaction) for ChIP evaluation were used. Subsequently, LightCycler® Multiwell Plate 384 (Roche) was securely and tightly covered with LightCycler® 480 Sealing Foil (Roche). Plate was briefly centrifuged, shaked by vortexing, and centrifuged again. Samples were subjected to the following qPCR program and analyzed. Average and standard deviation of C_P values of each triplicate were calculated. Outliers among each triplicate were excluded from analysis if the standard deviation was greater than 0.3.

qPCR program:

95 °C, 5 min
40 cycles 95 °C, 15 s
60 °C, 30 s
72 °C, 20 s
95 °C, 5s
50 °C, 1 min

Table 18 - Reaction mixtures for ChIP-qPCR and RT-qPCR analysis (total volume 10 µl)

ChIP-qPCR		RT-qPCR	
Reagents	**Volume**	**Reagents**	**Volume**
qPCR MasterMix*	5 µl	qPCR MasterMix*	5 µl
Primer 1 (10µM)	0.3 µl	Primer 1 (10µM)	0.3 µl
Primer 2 (10µM)	0.3 µl	Primer 2 (10µM)	0.3 µl
DNA (4.5 ng/µl)	4.4 µl	cDNA (100× diluted)	4.4 µl

***** MESA GREEN qPCR MasterMix Plus for SYBR® (Roche)

4.8.3.1. Specificity and efficiency determination of qPCR containing designed oligonucleotides

Templates for each reaction (performed in triplicates) were represented by series of six 1/10 dilutions (100 ng/µl, 10 ng/µl, 1 ng/µl, 0.1 ng/µl, 0.01 ng/µl, and 0.001 ng/µl). Reaction mixture, conditions and program were set in accordance with Table 19. Specificity of qPCR reactions containing designed oligonucleotides was determined by melting analysis. Melting analysis assesses dissociation characteristics of double stranded PCR product during heating, enabling to reveal the presence of diverse PCR products within one reaction. Denaturation of DNA is accompanied by fluorescent signal decrease

(fluorescent dye emits light only when bound to double-stranded DNA). Even minor alterations (1 nucleotide) in the sequence or size of DNA change its melting point. Thus, diverse products are denatured at different temperatures. Results of melting analysis are visualized in a graph where derivation of signal intensity is plotted against temperature and distinct DNA molecules are represented by peaks in different positions. If the qPCR is not specific, several melting peaks will occur in sole reaction. Results showed, however, only one melting peak, confirming that qPCR with designed primers give one specific product.

Efficiency of amplification was established using two different types of template, depending on further qPCR application. cDNA was used as a template for determination of efficiency of amplification for RT-qPCR experiments, while gDNA was used as a template for determination of efficiency of amplification for ChIP (Chromatin Immunoprecipitation). Series of six 1/10 dilutions of DNA (in case of gDNA in the same way as for qPCR specificity analysis) were added to reactions according to Tab 20. Resulting C_P values were plotted against proper DNA dilution/concentration, creating the standard curve in this manner. The efficiency (E) of reaction was calculated from the slope of the linear part of the standard curve using following equation.

$$E = 10^{\frac{-1}{slope}}$$

Table 19 - Reaction mixture per one qPCR (total volume 10 µl)

Reaction mixture per one qPCR	Volume
MESA GREEN qPCR MasterMix Plus for SYBR® (Eurogentec)	5 µl
Primer 1 (10µM)	0.3 µl
Primer 2 (10µM)	0.3 µl
DNA	1 µl
Sterile deionized H_2O	3.4 µl

qPCR program:

95 °C, 5 min

40 cycles — 95 °C, 15 s; 60 °C, 30 s; 72 °C, 20 s

95 °C, 5s

50 °C, 1 min

4.8.3.2. ChIP-qPCR analysis

The enrichment of DNA binding proteins in investigated loci is expressed as percentage of input (%IP; see ChIP protocol 4.10.). The percentage of input has been calculated according to following equation, where E is the efficiency of reaction containing specific pair of primers and C_{PA} is average of C_P values in given triplicate:

$$\%IP = \frac{E^{-C_{PA}\,immunoprecipitate}}{E^{-C_{PA}input}}$$

ChIP data might be also presented in form of fold enrichment, which describes enrichment of target protein in the studied locus compared to negative control. Signal (C_P values) at P4 (Ch I: 1928359-1928274) locus or geometric average of signals (C_P values) at locus M40 (Ch I: 499187-499310) and *act1* ORF were used as negative controls in this thesis, but it can be basically every locus where investigated protein does not bind. Fold enrichment has been calculated according to following figure:

$$Fold\ enrichment = \frac{\%IP_{sample}}{\sqrt{\%IP_{M40} \times \%IP_{act1}}}$$

4.8.3.3. RT-qPCR analysis

Data from qPCR were processed according to following equation, where all C_P values are averages of given triplicates; E represents efficiency of specific pair of primers, WT_0 marks values measured in untreated wild type cells. Resulting values express fold expression change compared to untreated wild type.

$$Fold\ expression = \frac{\sqrt{E^{Cp_{act1}} \times E^{Cp_{rho1}}}}{E^{Cp}} \times \frac{E^{Cp} WT_0}{\sqrt{E^{Cp_{act1}} \times E^{Cp_{rho1}}}}$$

Besides NTC, NRT control (see protocol 4.7.9.) has been also measured to establish relative quantity of contaminating DNA that was not degraded during RNA purification by DNase I and that might artificially increase qPCR signal (C_P values). Therefore, C_P values of NRT control should be at least 10 cycles greater than C_P values of analyzed samples.

4.9. Protein manipulation techniques

4.9.1. Preparation of native lysates

All procedures were performed on ice. 20 ml of liquid *S. pombe* culture (OD_{600} = 0.5) were transferred to falcon test tube (50 ml) and sedimented (1000g; 2 min; 4 °C). Supernatant was discarded, pellet resuspended in 3 ml of STOP buffer and sedimented (1000g; 2 min; 4 °C), resuspended in 1 ml of STOP buffer, transferred to the clean micro test tube, and sedimented again (1000g; 2 min; 4 °C). Supernatant was subsequently discarded and pellet frozen at -80 °C.

Approximately one third of the 2 ml screw-cap micro test tube was filled with chilled HCl-washed glass beads. Pelleted cells were resuspended in 200 µl of NP-40 buffer supplemented with appropriate volume of 100× concentrated FY protease inhibitors (Serva) and phosphatase inhibitor cocktail 2 and 3 (Sigma) and transferred to the screw-cap test tubes with beads. More beads were added if the original quantity floated in cell suspension – small part of the beads should stay dry. Cells were subsequently lysed in

FastPrep®-24 (M. P. Biomedicals) (60 s; 6.5 m/s). A hole was poked with a hot needle in the bottom and cap of the 2 ml screw-cap micro test tube that was immediately placed to the clean 1.5 ml micro test tube without a cap. These two test tubes were placed to the falcon test tube (50 ml) and the lysate was spun out of the beads (1000 g; 1 min; 4 °C). Lysate was subsequently transferred to clean micro test tube, centrifuged (20 000g; 10 min; 4 °C), and supernatant was collected to the clean micro test tube and stored in -80 °C if needed.

Buffers and solutions:

STOP buffer: 150mM NaCl; 50mM NaF; 25mM HEPES; 1.5mM NaN_3; pH = 8

NP-40 buffer: 6mM Na_2HPO_4, 4mM $NaH_2PO_4 \bullet H_2O$, 1% NONIDET P-40, 150mM NaCl, 2mM EDTA, 50mM NaF

4.9.2. Protein purification with trichloroacetic acid (TCA)

This protocol has been taken from [137, 138] and modified. Cells were cultivated (32 °C; 180 rpm) to OD_{600} = 0.5 and 20 ml of culture were collected before or after the treatment. Cells were sedimented (1000 g; 2 min; 4 °C), supernatant discarded, and pellet was resuspended in 3 ml of STOP buffer (see 4.9.1). Cells were sedimented again (1000 g; 2 min; 4 °C), resuspended in 1 ml of STOP buffer, transferred to the clean micro test tube, and sedimented (1000 g; 2 min; 4 °C). Supernatant was subsequently discarded, sediment resuspended in 50 µl of 10% TCA, and stored at -80 °C.

Approximately one third of the 2 ml screw-cap micro test tube was filled with chilled HCl-washed glass beads. Frozen pellets were melted by adding 150 µl of cold 12.5% TCA and transferred to the screw-cap micro test tube (2 ml). Cells were lysed in FastPrep®-24 (M. P. Biomedicals) (60 s; 6.5 m/s). A hole was poked with a hot needle in the bottom and cap of the 2 ml screw-cap micro test tube that was immediately placed to the clean 1.5 ml micro test tube without a cap. These two test tubes were placed to the falcon test tube (50 ml) and the lysate was spun out of the beads (1000 g; 1 min; 4 °C). Lysate was transferred to the clean micro test tube and centrifuged (20 000 g; 10 min; 4 °C). Sediment was collected and processed according to section 4.9.3.

4.9.3. Cysteine modification with iodoacetamide (IAA)

This protocol has been taken from [137, 138] and modified. Protein fraction precipitated with TCA (see 4.9.2.) was washed with 100 µl of acetone and air-dried (acetone was completely removed). Precipitate was subsequently dissolved in 300 µl of fresh IAA solution and incubated in 25 °C for 15 min. Cellular debris was sedimented (20 000 g; 10 min; 4 °C) and supernatant was transferred to the centrifuge filter Ultracell® YM-10 (Microcon®) and centrifuged (14 000 g; 40 min; 4 °C). 200 µl of dialysis solution was added to column and centrifuged (14 000 g; 20 min; 4 °C). Filter was washed with 200 µl of dialysis buffer again and centrifuged (14 000 g; 40 min; 4 °C). Filter was placed to the clean test tube upside down and proteins were spun out of the filter (14 000 g; 2 min; 4 °C). Protein concentration was subsequently established according to protocol 4.9.4.

Buffers and solutions:

IAA solution	0.75mM iodoacetamide; 1% SDS; 100mM TRIS-HCl (pH = 8); 1mM EDTA; FY protease inhibitors (Serva)
Dialysis buffer	10mM TRIS-HCl (pH = 8); 50mM NaCl; 10mM $MgCl_2$

4.9.4. DC™ Protein Assay

Protein content was measured in cell lysates using DC™ Protein Assay (Bio-Rad). Adequate amount of reagent A was combined with reagent S (20 µl of reagent S per 1 ml of reagent A). Bovine serum albumin (BSA) (2 mg/ml; Bio-Rad) was diluted according to Table 20 and used as protein concentration standard.

Samples were measured in triplicates. For each reaction 20 µl of reagent mixture A+S were transferred to clear 96-well plate. Cell lysates were 20× diluted (1 µl of lysate combined with 19 µl of NP-40 buffer) and 5 µl of diluted samples or protein standards were added to the wells with reagents A and S. These wells were subsequently filled with 200 µl of reagent B. Whole 96-well plate was incubated for 15 minutes in the dark and the absorbance of samples at 750 nm was measured using Varioskan™ Flash (Thermo Fisher).

An average absorbance values were computed from all triplicates. Average absorbances of standards were plotted against their concentration and linear regression of standard curve was created. Protein concentrations of samples were calculated according to

the equation of linear regression. Cell lysates were diluted with NP-40 buffer to the unified concentration (usually to 10 μg/μl).

Table 20 – BSA protein standards for DC™ Protein Assay

Concentration	NP-40	BSA 2mg/ml
0.2 mg/ml	45 μl	5 μl
0.5 mg/ml	37.5 μl	12.5 μl
1 mg/ml	25 μl	25 μl
1.5 mg/ml	12.5 μl	37.5 μl

4.9.5. Denaturing polyacrylamide gel electrophoresis (SDS-PAGE)

Set Mini-PROTEAN® III (Bio-Rad) was used for SDS-PAGE. The device for hand casting of gels was compiled following manufacturer's orders. Separating polyacrylamide gel was prepared according to Table 21. Prepared solution was transferred between two glasses (two thirds of the area between glasses was filled), divided by 0.75 mm thick spacers, immediately after the addition of ammonium persulfate and covered with thin layer of isopropanol. Isopropanol was removed and gel was washed with distilled water several times when the process of acrylamide polymerization was finished. Residual water was carefully removed with the piece of filtrating paper (contact with gel must be avoided). The form was filled with freshly prepared stacking gel (Table 21) and a comb was placed into the form.

Gel form was put into electrophoretic chamber, poured with 1% SDS (sodium dodecyl sulfate) buffer, and the comb was removed. Protein lysates were mixed with appropriate amount of 6× concentrated Laemmli buffer (2 μl of Laemmli buffer per 10 μl of cell lysate), denatured in 95 °C for 10 min and cooled on ice. The volume of cell lysate containing 100 μg of proteins and 5 μl of PageRuler™ Plus Prestained Protein Ladder (Thermo Scientific) as a marker of protein molecular weight were loaded to the gel using Hamilton syringe. Proteins were subsequently separated by electrophoresis (20 mA per gel).

Table 21 – Polyacrylamide gel composition

Reagent	10% separating gel	Stacking gel
AA/BIS	1.67 ml	325 µl
4× TRIS-HCl/SDS; pH = 8.8	1.25 ml	-
4× TRIS-HCl/SDS; pH = 6.8	-	625 µl
Deionized H_2O	2.08 ml	1.55 ml
TEMED	3.4 µl	2.5 µl
10% Amonium persulfate	16.5 µl	12.5 µl

Buffers and solutions:

AA/BIS	30% acrylamide (Sigma); 0.8% N,N´-methylenbisacrylamide; sterilized by filtration (syringe filters PES 0.2 µl; Fisher Scientific)
4× TRIS-HCl/SDS; pH = 8.8	1.5M TRIS; 0.4% SDS; pH = 8.8 (HCl); sterilized by filtration (syringe filters PES 0.2 µl; Fisher Scientific)
4× TRIS-HCl/SDS; pH = 6.8	1.5M TRIS; 0.4% SDS; pH = 6.8 (HCl); sterilized by filtration (syringe filters PES 0.2 µl; Fisher Scientific)
6× Laemmli buffer (10 ml)	1.2 g SDS; 6 mg bromophenol blue; 4.7 ml glycerol; 1.2 ml 0.5M Tris (pH = 6.8); 2.1 ml deionized H_2O; 0.93 g DTT (dithiothreitol)
SDS buffer	25mM TRIS; 190mM glycine; 0.5% SDS; pH = 8.3

4.9.6. Non-reducing polyacrylamide gel electrophoresis (SDS-PAGE)

The composition and casting of polyacrylamide gel was identical to protocol 4.9.5. (SDS-PAGE) These two protocols differ only in the composition of Laemmli buffer which lacks DTT for non-reducing SDS-PAGE.

4.9.7. Western blotting

TransBlot® Turbo™ (Bio-Rad) Transfer System was used for gel-to-nitrocellulose membrane (Bio-Rad) protein transfer. Three pieces of filtration paper (Whatman, 3 mm) were stacked to a column, soaked with Towbin buffer, and put into bottom part of

TransBlot cassette. The piece of nitrocellulose membrane was moistened with Towbin buffer and placed at the top of the filtration paper stack. Polyacrylamide gel containing separated proteins was carefully removed from gel-casting device, washed in Towbin buffer, precisely put on the nitrocellulose membrane, and covered with other wet stack of three filtration papers. TransBlot cassette was inserted to TransBlot® Turbo™ Transfer System and proteins were transferred for 30 min with constant current I = 1 A. Subsequently, membrane area that should contain loading control (protein Cdc2) was cut off with lancet and all pieces of membrane were blocked in 5% milk (Bio-Rad) solution in TBST for 30 min in 37 °C.

Buffers and solutions:

Towbin buffer	25mM TRIS; 192mM glycin; 20% methanol; pH = 8.05
TBS	20mM TRIS; 500mM NaCl; pH = 7.5
TBST	20mM TRIS; 500mM NaCl; 0.05% Tween 20 (Bio-Rad) pH = 7.5

4.9.8. Immunodetection of proteins

Blocked pieces of nitrocellulose membrane were incubated in 4 °C with primary antibodies diluted in 5% milk-TBST solution according to Table 1 on the rocker overnight. Membranes were three times washed for 10 min in cold TBST and subsequently incubated with proper dilution of secondary antibodies (Table 1) conjugated with HRP (horseradish peroxidase) for 60 min in room temperature. Then the antibody solutions were removed and membranes were washed two times in TBST for 10 min and subsequently washed 10 min in TBS.

Proper volumes (0.5 ml per membrane) of both Amersham ECL Prime Western Blotting Detection Reagent (GE Healthcare Life Sciences) components were tempered to room temperature 20 min before the application. These two components were mixed together and applied on the membrane. After 1 min of incubation, membranes were put between two pieces of transparent foil and chemiluminiscence signal was detected with CCD camera LAS 4000 (Fujifilm) and ImageQuant™ software.

4.10. Chromatin immunoprecipitation

4.10.1. Fixation of cells

50 ml of liquid *S. pombe* culture (OD_{600} = 0.5) were poured to the falcon test tube (50 ml). 1.35 ml of 37% formaldehyde (Sigma Aldrich) was added and cells were incubated in room temperature shaking. After 30 min of incubation, 2.5 ml of 2.5M glycine was added to the fixed cell culture. 10 min-long incubation in room temperature followed.

Cells were spun (1000 g; 3 min; 20 °C), washed with 40 ml of deionized water, and spun again. Resulting pellet was resuspended in 1 ml of deionized water, transferred to the clean micro test tube and centrifuged (1000 g; 3 min; 20 °C). Sediment was frozen and stored in -80 °C.

4.10.2. Chromatin preparation

All following procedures were performed on ice. LB buffer has been prepared first. Needed volume (1.4 ml per sample) of LB buffer was mixed with one hundredth of 100× concentrated FY protease inhibitors (Serva). Sediment of fixed cells was resuspended in 370 µl of ice-cold LB buffer (with protease inhibitors).

2 ml screw-cap micro test tubes were filled with ~600 µl of chilled HCl-washed glass beads. Resuspended cells were transferred to the glass beads and lysed in FastPrep®-24 (M. P. Biomedicals) - 3× 13 s at speed 5.5 with 5 min incubations on ice in between. The breaking efficiency after three cycles should be ~70 % (verified by microscopy). The bottom and the cap of test tubes containing lysed cells and glass beads were penetrated with hot needle and these tubes were put into clean 1.5 ml micro test tubes with removed cap. These systems of two test tubes were put into falcon test tubes (50 ml) and lysate was spun out of the beads (1000 g; 1 min; 4 °C). Beads were subsequently washed with 100 µl of LB buffer (containing FY protease inhibitors) and spun again (1000g; 1 min; 4 °C). Cell lysates were transferred to the clean micro test tubes and centrifuged (20 000g; 10 min; 4 °C). Sediment was resuspended in 600 µl of LB buffer (containing FY protease inhibitors), centrifuged again (20 000g; 10 min; 4 °C), and resulting pellet was resuspended in 270 µl of LB buffer (containing FY protease inhibitors).

Cell lysates were sonicated with sonicator Bioruptor® (Diagenode) at high intensity (20 cycles comprised of 30 s long sonicating phase and 30 s long resting phase) generating ~500 bp long DNA fragments. Sonicated samples were spun (20 000 g; 10 min; 4 °C) and supernatant was collected to clean micro test tubes.

Protein content was determined with spectrophotometer NanoDrop 2000 (Thermo Scientific), measuring the absorbance of sample at 280 nm and appropriate volume of LB buffer (with FY protease inhibitors) was added to each sample to bring the protein concentration to the same level. 30 µl of chromatin solution were withdrew and stored in -80 °C for further analysis as an immunoprecipitation input. Approximately 170 µl of residual chromatin solution (~80 µg/µl) were subjected to immunoprecipitation.

Buffers and solutions:

LB buffer 50mM HEPES (pH = 7.6); 1mM EDTA (pH = 8); 150mM NaCl; 1% Triton X-100; 0.1% Na-Doc

4.10.3. Chromatin immunoprecipitation of TAP-tagged proteins

30 µl of IgG coated magnetic beads (Pan Mouse IgG coated Dynabeads® Life Technologies; catalog number: 11041) were two times washed with block solution (1 ml of cold LB buffer containing 0.5 mg/ml BSA) using magnetic stand. 170 µl of chromatin solution were added to blocked magnetic beads and gently mixed in rotating wheel overnight in 4 °C.

4.10.4. Chromatin immunoprecipitation of Pk-tagged proteins

5 µl (1 µg/µl) of Mouse anti V5 antibody (Serotec) were added to ~170 µl of sonicated chromatin solution and incubated at 4 °C in rotating wheel for 4 hours. Incubated samples were mixed with 30 µl of magnetic beads coated with protein A (Dynabeads® Novex® Life Technologies; catalog number: 100.02d) that were two times washed with block solution (1 ml of cold LB buffer containing 0.5 mg/ml BSA) using magnetic stand. Chromatin solution was subsequently incubated at 4 °C in rotating wheel overnight.

4.10.5. DNA purification with Chelex®-100

Beads were collected using magnetic stand and washed six times with 1 ml of ice-cold IP buffer. IP buffer was completely removed and 100 µl of 10% Chelex®-100

(Bio-Rad) were added to all beads and inputs (prepared according to 4.10.2.). Samples were 10 s vortexed and boiled in 95 °C for 10 min. Samples were slowly cooled down and mixed with 1 µl of Proteinase K (20mg/ml; Roche), vortexed, and incubated for 30 min in 55 °C, shaking (1000 rpm). Proteinase K was inactivated by 10 min of incubation in 95 °C. Samples were centrifuged (12 000 g; 1 min; 4 °C) and top 80 µl were transferred to the clean micro test tube. Sediment was washed with 120 µl of deionized water, centrifuged again (12 000 g; 1 min; 4 °C), and top 120 µl of supernatant were withdrew and pooled with previously taken 80 µl.

DNA concentration was established by measuring the absorbance at 260 nm using spectrophotometer NanoDrop 2000 (Thermo Scientific). Proper amount of deionized water was added to each sample to bring the concentration of all samples to 4.5 ng per µl.

Buffers and solutions:

IP buffer 50mM TRIS (pH = 7.5); 1% Triton X-100; 150mM NaCl; 5mM EDTA; 0.5% NP-40

4.11. β-galactosidase activity assay

Cells were inoculated to 10 ml of defined minimal medium EMM without leucine and cultivated (32 °C; 180 rpm) overnight. Cell culture was subsequently diluted to OD_{600} = 0.05 (10 ml) and growth accurately to OD_{600} = 0.5.

8 ml (total biomass equals 4OD) of cell culture were transferred to falcon test tube (15 ml), spun (1000 g; 2 min; 20 °C), sediment was washed with 5 ml of Z buffer and spun again (1000 g; 2 min; 20 °C). Sediment was resuspended in 1 ml of Z buffer and mixed with 3.4 µl of mercaptoethanol (1 µl per 300 µl of cell suspension). Falcon test tube was put on ice and 250 µl of HCl-washed chilled glass beads were transferred to screw-cap micro test tube (2 ml) and topped with 300 µl of the cell suspension. Cells were lysed using FastPrep®-24 (M. P. Biomedicals) set to 3× 20 s at speed 5.5. Samples were cooled on ice between each lysis cycle. Cell lysates were mixed with 300 µl of cold Z buffer, vortexed and protein concentration was established by measuring samples absorbance at 280 nm using spectrophotometer NanoDrop 2000 (Thermo Scientific). Proper volume of Z buffer was added to each sample to bring its protein concentration to 0.4 µg/µl.

Then, 250 µl of cell lysate (protein concentration 0.4 µg/µl), 350 µl of cold Z buffer, and 80 µl of ONPG (o-nitrophenyl-D-galactopyranoside; Sigma) solution (4 mg/ml) in Z buffer were transferred to clean micro test tube (1.5 ml). This mixture was incubated in 30 °C for 15 min shaking (900 rpm). Reaction was stopped immediately after the incubation by addition of 250 µl of 1M Na_2CO_3. Sample was vortexed, briefly centrifuged, and its absorbance at 420 nm was measured using spectrophotometer NanoDrop 2000 (Thermo Scientific)

Buffers and solutions:

Z buffer 60mM $Na_2HPO_4.12H_2O$; 40mM $NaH_2PO_4.2H_2O$; 10mM KCl; 900µM $MgSO_4.7H_2O$; pH = 7

5. RESULTS

5.1. Cbf11 but not Cbf12 is indirect repressor of several stress responsive genes

Unpublished preliminary experiments performed by Dr. Převorovský found that *cbf11Δ* cells are resistant to H_2O_2 compared to wild type (Fig. 6). Consistently with previous observation, subsequent microarray analyses shown augmented expression of antioxidants catalase *ctt1*, glutathione-S-transferase II *gst2*, transcription factor *atf1*, and phosphatase *pyp2* (Fig. 7). The two last mentioned are important regulators of cellular stress responses [2]. Moreover, ChIP-seq (Chromatin Immunoprecipitation-sequencing) data provided by Dr. Převorovský (Fig. 8) showed potential but weak Cbf11 binding to the promoter regions of *ctt1*, *gst2*, *pyp2* and *atf1* (see Materials and Methods for binding sites coordinates). Different analysis of the fission yeast transcriptome revealed increasing expression of *cbf12* during oxidative stress [42]. Thus, several lines of evidence suggest CSL transcription factors might regulate the oxidative stress response in *S. pombe*. On the basis of our expression profiling and ChIP-seq data, *ctt1*, *gst2*, *atf1*, *pyp2*, *cbf11* and *cbf12* genes were selected for more detail transcription analysis using RT-qPCR (Reverse Transcription-quantitative Polymerase Chain Reaction). Genes for actin *act1* and small GTPase *rho1* were chosen as references, because their expression is unchanged during oxidative stress [42].

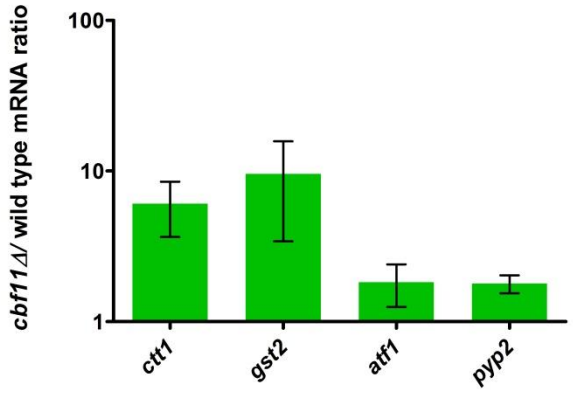

Fig. 7 – The expression microarray results showing upregulation of *ctt1*, *gst2*, *atf1*, and *pyp2* in *cbf11Δ* cells. The genome-wide expression analysis was performed by Dr. Převorovský. Columns represent mean of ratios of transcript level of studied genes in *cbf11Δ* cells and wild type. SD is represented by error bars.

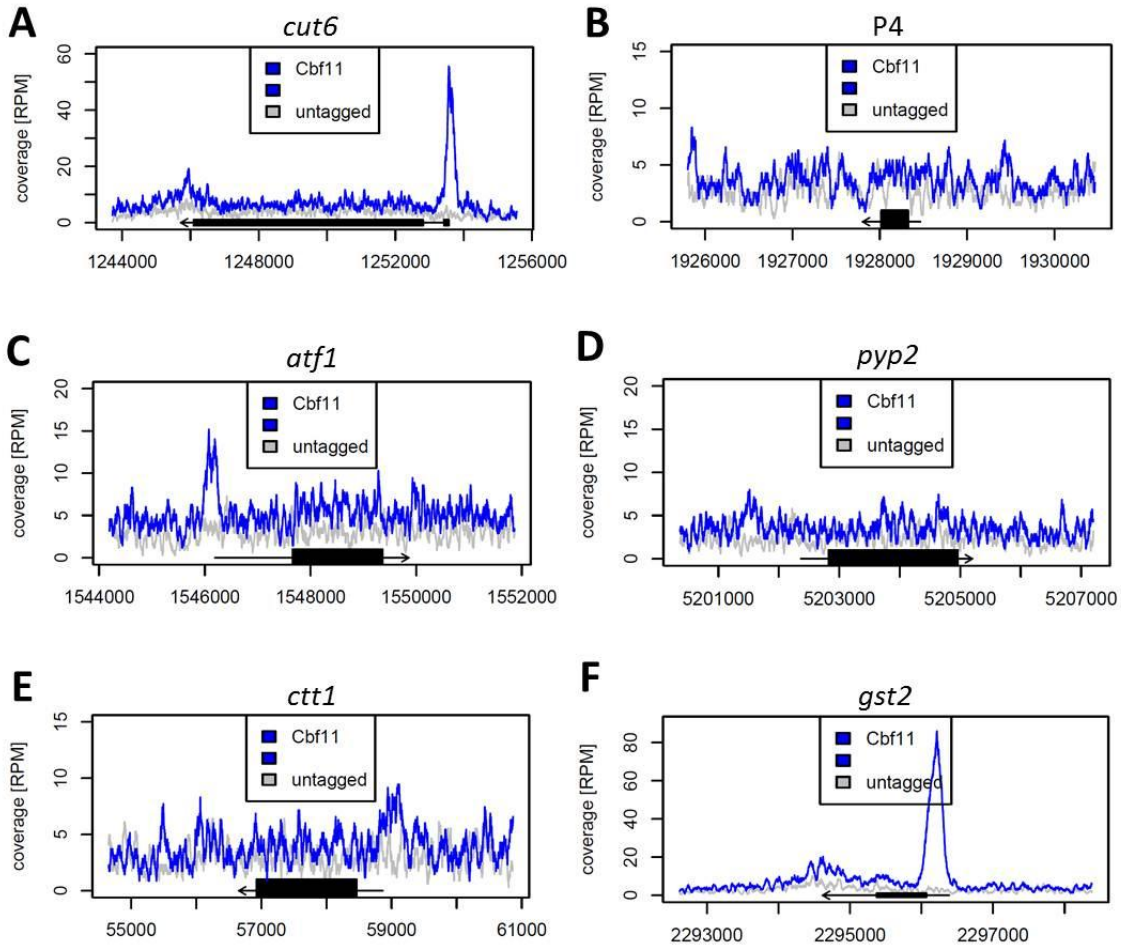

Fig. 8 – The enrichment of Cbf11 protein in the promoters of relevant genes during S-phase/cytokinesis in *cbf11-ctap* cells. Dr. Převorovský designed, performed, and analyzed ChIP-seq and created displayed graphs. An intensity of unspecific background signal obtained from cells lacking TAP-tagged Cbf11 (TAP tag was used for immunoprecipitation) is determined by the grey curve, while the blue one represents Cbf11 enrichment at target sequences. ORFs (Open Reading Frames) are marked with thick black rectangle, untranslated regions with thin black line, and arrows show the orientation of the gene. The Cbf11 was significantly enriched in the promoter of *cut6* (**A**), gene whose absence causes so called cut phenotype which has been observed also in *cbf11Δ* cells [126], suggesting functional connection of *cbf11* and *cut6*. In contrast, no Cbf11 binding was detected in intergenic locus P4 (**B**). These two promoters were depicted in this figure to illustrate differences between expressive and poor Cbf11 enrichment, which should contribute to the better analysis of figures **C-F**.

5.1.1. Gene expression analysis in CSL mutants

5.1.1.1. Validation of primers for qPCR

Suitable primers for amplification of *ctt1*, *pyp2* and *rho1* ORFs (Open Reading Frames) were not present in our laboratory and had to be designed for this project. The PCR using *S. pombe* genomic DNA (gDNA) as a template followed by agarose gel electrophoresis confirmed that PCR reactions with tested primers give products. Position of amplified DNA in each reaction corresponded with expected amplicon sizes (120 bp for *ctt1*, 93 bp for *pyp2* and 102 bp for *rho1*) (Fig. 9). Despite of weak signal in no-template control for *pyp2*-specific pair of primers, other analyses convincingly confirmed their functional specificity (Fig. 10). The observed signal might be therefore a result of cross-contamination of samples during agarose gel loading.

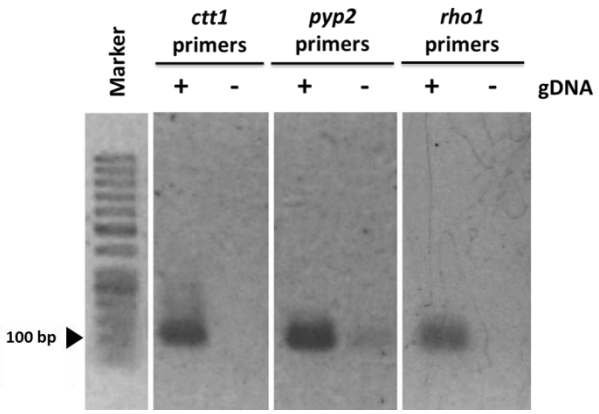

Fig. 9 – PCR validation of primers designed for amplification of *ctt1*, *pyp2* and *rho1* ORFs. Designed primers were examined whether they could produce an amplicon of predicted size in PCR reaction with a gDNA as a template. The PCR program and reaction mixture composition are described in Materials and Methods in detail. Products of PCR amplification were mixed with 6x LD buffer, loaded to 2% agarose gel and separated by electrophoresis. GeneRuler 50 bp DNA Ladder (Thermo Scientific) was used as a marker of DNA fragment size.

Number of products that each pair of primers produces from gDNA during PCR and efficiency of cDNA amplification was determined by qPCR. Melting analysis revealed that there was only one product (additional products typically generate extra melting peaks) in each performed qPCR reaction (Fig. 10). Hence, designed primers are thought to be specific for target sequences. Then, dilution series of cDNA were used as a template for qPCR reaction. Obtained C_P values were plotted against cDNA concentration and the

efficiency of each pair of primers was calculated from the slope of linear part of the standard curve (Fig. 11).

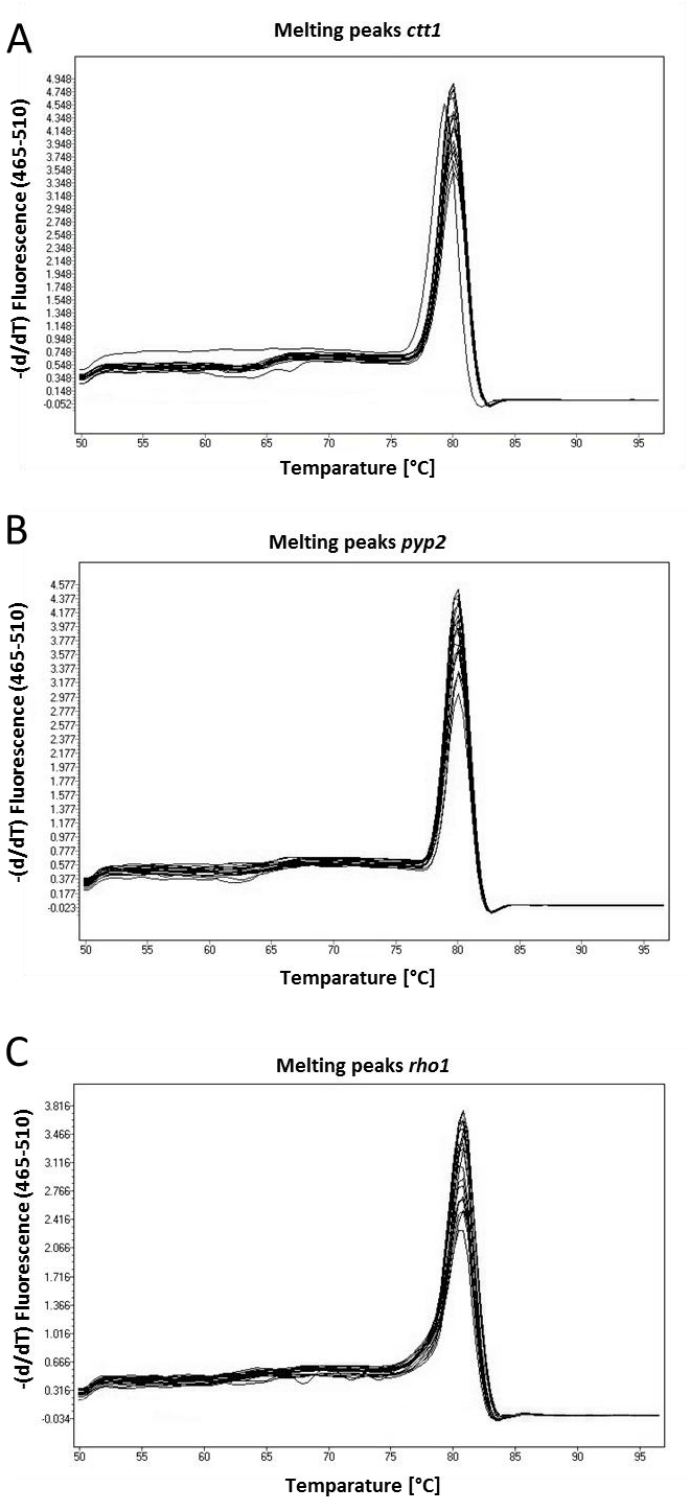

Fig. 10 – Melting analysis of qPCR products. Diagrams show melting peaks of qPCR products of PCR reactions containing primers designed for annealing into ORFs of **A**: *ctt1*, **B**: *pyp2*, and **C**: *rho1*. Only one clear peak was detected in each reaction containing given pair of primers, suggesting that only one product has been amplified in these PCR reactions.

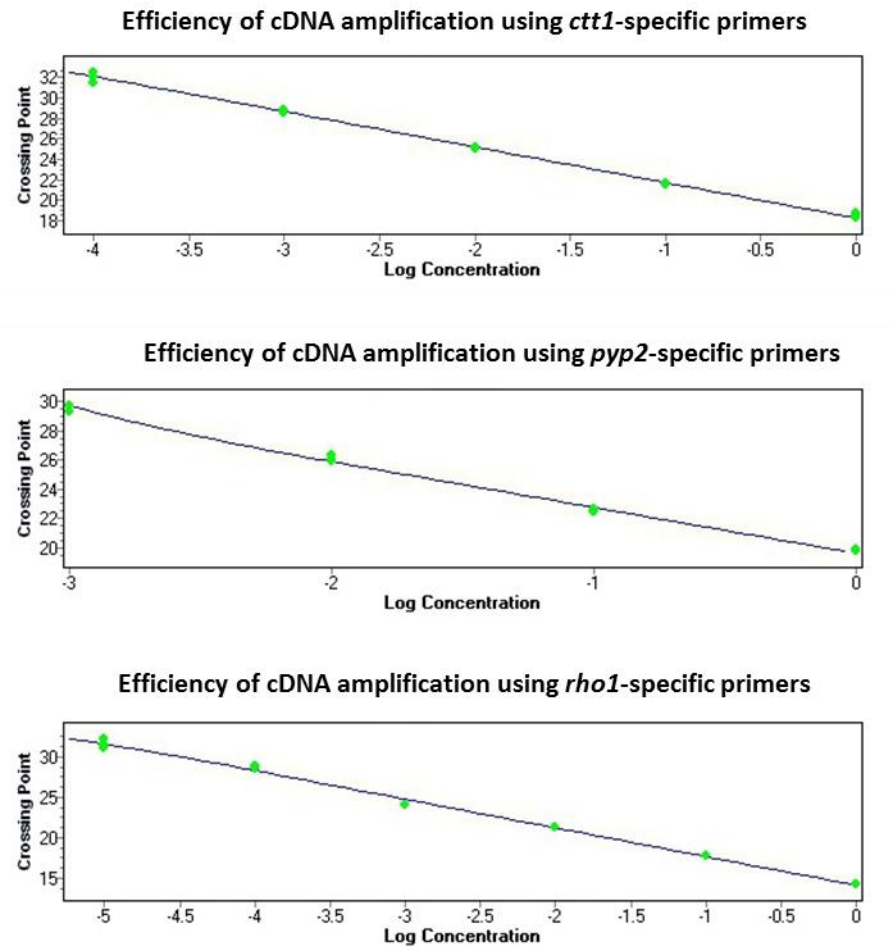

Fig. 11 – Efficiency of cDNA amplification with different pairs of primers. The y axis represents C_P value (crossing point) and x axis represents the relative concentration of cDNA. Efficiency of cDNA amplification for each pair of primers was established from the standard curve slope.

5.1.1.2. The expression of stress-responsive genes in *cbf11Δ* and *cbf12Δ* cells

To decipher the role of each CSL paralog in response to oxidative stress in fission yeast, transcripts of *ctt1*, *gst2*, *pyp2*, *atf1*, *cbf11* and *cbf12* were quantified by RT-qPCR in wild type, *cbf11Δ* and *cbf12Δ* cells in accordance with the scheme depicted in Fig. 12.

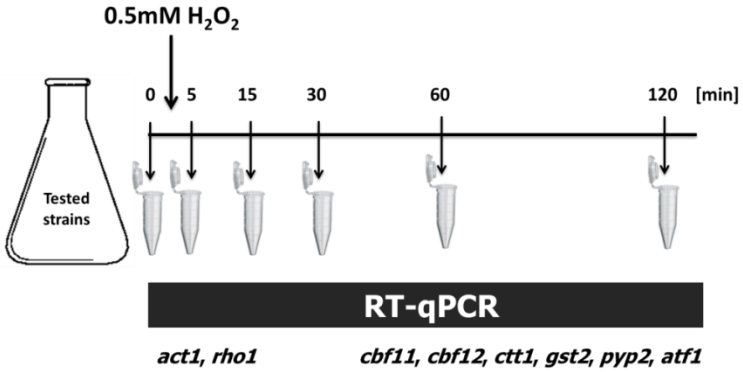

Fig. 12 – The experimental design of gene expression analysis. Cells were grown in complete liquid YES medium to OD_{600} = 0.5 and harvested before and 5, 15, 30, 60 and 120 min after the treatment with 0.5mM hydrogen peroxide. RNA purification was followed by reverse transcription and cDNA of interest was quantified using qPCR. *act1* and *rho1* cDNAs were used as references.

Consistently with our preliminary data, important H_2O_2 scavenger – *ctt1* is upregulated in unstressed *cbf11Δ* cells compared to wild type. Amount of *ctt1* transcript in *cbf11Δ* strain is further augmented by hydrogen peroxide and its expression culminates 30 min upon the treatment (Fig. 13A). Similar but less robust pattern was observed in the expression of *pyp2* and *atf1* (Fig. 13C, D), genes whose products are involved in MAPK stress signaling [2]. It might be hard to distinguish whether *pyp2* and *atf1* genes are really upregulated before and 5, 15, and 30 min after the H_2O_2 treatment from Fig. 13C, D, however, the statistical analysis (paired two sample t-test) confirmed that the level of *pyp2* and *atf1* mRNA is significantly increased ($p < 0.05$) in this particular time points in *cbf11Δ* strain compared to wildtype. Interestingly, the level of *gst2* transcript is exceedingly increased in *cbf11Δ* cells compared to wild type. The level of mRNA *gst2* is ~80-fold higher in *cbf11* knock-out cells compared to wild type and does not dramatically change after H_2O_2 treatment (Fig. 13B). Enhanced expression of *cbf12* was detected in stressed and unstressed *cbf11Δ* cells (Fig. 13E) but deletion of *cbf12* did not change the expression of cbf11 at all (Fig. 13F). The pattern of *cbf12* expression in Fig. 13E is similar in either wild type or *cbf11Δ* cells but relative amount of transcript is ~4-fold enriched in *cbf11* mutants before and after the stress induction. Previous study described functional antagonism between paralogs Cbf11 and Cbf12 [126]. Derepression of *cbf12* in *cbf11Δ* cells (Fig. 13E) further supports this idea. On the other hand, *cbf12* does not seem to affect expression of investigated genes in physiological concentration as deletion of *cbf12* has only negligible effect on expression of *ctt1*, *gst2*, *pyp2*, *atf1*, and *cbf11*, if any (Fig. 13).

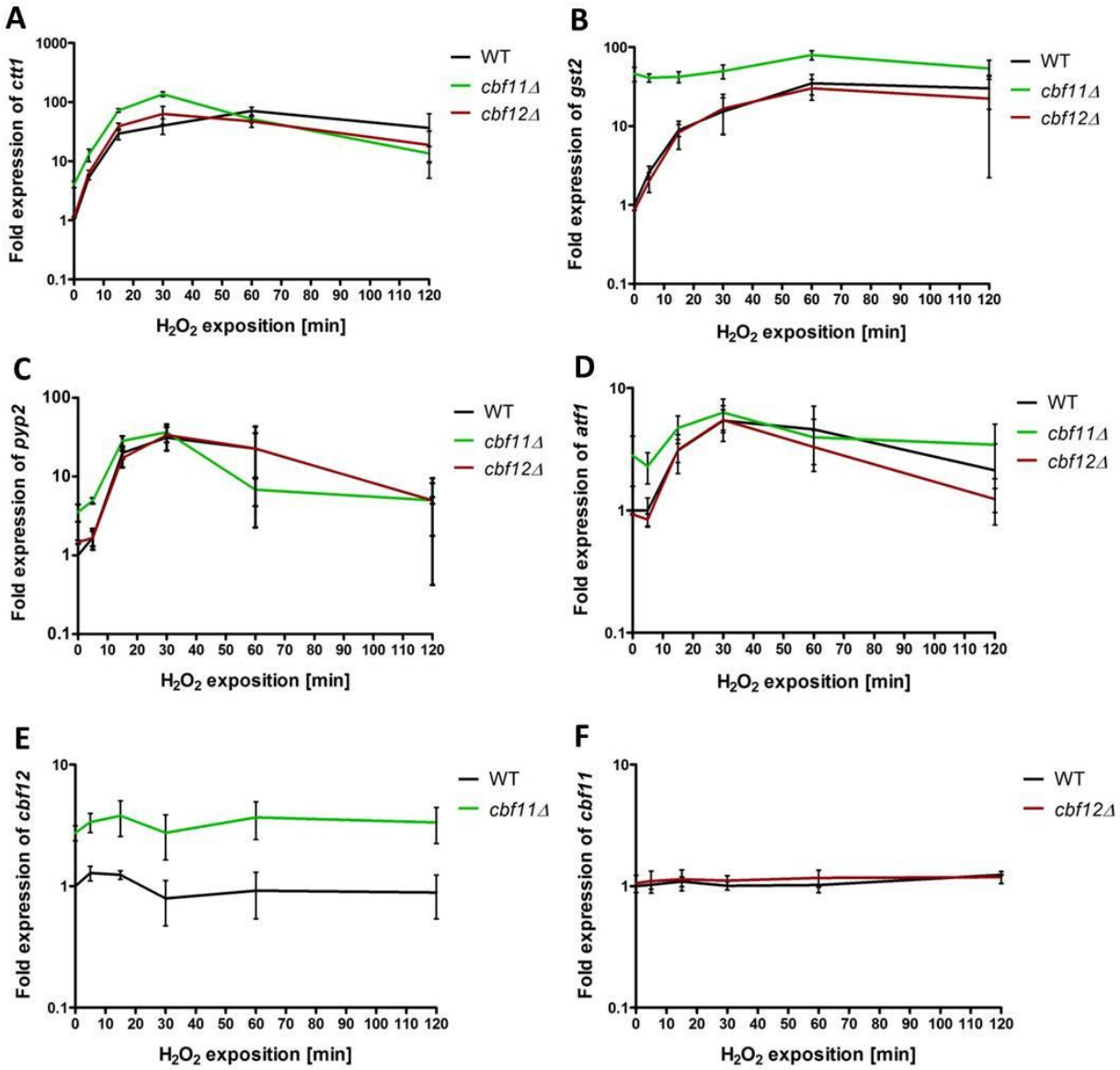

Fig. 13 – Gene expression analysis by RT-qPCR of *cbf11Δ* and *cbf12Δ* cells during oxidative stress. Wild type, *cbf11Δ* and *cbf12Δ* cells were treated with 0.5mM H_2O_2, processed according to scheme in Fig. 4, and relative levels of *ctt1* (**A**), *gst2* (**B**), *pyp2* (**C**), *atf1* (**D**), *cbf11*(**E**), and *cbf12* (**D**) transcripts were quantified. Data were normalized to *act1* and *rho1* transcript levels and to target gene transcript level in untreated wild type cells. Each curve represents mean of three independent experiments. Error bars represent standard deviation (SD). No-template control was negative.

These data suggest that Cbf11 represses oxidative stress responsive genes *ctt1*, *gst2*, *pyp2*, and *atf1*. Consistently, deletion of *cbf11* results in derepression of these genes in both stress and non-stress conditions. The function of transcription factor Cbf12 in

regulating *ctt1, gst2, pyp2*, and *atf1* genes at transcriptional/post-transcriptional level is not likely.

5.1.2. Analysis of Cbf11 binding into promoters of *ctt1, gst2, pyp2*, and *atf1*

Previous results showed that Cbf11 is involved in the regulation of stress responsive genes *ctt1*, *gst2*, *pyp2*, and *atf1*. To investigate, whether observed Cbf11-dependent gene repression is caused by direct binding of transcription factor Cbf11 to target genes promoters, the chromatin immunoprecipitation has been performed. Cells producing Cbf11 with C-terminal TAP (Tandem Affinity Purification) tag, were collected before (time 0) and 30 min after the treatment with 0.5mM hydrogen peroxide, lysed and lysates were immunoprecipitated with IgG coated magnetic beads. TAP tag contains IgG binding domains of *Staphylococcus aureus* protein A that allows tagged protein (Cbf11) to create immunocomplex with antibody-covered beads. Primers specific for promoter regions of *gst2* and *atf1* were already present in our lab, but primers for amplification of promoter regions of *ctt1* and *pyp2* had to be designed.

5.1.2.1. Validation of primers for amplification of *ctt1* and *pyp2* promoters

Primers for amplification of *ctt1* and *pyp2* promoters were designed to positions where Dr. Převorovský detected weak, potential binding of CSL transcription factors with ChIP-seq. (Fig. 8) Designed primers were examined by PCR with gDNA as a template and PCR products were analyzed by agarose gel electrophoresis. Both PCR reactions containing relevant pair of primers gave a product of expected size (141 bp for *ctt1* and 99 bp for *pyp2* promoters), while no signal was detected in NTC (Fig. 14A). Subsequent qPCR melting analysis confirmed specificity of designed primers. There is only one remarkable peak in either Fig. 14B or 14C suggesting there is only one product in each qPCR reaction. Dilution series of gDNA were amplified and resulting C_P values were plotted against gDNA concentration, creating a standard curve whose slope was used for calculation of efficiency of qPCR containing given pair of primers. Thus, primers for amplification of promoter regions of *ctt1* and *pyp2* genes are specific, selective and suitable for ChIP evaluation.

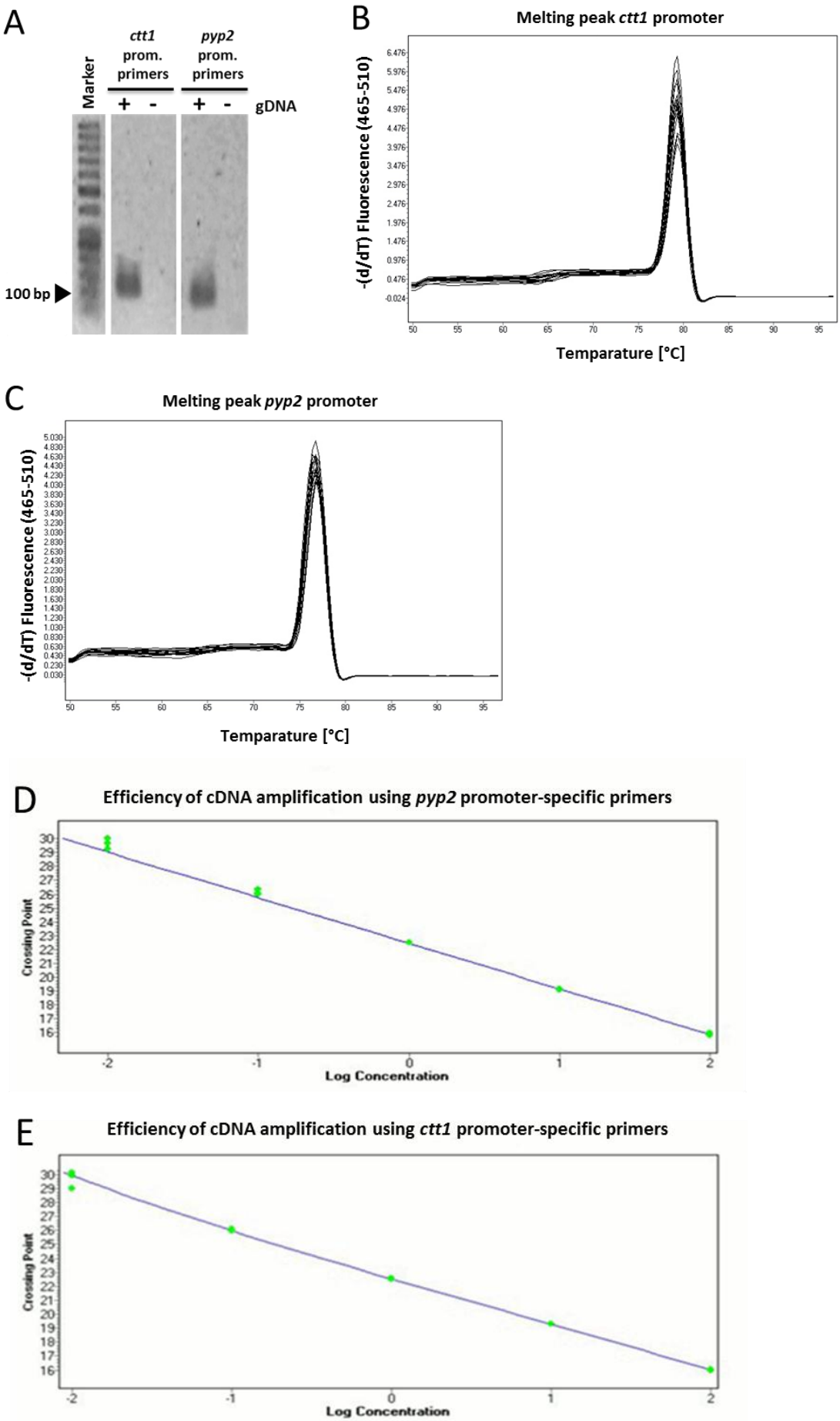
A
ctt1 prom. primers
pyp2 prom. primers
Marker
+ - + -
gDNA
100 bp
B
Melting peak ctt1 promoter
-(d/dT) Fluorescence (465-510)
Temparature [°C]
C
Melting peak pyp2 promoter
-(d/dT) Fluorescence (465-510)
Temparature [°C]
D
Efficiency of cDNA amplification using pyp2 promoter-specific primers
Crossing Point
Log Concentration
E
Efficiency of cDNA amplification using ctt1 promoter-specific primers
Crossing Point
Log Concentration

Fig. 14 - Validation of primers designed for amplification of putative Cbf11 binding sites in *ctt1* and *pyp2* promoter regions. (**A**) Primers were examined whether PCR that contains them could produce an amplicon of predicted size with a gDNA as a template. The PCR program and reaction mixture composition are described in Materials and Methods in detail. GeneRuler 50 bp DNA Ladder (Thermo Scientific) was used as a marker of nucleic acid size. (**B, C)** Diagrams show melting peaks of products of qPCR reactions containing primers designed for annealing into promoters of *ctt1* (**B**) and *pyp2* (**C**). The y axis of standard curves (**D**, **E**) represents C_P value and x axis represents the relative concentration of template. Efficiency of gDNA amplification for each pair of primers was established from the slope of depicted standard curves.

5.1.2.2. Cbf11 is not enriched in promoters of *ctt1*, *gst2*, *pyp2*, and *atf1*

Previous results indicate Cbf11 is a negative regulator of *ctt1*, *gst2*, *pyp2*, and *atf1* genes. Thus, it has been expected that this transcription factor might be bound to the promoter regions of regulated genes, avoiding their activation in normal conditions. This model also assumed that Cbf11 dissociates from target promoters after the induction of oxidative stress, enabling proper activation of stress-responsive genes in this manner. However, chromatin immunoprecipitation results (Fig. 15) show that Cbf11 binding to the promoters of *atf1* and *gst2* is undistinguishable (confirmed by paired two sample t-test; $p > 0.1$) from the negative control (P4 locus, where no Cbf11-TAP binding was detected with ChIP-seq; see Fig. 8) and binding to *ctt1* and *pyp2* promoters is even significantly lower (two sample t-test; $p < 0.05$) than binding to P4 locus. Additionally, the treatment with 0.5mM H_2O_2 causes no significant changes in Cbf11-TAP binding to *atf1*, *gst2*, *ctt1*, and *pyp2* promoters (two sample t-test; $p > 0.05$). Interestingly, the ability of Cbf11 to bind *cut6* promoter (positive control) seems to be affected during oxidative stress. Thus, Cbf11 likely repress *ctt1*, *gst2*, *atf1* and *pyp2* indirectly. One of the possible mechanisms how Cbf11 can decrease transcript level of studied genes might be modulation of the oxidative stress-related signaling.

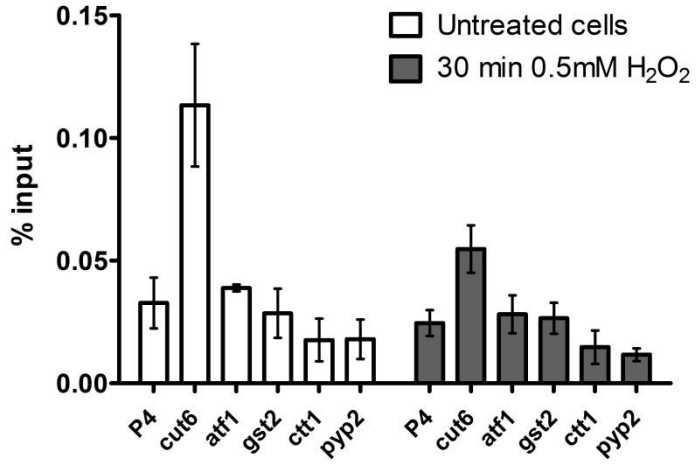

Fig. 15 – Cbf11 binding to promoter regions of investigated genes in normal conditions and during oxidative stress. Cells producing TAP tagged Cbf11 were harvested before and 30 min after 0.5mM hydrogen peroxide treatment and processed according to ChIP protocol (see Materials and Methods). Y axis represents % input DNA. Plotted values are means of three independent experiments and SD is signified by error bars. Promoter of *cut6* was used as a positive control and P4 locus, where no Cbf11 binding was detected, served as a negative control (see Fig. 8).

5.2. Cbf11 regulates oxidative stress response via Sty1/Atf1 pathway

Preceding data demonstrate indirect upregulation of some stress-responsive genes in *cbf11Δ* cells and their resistance to hydrogen peroxide, for which Cbf11 has been considered as their negative regulator. Since Sty1/Atf1 pathway is the major signal transducing system employed in triggering of diverse cellular responses to environmental stress [42] and expression of its components is affected in *cbf11Δ* cells (Fig. 7), the role of Sty1/Atf1 pathway in observed resistance and gene derepression has been questioned. To decipher the role MAPK signaling in *cbf11Δ* cells, mRNA levels of *ctt1*, *gst2*, *pyp2* and *atf1* has been measured by RT-qPCR (in accordance with scheme in Fig. 12) in strains with the single deletion of *sty1* or *atf1* and in double knock-out cells *sty1Δ cbf11Δ* and *atf1Δ cbf11Δ*.

5.2.1. Upregulation of *ctt1*, *gst2*, *pyp2*, and *atf1* expression in *cbf11Δ* cells is Sty1-dependent

Cells with deletion of *sty1* gene exert significantly decreased *ctt1* transcript level compared to wild type before and after the hydrogen peroxide treatment, which indicates

the importance of Sty1 in both basal and stress-induced expression of catalase. Catalase expression profile was similarly decreased in *sty1Δ* cells and double deletant *sty1Δ cbf11Δ* (Fig. 16A), suggesting that Sty1 is mandatory for *ctt1* upregulation also in *cbf11Δ* cells. Nonetheless, the hydrogen peroxide induced elevation of *ctt1* mRNA can be observed also in *sty1* deficient strains. Thus, catalase seems to be activated by multiple pathways during oxidative stress.

In contrast with *ctt1* whose mRNA levels are significantly decreased in the absence of Sty1, basal expression of *gst2* is elevated in *sty1Δ* cells but its further upregulation during oxidative stress is abrogated (Fig. 16B). This observation suggests that more pathways might be involved in *gst2* regulation, where one should be important for *gst2* regulation in normal conditions and during early phases of oxidative stress, while the second, probably Sty1, is important rather in later events. Deletion of *sty1* in *cbf11Δ* strain decreases levels of *gst2* mRNA to the level observed in *sty1Δ* cells (Fig. 16B), indicating Sty1 is important for *gst2* upregulation in *cbf11Δ* cells.

Basal level of *pyp2* transcript is unchanged in wild type, *sty1Δ*, and *sty1Δ cbf11Δ* cells. Single deletion of *cbf11*, in contrast, results in enhancement of *pyp2* mRNA level. Only slight enhancement of *pyp2* transcript level can be observed 120 min after the H_2O_2 treatment in *sty1Δ* and *sty1Δ cbf11Δ* cells (Fig. 16C). Activation of *pyp2*, therefore, seems to be Sty1-dependent in both wild type and *cbf11Δ*. Results suggest that in wild type, *pyp2* is activated only in the presence of stressor, which is not true for *cbf11Δ*.

A weak downregulation of *atf1* basal expression can be observed in *sty1Δ* cells and concentration of *atf1* is even decreasing during oxidative stress in strain with *sty1* deletion. Thus, Sty1 seems to be essential for *atf*1 expression in wild type. Cells with *cbf11* deletion exert increased level of *atf1* mRNA compared to wild type. Importantly, deletion of *sty1* in *cbf11Δ* repeals *atf1* upregulation that has been observed in *cbf11* deficient strain (Fig. 16D). These results implicate that Sty1 is important for *atf1* upregulation in *cbf11Δ* cells as well.

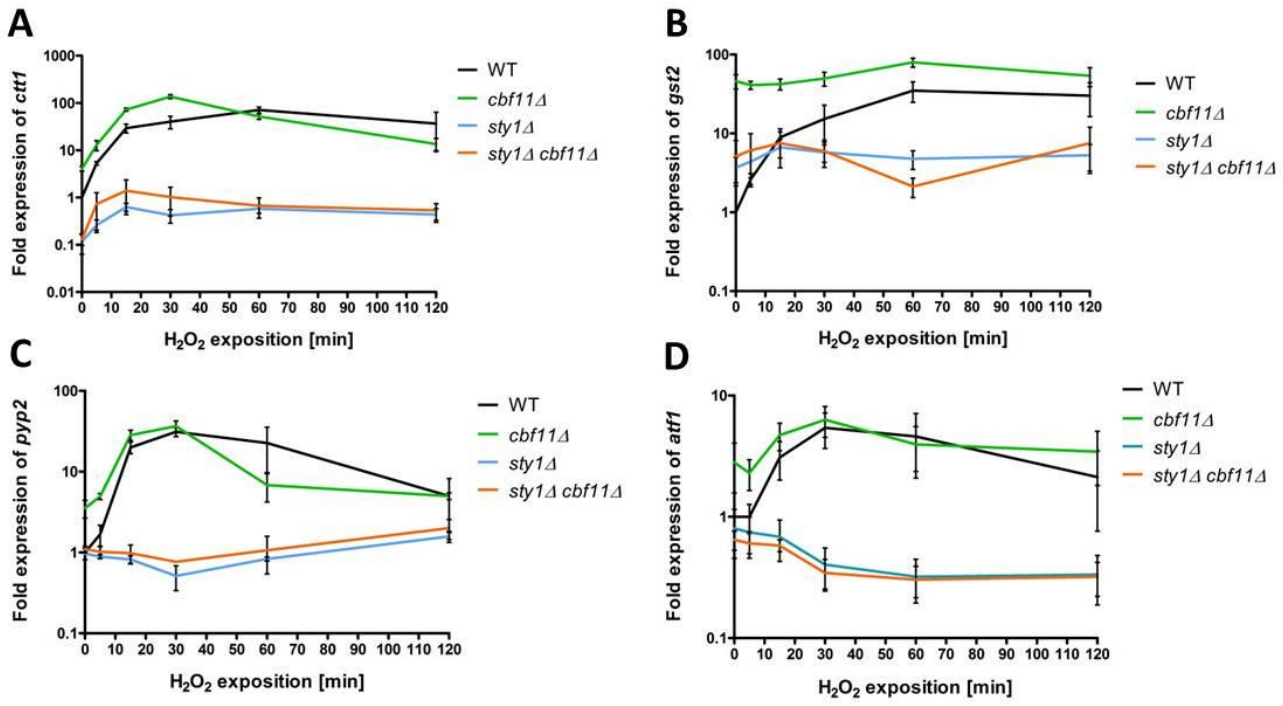

Fig. 16 – Sty1 dependent expression of *ctt1*, *gst2*, *pyp2* and *atf1* genes during oxidative stress. Wild type, *cbf11Δ*, *sty1Δ* and *sty1Δ cbf11Δ* cells were treated with 0.5mM H_2O_2, processed according to the scheme in Fig. 12 and relative levels of *ctt1* (**A**), *gst2* (**B**), *pyp2* (**C**), and *atf1* (**D**) mRNA were quantified. Data were normalized to *act1* and *rho1* transcript levels and to target gene transcript level in untreated wild type cells. Each curve represents mean of three independent experiments. Error bars represent standard deviation (SD). No-template control was negative.

5.2.2. Upregulation of *pyp2* but not *ctt1* and *gst2* is Atf1-dependent in *cbf11Δ*

Previous results revealed that upregulation of *ctt1*, *gst2*, *pyp2* and *atf1* in *cbf11Δ* cells is Sty1-dependent. To obtain more detail information about the relationship between Cbf11 and Sty1 pathway, the levels of mRNA of *ctt1*, *gst2*, and *pyp2* genes were evaluated also in *atf1Δ* and *atf1Δ cbf11Δ* strains. Interestingly, deletion of *atf1Δ* in *cbf11Δ* strain affects mRNA levels of *ctt1*, *gst2*, and *pyp2* differently, suggesting that Cbf11 is involved in multiple mechanisms that regulate these genes (Fig. 17). Atf1 has been identified as a positive regulator of catalase and Atf1 deficient cells are, additionally, sensitive to various stresses [42, 89, 94, 140]. Consistently with this observation, *atf1Δ* cells exert significantly decreased level of catalase mRNA before and after hydrogen peroxide treatment (Fig 17A). Despite this well described phenomenon, hydrogen peroxide treatment can still cause significant but less robust upregulation of *ctt1* in *atf1Δ* cells

compared to wild type, indicating that hydrogen peroxide might induce catalase expression through multiple mechanisms. Indeed, transcription factor Pap1 has been reported to be involved in the regulation of *ctt1* [69, 141]. Intriguingly, deletion of *atf1* in *cbf11Δ* cells decreases the amount of *ctt1* mRNA to the similar level that has been observed in wild type (Fig. 17A).

Consistently with Fig. 16B, Atf1 and Sty1 are equally important for proper expression of *gst2* especially during late phases of oxidative stress in wild type. However, upregulation of *gst2* gene appears to be Atf1 independent in *cbf11*-deficient strain, because deletion of *atf1* in *cbf11Δ* strain does not change the level of *gst2* mRNA during oxidative stress (Fig. 17B), suggesting that Cbf11 might be involved also in other signaling pathway.

On the other hand, regulation of *pyp2* seems to be Atf1-dependent in both wild type and *cbf11Δ* cells. Decline of *pyp2* mRNA level in treated *atf1Δ* and double deletant *atf1Δ cbf11Δ* is very similar (Fig. 17C); however, basal *pyp2* expression in double deletant *atf1Δ cbf11Δ* is rather similar to the *cbf11Δ* cells. Interestingly, even single deletion of *atf1* increases basal level of *pyp2* transcript. These results together with Fig. 16C suggest that Sty1/Atf1 pathway is necessary for proper *pyp2* activation during oxidative stress both in wild type and *cbf11Δ*.

Taken together, these results suggest Cbf11 represses expression of investigated genes via multiple mechanisms. Cbf11 is likely tightly connected with MAPK Sty1 and to some extent also with its substrate Atf1. Hence, Sty1 appears to be a key molecule for *ctt1*, *gst2*, *pyp2* and *atf1* upregulation in *cbf11Δ* strain and its resistance to hydrogen peroxide. For this reasons protein levels and phosphorylation state of Sty1 were examined.

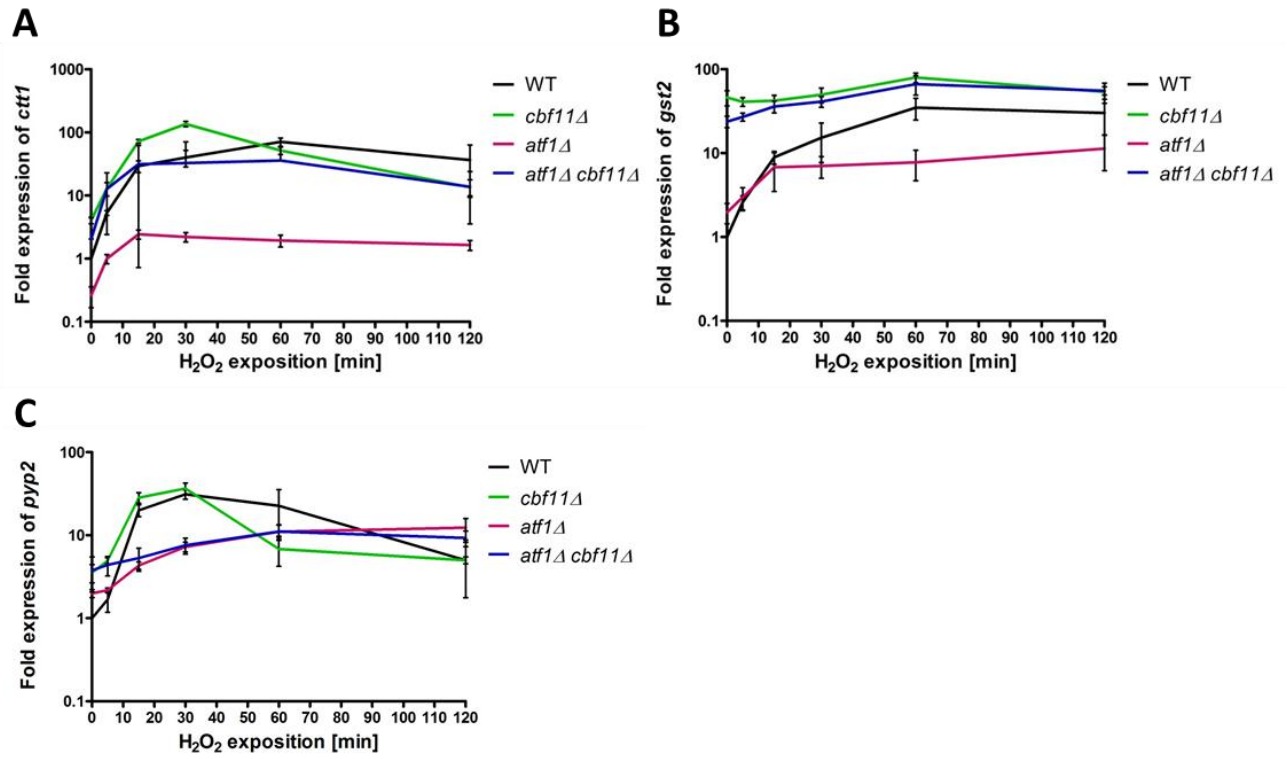

Fig. 17 - Atf1 dependent upregulation of *ctt1* and *pyp2* and Atf1 independent upregulation of *gst2* during oxidative stress in *cbf11Δ*. Wild type, *cbf11Δ*, *atf11Δ* and *atf1Δ cbf11Δ* cells were treated with 0.5mM H_2O_2, harvested according to the scheme depicted in Fig. 4 and relative levels of *ctt1* (**A**), *gst2* (**B**), and *pyp2* (**C**) transcripts were quantified. Data were normalized to *act1* and *rho1* transcript levels and to target gene transcript level in untreated wild type cells. Each curve represents mean of three independent experiments while error bars represent standard deviation (SD). No-template controls were negative.

5.3. Analysis of Sty1 phosphorylation state in *cbf11Δ* cells

Strain with HA-tagged Sty1 was already present in our laboratory, but strain that harbors both tagged Sty1 and deletion of *cbf11* had to be prepared for the investigation of Sty1 protein levels and its phosphorylation state.

5.3.1. Deletion of *cbf11* in *sty1-ha* cells

The deletion of *cbf11* gene in *sty1-ha6his* strain was performed using plasmid pMP91 [142] that contains Nat MX6 cassette (Fig. 18A) which is composed from gene for nourseothricine resistance (*natR*) surrounded by two sequences that are complementary to 5' and 3' flanking regions of *cbf11* ORF. After the transformation of the cells, the hybridization of the linearized plasmid to flanking regions of *cbf11* in the genome might

result in homologous recombination which interchanges *cbf11* gene for *natR* that subsequently serves as a selection marker.

Plasmid was isolated from bacteria *E. coli* and digested by restriction endonucleases XbaI, XhoI and BglII for its validation. Cleavage sites are depicted in Fig. 18C. Restriction cleavage produced DNA fragments of expected size (3707 bp, 811 bp, and 517 bp) as can be read from Fig. 18B. Therefore identity of purified plasmid (pMP91) was confirmed. Then the pMP91 was linearized with XbaI and introduced into *sty1-ha6his* cells. Only two colonies (marked C1 and C2) grew on selection YES plate and were subsequently analyzed. Genomic DNA was purified from these two clones and used as a template for PCR. Amplicons of designed primers overlap partially with inserted Nat MX6 cassette and partially with genome sequence adjacent upstream or downstream to deletion cassette. Each PCR reaction containing gDNA of C2 clone provide product of expected sizes (953 bp for upstream, 5' UTR region and 823 bp for downstream, 3' UTR region) while no signal was detected in no-template controls (Fig. 18C). PCR reaction containing gDNA isolated from clone C1 did not provide any product, indicating that integration of Nat MX6 was unspecific in C1 clone, for which C1 was excluded from further analysis for this reason. Thus, medium containing nourseothricine selected successfully C2 cells transformed with *natR* and following PCR confirmed that Nat MX6 cassette was integrated to the specific locus in C2 clone. *sty1-ha6his cbf11Δ* strain was therefore validated and prepared for upcoming experiments.

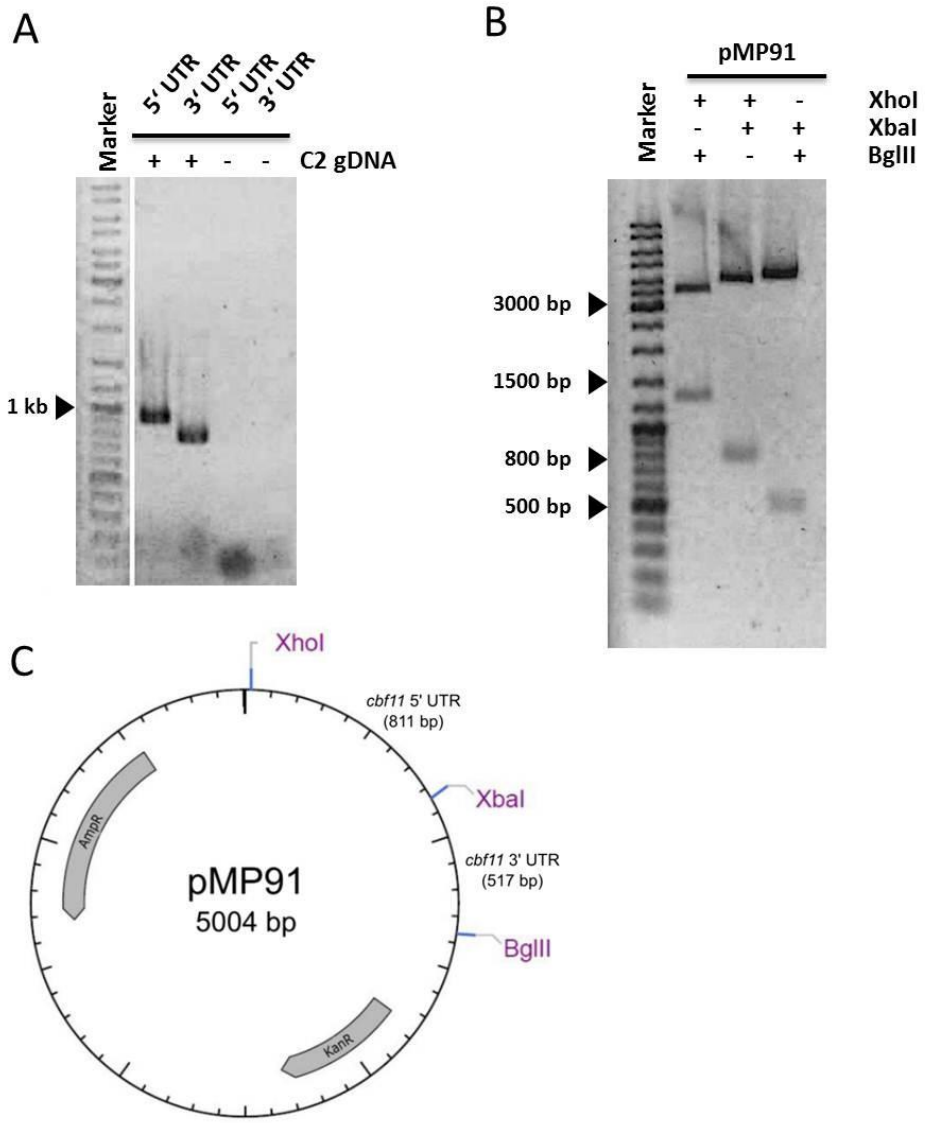

Fig. 18 – Preparation and validation of *cbf11* deletion with pMP91 plasmid. Products of PCR reactions containing pair of primers that anneal to the upstream or downstream region of the insert and 5' or 3' flanking regions of deleted *cbf11* ORF respectively. Genomic DNA isolated from C2 colony was used as a PCR template. PCR products were separated in 1% agarose gel and their molecular weight matches to the theoretically computed size (953 bp for upstream region and 823 bp for downstream region). No signal was detected in no-template control. GeneRuler Mix DNA Ladder (Thermo Scientific) was used as a marker of molecular weight (**A**). Plasmid was digested with XbaI, XhoI anf BglII restriction endonucleases according to the protocol in Materials and methods. Electrophoresis of reaction mixture in 1% agarose gel revealed two products of expected size in each line (1327 bp for whole insert, 811 bp for its upstream part, and 517 bp for downstream part). GeneRuler Mix DNA Ladder (Thermo Scientific) was used as a marker of a nucleic acid molecular weight (**B**). The map of pMP91 plasmid with marked restriction sites that were used for restriction analysis (**C**).

5.3.2. Activatory phosphorylation of Sty1 is diminished in *cbf11Δ* cells

For western blot analysis, *sty1-ha6his* and *sty1-ha6his cbf11Δ* cells were harvested before and 30 min upon the treatment with 0.5mM H_2O_2 and lysed. This particular time was chosen because mRNA levels of majority of examined genes culminated at this point during previous timecourse experiments and it has been expected that also other effects should be the most pronounced at this time point. The activatory phosphorylation of Sty1 at Thr171 and Tyr173 was determined using commercially available antibody against mammalian Sty1 ortholog – phosphorylated p38 (anti p38-P) kinase. Anti p38-P antibody has been proven to specifically detect also phosphorylated Sty1 earlier [85, 139, 143].

Spot test performed by Dr. Převorovský shown *cbf11Δ* cells are resistant to oxidative stress (Fig. 6) Consistently, the significant upregulation of stress responsive genes has been detected in the cells lacking Cbf11 (Fig. 13) and this upregulation was Sty1-dependent (Fig. 16). Additionally, active Sty1 kinase (phosphorylated on Thr171 and Tyr173) is essential for resistance to various stresses. Consistently, strains with mutation of these two residues exerted profound stress sensitivity [85, 86, 88]. In spite of this large body of evidence, Sty1-HA6HIS is not activated in *sty1-ha6his cbf11Δ* cells before hydrogen peroxide treatment and only very low level of Sty1 phosphorylation occurred 30 min after the treatment compared to wild type (Fig. 19A). The explanation that lower anti p38-P signal might be caused by decreased level of HA-tagged Sty1 protein in *sty1-ha6his cbf11Δ* cells is not very probable as total HA-tagged Sty1 fraction does not apparently change in tested strains or conditions (Fig. 19A). To exclude the hypothetical possibility that HA tag disrupts the structure of Sty1 and abolishes its phosphorylation in this manner, the same experiment was performed using wild type and *cbf11Δ* cells instead of cells comprising tagged Sty1. Indeed, the activatory phosphorylation of Sty1 was compromised also in *cbf11Δ* cells (Fig. 19B). No signal was detected in *sty1Δ* cells suggesting observed bands are Sty1-P specific. The basal phosphorylation level of Sty1 is present in both unstressed wild type and *cbf11Δ* cells (Fig. 19B) which is consistent with the literature [84, 91]. This finding suggests phosphorylation of Sty1 is not completely inhibited in *cbf11Δ* cells – it seems that the lack of Cbf11 rather impairs hyperactivation of Sty1 during oxidative stress. On the other hand, others have shown that osmotic stress-induced phosphorylation and consequent nuclear translocation of Sty1 occurs 10 min after the stress induction and the cytosolic localization of Sty1 is reconstituted in following 10 minutes [88]. It is therefore possible, that Sty1 kinase signaling might be executed in

less than 30 min in *cbf11Δ* cells and Fig. 19A, B reveals already dephosphorylated Sty1. Thus, time-course experiment has been performed. Wild type and *cbf11Δ* cells were treated before and 5, 15, and 30 min upon the treatment with 0.5mM hydrogen peroxide and Sty1-P amounts were determined. Interestingly, minor but most significant signal occurs 5 min upon the treatment and gradually fades away to the intensity detected in untreated cells (30 min after the H_2O_2 treatment) in *cbf11Δ* cells (Fig. 19C), indicating that hyperphosphorylation of Sty1 is not inhibited but rather attenuated in *cbf11Δ* strain.

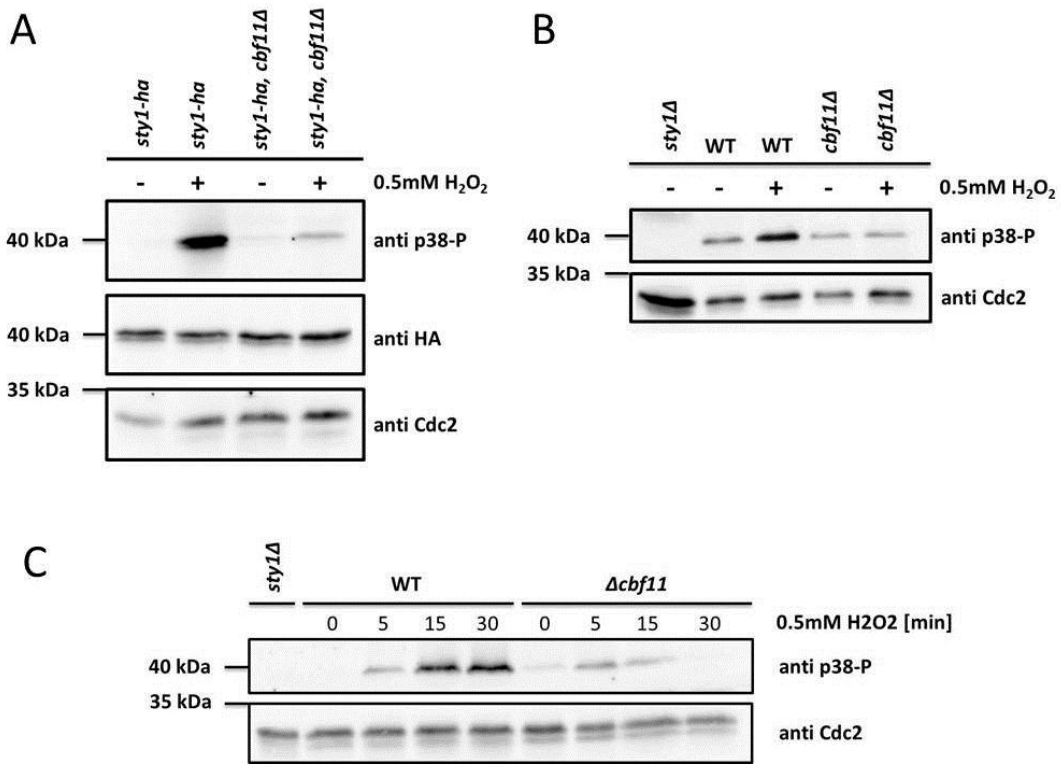

Fig. 19 – Phosphorylation of Sty1 at Thr171 and Tyr173 before and after the H_2O_2 treatment in wild type and *cbf11Δ* cells. Protein lysates prepared from *sty1-ha6his, sty1-ha6his cbf11Δ* (**A**), wild type, *sty1Δ*, and *cbf11Δ* cells untreated or treated with 0.5mM hydrogen peroxide for 30 min (**B**) or for indicated time (**C**) were separated by 10% poly-acrylamide gel electrophoresis (PAGE). Active, phosphorylated form of Sty1 was detected with antibody raised against phosphorylated form of orthologous protein p38. Amount of total HA-tagged Sty1 was established using specific anti HA antibody. Cdc2, the cyclin-dependent protein kinase, was detected with commercially accessible anti Cdc2 antibody (PSTAIRE) as a loading control. Positions of all bands are consistent with expected molecular weight of each detected protein. Figure **A** and **C** are representatives of two independent experiments and figure **B** is representative of three independent experiments.

Taken all data together, it has been shown that deletion of *cbf11* results in derepression of *ctt1*, *gst2*, *pyp2*, *atf1*, and *cbf12*. Thus, transcription factor Cbf11 appears

to be negative regulator of these genes. As no Cbf11-TAP binding to the promoters of these genes was detected, it has been postulated that Cbf11 is indirect negative regulator. Data further revealed that observed gene upregulation in *cbf11Δ* was Sty1 dependent. In contrast to our expectations, activatory phosphorylation of Sty1 is diminished in stress-resistant *cbf11Δ* cells (compared to wild type) after the treatment with hydrogen peroxide.

5.4. Cbf11 modulates oxidative stress response via Pap1 pathway

5.4.1. Expression analysis of strains with deletion of *pap1*

Several pieces of evidence implicate that *ctt1* and *gst2* are not regulated solely by Sty1/Atf1 pathway. Indeed, others previously describe regulation of these two genes by Pap1 pathway that triggers specific response to oxidative stress in *S. pombe*. Thus, the level of mRNA of *ctt1*, *gst2*, *atf1*, and *pyp2* has been measured in *pap1Δ* and *pap1Δ cbf11Δ* cells by RT-qPCR in accordance with the experimental scheme depicted in Fig. 12. Deletion of *pap1* gene causes remarkable decline of the *ctt1* transcript level in both stressed and unstressed cells but does not completely prevent catalase upregulation in the presence of hydrogen peroxide, which is consistent with literature [69, 141]. Importantly, catalase derepression observed in *cbf11Δ* cells is prevented in *pap1Δ cbf11Δ* cells. Moreover, *ctt1* transcript level reduction is similar in *pap1Δ cbf11Δ* and *pap1Δ* cells (Fig. 20A), suggesting that Cbf11 regulates *ctt1* gene in Pap1-dependent manner.

Pap1 has been also identified as a major regulator of *gst2* earlier [76, 144]. Indeed, expression of *gst2* is impaired in *pap1Δ* cells. The fact that double knock-out *pap1Δ cbf11Δ* cells exerts very similar levels of *gst2* mRNA as *pap1Δ* cells in both treated and untreated cells (Fig. 20 B) further supports the hypothesis that Pap1 might be involved in gene derepression observed in *cbf11Δ*. Connection between Pap1 and Cbf11 is probably not exclusive, because double knock-out *pap1Δ cbf11Δ* cells exert significantly (paired two sample t-test; $p < 0.05$) increased basal expression *gst2* compared to *pap1Δ* strain.

The expression profile of *atf1* in *pap1Δ* and *pap1Δ cbf11Δ* cells is analogous to wild type during oxidative stress (Fig. 20C). Thus, Pap1 has probably only negligible role in Cbf11-mediated repression of *atf1*.

Deletion of *pap1* results in overexpression of *pyp2* that was similar to the expression profile of *pyp2* in *pap1Δ cbf11Δ*, indicating that *pyp2* derepression observed in *cbf11Δ* is not generally Pap1-dependent (Fig. 20D). It is more likely that Pap1 and Cbf11 can both repress *pyp2* via different pathways, as absence of each of these proteins or both of them results in gradual *pyp2* overexpression.

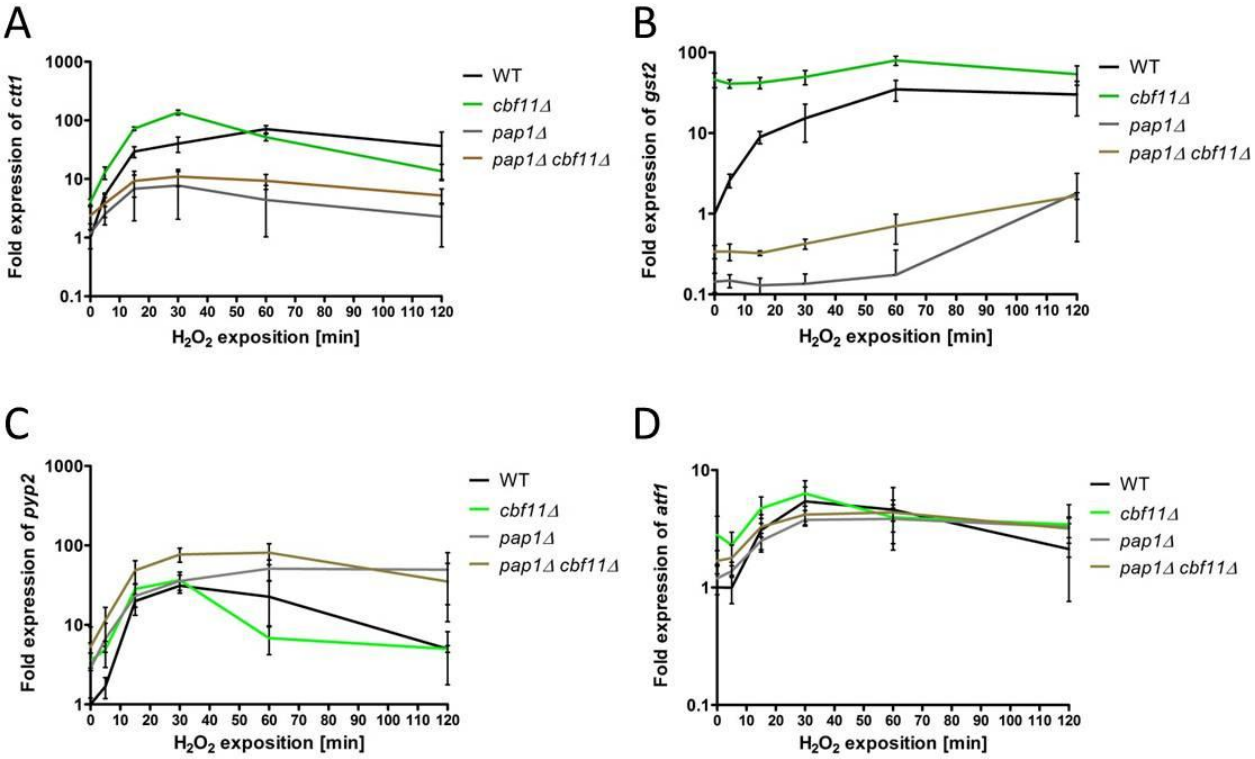

Fig. 20 – Expression profiles of *pap1Δ* and *pap1Δ cbf11Δ* during oxidative stress. Wild type, *cbf11Δ*, *pap1Δ* and *pap1Δ cbf11Δ* cells were treated with 0.5mM H_2O_2, processed according to the scheme in Fig. 12 and relative concentrations of *ctt1* (**A**), *gst2* (**B**), *atf1* (**C**), and *pyp2* (**D**) mRNA were quantified. Data were normalized to *act1* and *rho1* transcript levels and to target gene transcript level in untreated wild type cells. Each curve represents mean of three independent experiments. Error bars represent standard deviation (SD). No-template controls were negative.

5.4.2. Unstressed *cbf11Δ* cells express increased Pap1 activity

Because Pap1 is transcription regulator of *ctt1* [69, 141] and *gst2* [76, 144] genes which are both upregulated in cells with deletion of *cbf11* and this upregulation is obviously Pap1-dependent, the activity of Pap1 in *cbf11Δ* strain has been examined.

5.4.2.1. Construction of reporter vector pMP127

The reporter vector for evaluation of the activity of transcription factor Pap1 was constructed by Dr. Převorovský who cloned two copies (in sense and antisense orientation) of AP-1 binding site from human collagenase (5'-TGACTCA-3' [145]) using Col-AP-1 oligonucleotides [135] with NheI compatible overhangs into pREPORT-U plasmid according to [136], creating vector pMP120. Because *ura4* was used previously as a selection for *pap1* deletion, the selection marker gene of pMP120 was switched from *ura4* to *LEU2* from pREPORT-L [136].

Both *ura4* and *LEU2* genes were cleaved-out from the plasmid (pMP120 and pREPORT-L) by restriction endonuclease HindIII. Products of restriction cleavage were separated by agarose gel electrophoresis and *ura4*-lacking plasmid backbone of pMP120 and *LEU2* gene from pREPORT-L were cut out from the gel, purified and pMP120 backbone was treated with FastAP phosphatase to prevent its self-ligation without insert. Then *LEU2* and pMP120 backbone were subjected to ligation and electropored into competent *E. coli* cells that were subsequently grown on solid LB plates with ampicilin. Six colonies were formed and their DNA was purified and analyzed by restriction cleavage. Cleavage by HindIII should prove whether plasmid contains full-length *LEU2* (2232 bp) while cleavage by HpaI should reveal orientation of inserted gene (7574 bp, 2615 bp, 651 bp, and 624 bp for forward orientation; 9318 bp, 871 bp, 651 bp, and 624 bp for reverse orientation). According to the Fig. 21A, clones 1, 2, 4, and 5 contained insert of expected length. These clones were then tested by HpaI - clone 1 contains *LEU2* in reverse orientation while clones 2, 3, and 5 in forward (Fig. 21B). 651 bp and 624 bp long fragments appears as one band probably due to insufficient separation of these fragments with similar size. Because pREPORT-L also contains reverse *LEU2* [136], plasmid DNA was purified from clone 1 and named pMP127.

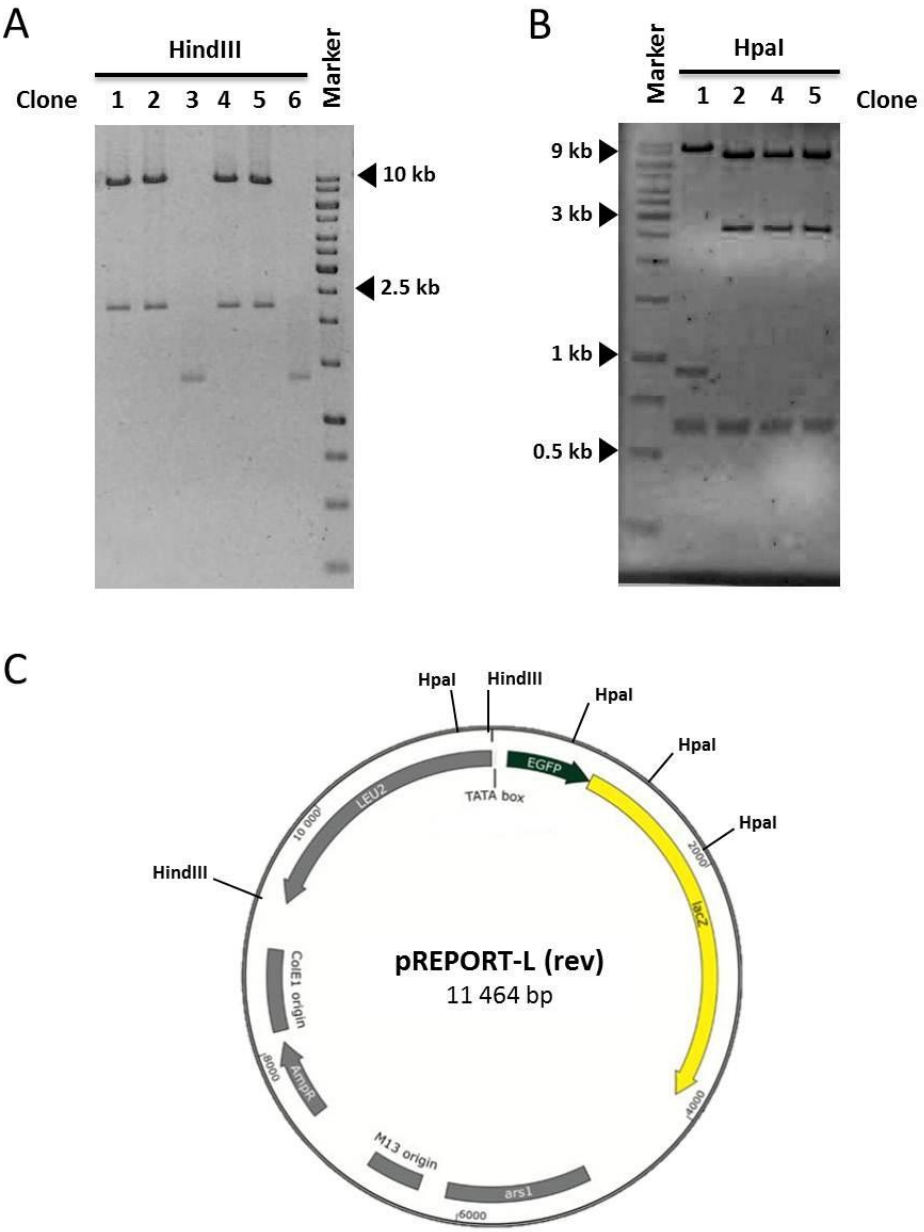

Fig. 21 – Restriction analysis of *E. coli* clones potentially transformed with pMP127. Plasmid DNA purified from colonies that grown on selection solid medium after electroporation was subjected to restriction cleavage by endonuclease HindIII and separated by 1% agarose gel electrophoresis. Vector with the insert size corresponding to *LEU2* marker gene (2232 bp) was present in clones 1, 2, 4, and 5 within HindIII restriction site (**A**). Plasmid DNA from clones with proper insert was cleaved by restriction endonuclease HpaI and products of this reaction were separated by 1% agarose gel electrophoresis. The size of fragments of cleaved vector from clone 1 (9318 bp, 871 bp, 651 bp, and 624 bp) correspond to the vector with *LEU2* marker gene in reverse orientation. The size of fragments generated by cleavage of DNA from other insert-containing vectors (7574 bp, 2615 bp, 651 bp, and 624 bp) corresponds to the plasmid with *LEU2* marker in forward orientation (**B**). Figure **C** was taken and adjusted from [136] and display pREPORT-L (*LEU2* in reverse orientation) vector with marked HindIII and HpaI restriction sites. Size of nucleic acid fragments was determined using GeneRuler 1 kb DNA ladder (Thermo Scientific) (**A**, **B**).

5.4.2.2. β-galactosidase assay

Wild type, *cbf11Δ*, and *pap1Δ* cells were transformed with plasmid pMP127 and selected at EMM agar plates without leucine. Cells were cultivated in liquid EMM without leucine precisely to OD_{600} = 0.5, harvested, and subjected to β-galactosidase assay. The level of the assay background signal was established in *pap1Δ* cells where Pap1-binding sites in the promoter of *lacZ* in pMP127 cannot be occupied by transcription factor Pap1 that is absent in these cells. Slightly higher activity compared to *pap1Δ* strain was measured in unstressed wild type cells (Fig. 22). Importantly, β-galactosidase activity was ~2.7 higher in Cbf11 deficient cells compared to wild type.

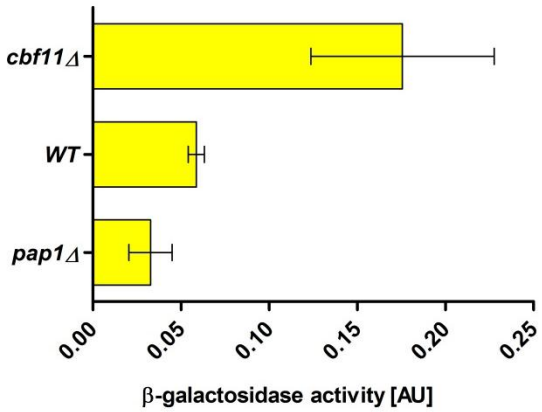

Fig. 22 – Activity of β-galactosidase expressed from pMP127 in different strains. Wild type, *cbf11Δ*, and *pap1Δ* cells transformed with pMP127 were diluted to liquid EMM medium without leucine to OD_{600} = 0.075 and cultivated precisely to OD_{600} = 0.5, harvested, lysed, and β-galactosidase activity of lysates was established by addition of its substrate – ONPG. Reaction gives yellow product that absorbs visible light with wave length 420 nm. Depicted graph shows average values of three independent experiments and error bars represent SD.

5.4.3. Hydrogen peroxide treatment increases Pap1 binding to *ctt1* and *gst2* promoters in *cbf11Δ* cells

Previous results might imply that Pap1 is a key molecule for *cbf11Δ* strain resistance to hydrogen peroxide. Experiment with reporter vector pMP127 additionally suggests that Pap1 is more active in *cbf11Δ* cells (Fig. 22). However, these data were obtained using artificial conditions (structure of chromosomal binding site might differ from plasmid). It is known Pap1 binds to the promoters of *ctt1* and *gst2* in wild type cells [76, 94, 134]. Pap1 occupancy at promoters of *ctt1* and *gst2* was therefore determined with ChIP in *cbf11Δ* cells. Promoters of *pyp2* and *sty1* were also analyzed to examine

hypothesized signaling crosstalk between Pap1 and Sty1/Atf1 pathways [69]. Additionally RT-qPCR data show *pyp2* upregulation in *pap1Δ* cells (Fig. 20C). Thus, we wanted to investigate whether more active Pap1 can regulate also Sty1 signaling that is necessary for upregulation of all tested genes in *cbf11* deficient cells (Fig. 16).

5.4.3.1. Design and validation of oligonucleotides for ChIP evaluation

Pap1 binding sites in GP3 (*gst2*) and CP3 (*ctt1*) promoter regions (Fig. 23A) have been identified in previous studies [76, 134]. *In silico* analysis was used for prediction of additional potential Pap1 binding sites in promoters of *ctt1*, *gst2*, *pyp2*, and *sty1* genes. Amplicons for qPCR evaluation of ChIP were subsequently designed specifically to overlap with these potential Pap1 binding sites (Fig. 23A). The ability of PCR reaction containing designed primers to give specific product was tested by PCR. Each reaction containing applied oligonucleotides provided one product of expected size (Fig. 23A, B). No product was observed in NTCs. Subsequent qPCR and melting analysis of PCR products confirmed each reaction containing given pair of designed oligonucleotides amplify one specific product that is represented by one melting peak (Fig. 24). Dilution series of gDNA were amplified and resulting C_P values were plotted against gDNA concentration, creating a standard curves (Fig. 25) whose slope was used for calculation of efficiency of qPCR containing given pair of primers. Thus, primers for amplification of promoter regions of *ctt1*, *gst2*, *pyp2*, and *sty1* genes are specific and suitable for ChIP evaluation.

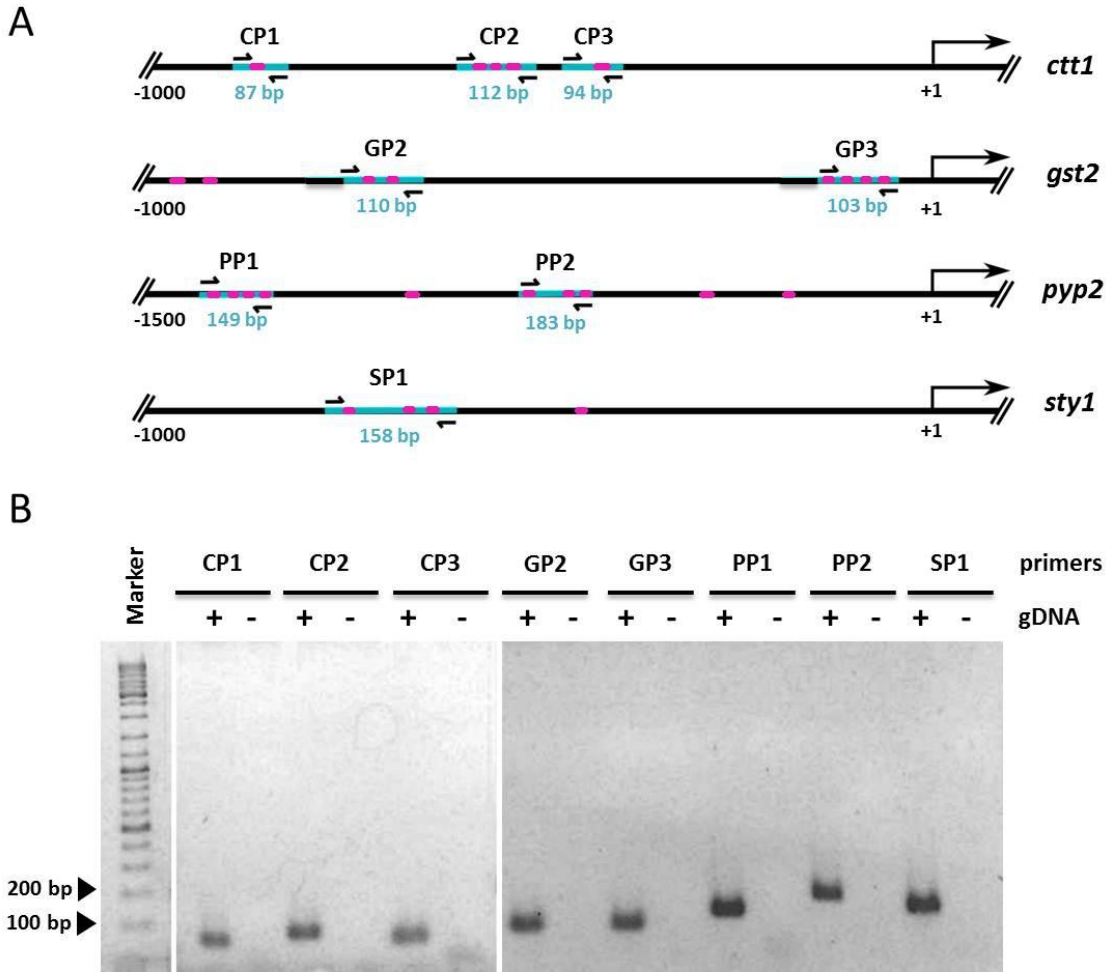

Fig. 23 – Validation of oligonucleotides for qPCR evaluation of ChIP. Figure illustrates schematic positions and sizes of designed amplicons related to the transcription start site of *ctt1*, *gst2*, *pyp2*, and *sty1* genes; purple dots depict positions of predicted Pap1 binding sites (**A**). Designed pairs of primers were added to PCR reactions with gDNA as a template. Reaction products were separated by 2% agarose gel electrophoresis. PCR reactions containing designed pair of primers provide products of expected size. No product was observed in NTCs. GeneRuler Ladder Mix (Thermo Scientific) was used as a marker of molecular weight (**B**).

.

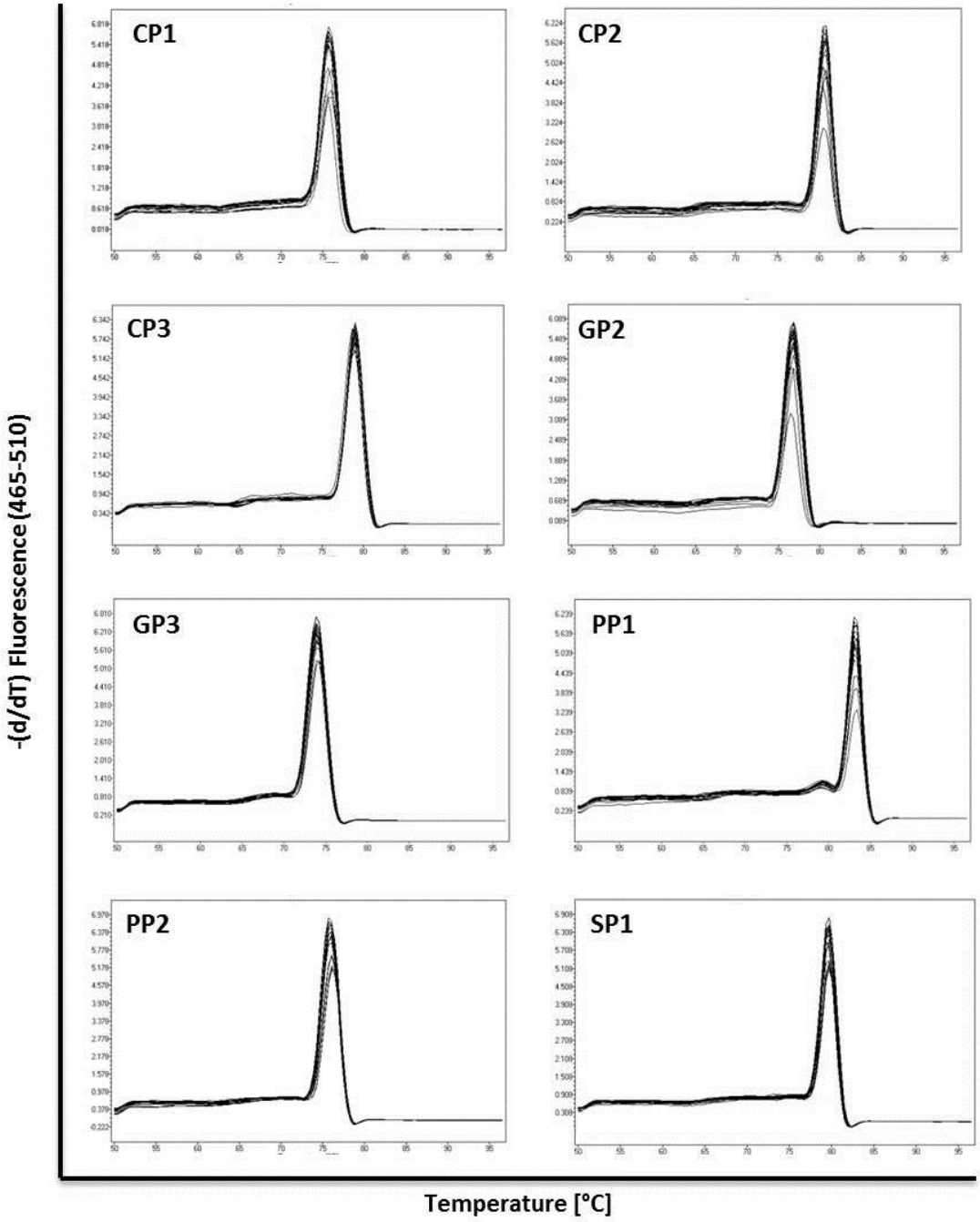

Fig. 24 – Melting analysis of products of qPCR containing designed oligonucleotides for amplification of possible Pap1 binding sites in promoter regions of *ctt1*, *gst2*, *pyp2*, and *sty1*. Designed oligonucleotides were added to qPCR reaction mixture with 19.8 ng of gDNA as a template and products of each reaction were subjected to melting analysis. Figure shows that there is only one qPCR product in each reaction, confirming specificity of designed primers. Amplicon positions and lengths are described in Fig. 23.

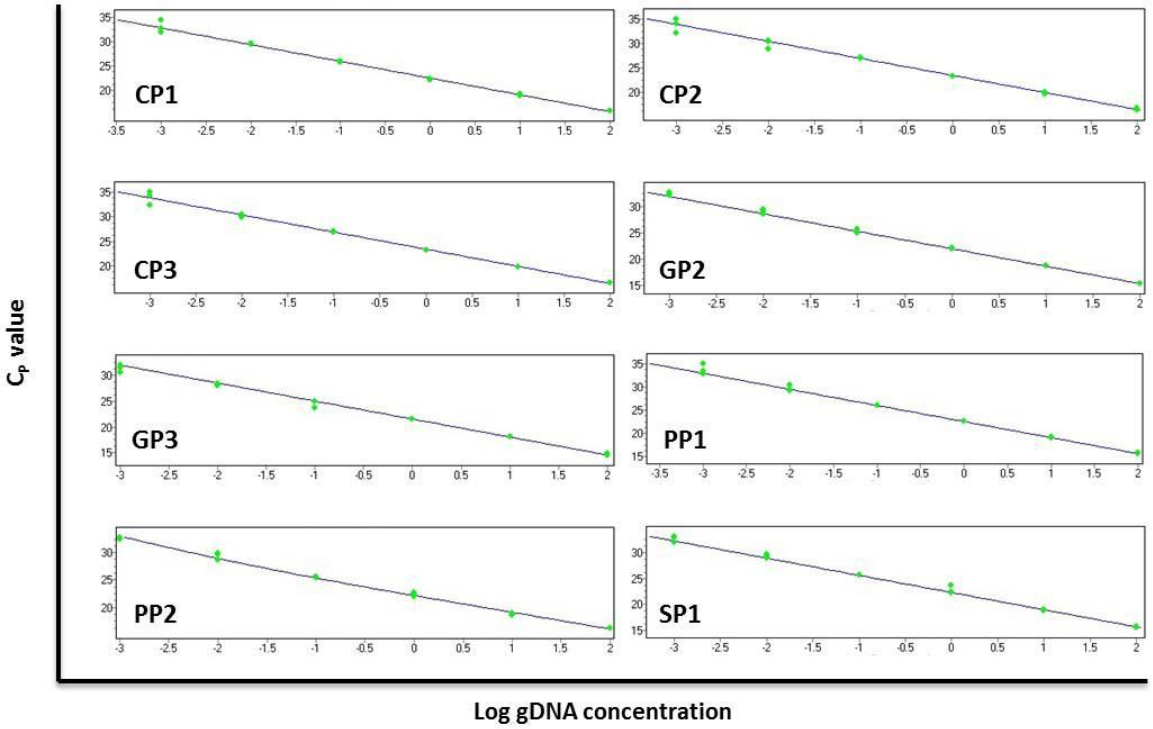

Fig. 25 – Standard curves of qPCR containing pair of primers designed for amplification of possible Pap1 binding sites in promoter regions of *ctt1*, *gst2*, *pyp2*, and *sty1* genes. Designed oligonucleotides were analyzed by qPCR with dilution series of gDNA as a template. Resulting C_P values were plotted against gDNA concentration forming standard curves whose linear part was used for calculation of qPCR reaction efficiency.

5.4.3.2. Pap1 binding to its potential binding sites in promoter regions of *ctt1*, *gst2*, *pyp2*, and *sty1*

The Pap1 binding to the promoter of *ctt1* was measured in three distinct loci called CP1, CP2, and CP3 (Fig. 23A). Strains with tagged Pap1 (*pap1+(3Pk)* and *pap1+(3Pk) cbf11Δ*) were cultivated according to ChIP protocol and harvested before and 30 min after the treatment with 0.5mM hydrogen peroxide. Signal from the most distal CP1 region was rather subtile and statistically undistinguishable ($p > 0.07$; paired two sample t-test) from negative controls (locus M40 and *atf1* ORF) for which CP1 was excluded from following analysis.

Activity of Pap1 is increased in *cbf11Δ* cells (Fig. 22). Thus, it has been expected that Pap1 binding to the promoters of upregulated genes (Fig. 13) would be enhanced in *cbf11Δ* cells. Nonetheless, no significant difference ($p > 0.05$; paired two sample t-test) in Pap1 binding to CP2 and CP3 regions was observed between unstressed *cbf11Δ* and wild type (*pap1+(3Pk)*) strains (Fig. 26). H_2O_2 treatment resulted in significant but weak

(p = 0.0077; paired two sample t-test) increase of Pap1 enrichment in CP2 region in wild type cells. Interestingly, this enrichment elevation (in either CP2 or CP3 regions) was much more pronounced in *cbf11Δ* cells (Fig. 26).

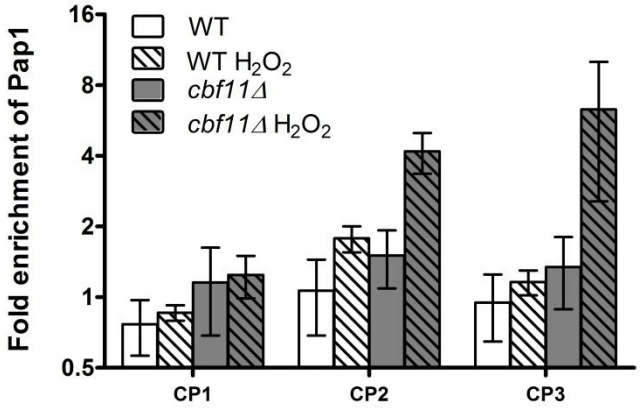

Fig. 26 – Pap1 binding to the promoter region of *ctt1* gene. Wild type (*pap1+(3Pk)*) and *cbf11Δ* (*pap1+(3Pk) cbf11Δ*) cells were cultured and harvested before and 30 min after the treatment with 0.5mM hydrogen peroxide. Lysed cells were subjected to ChIP and enrichment of Pap1 at three distinct regions of *ctt1* promoter (CP1, CP2 and CP3; see Fig. 23A) was established by qPCR. Axis y shows relative Pap1 occupancy compared to geometric average of negative controls (locus M40 and *act1* ORF). Columns represent means of three independent experiments while error bars represent standard deviation.

Only weak Pap1 binding and no substantial changes in different conditions and strains were detected in GP2 region. Despite higher Pap1 activity in *cbf11Δ* cells (Fig. 22), no Pap1 enrichment was observed in untreated *cbf11* deficient strain compared to wild type (*pap1+(3Pk)*) in GP3 region. Pap1 occupancy in GP3 region was remarkably decreased after the H_2O_2 treatment in wild type cells (*pap1+(3Pk)*) compared to untreated cells, but the amount of Pap1 bound to this region remained almost unchanged before or after the treatment in *pap1+(3Pk) cbf11Δ* (Fig. 27).

According to Fig. 28, no Pap1 binding was detected in PP1, PP2, and SP1 promoter regions as signal in all of these loci was lower than signal obtained from negative control (locus M40 and ORF of *act1*).

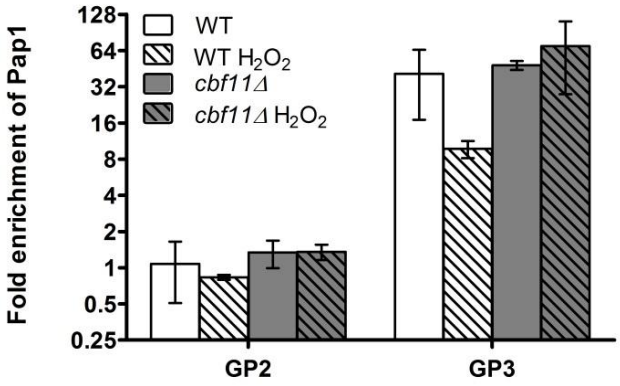

Fig. 27 – Pap1 binding to the promoter region of *gst2* gene. Wild type (*pap1+(3Pk)*) and *cbf11Δ* (*pap1+(3Pk) cbf11Δ*) cells were cultured and harvested before and 30 min after the treatment with 0.5mM hydrogen peroxide. Lysed cells were subjected to ChIP and enrichment of Pap1 in two distinct regions of *gst2* promoter (GP2 and GP3; see Fig. 23A) was established by qPCR. Axis y shows relative Pap1 occupancy compared to geometric average of negative controls (locus M40 and *act1* ORF). Columns represent means of three independent experiments while error bars represent standard deviation.

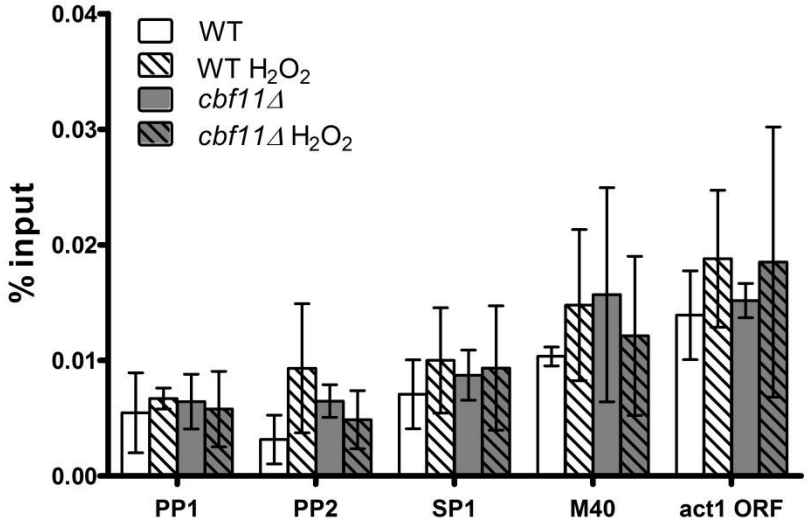

Fig. 28 - Pap1 binding to the promoter regions of *pyp2* and *sty1* gene. Wild type (*pap1+(3Pk)*) and *cbf11Δ* (*pap1+(3Pk) cbf11Δ*) cells were cultured and harvested before and 30 min after the treatment with 0.5mM hydrogen peroxide. Lysed cells were subjected to ChIP and enrichment of Pap1 in two distinct regions of *pyp2* promoter (PP1 and PP2; see Fig. 23A) and in SP1 region in *sty1* promoter was established by qPCR. Locus M40 and *act1* ORF were selected as negative controls. Columns represent means of three independent experiments while error bars represent standard deviation.

5.4.4. Analysis of cysteine oxidation in Pap1

Experiment with reporter vector pMP127 (Fig. 21C, 22) showed hyperactivation of Pap1 in unstressed *cbf11Δ* cells. However, no increase of Pap1 binding to its binding sites in the promoters of *ctt1* and *gst2* genes (Fig 26, 27) has been observed in unstressed *cbf11Δ* cells compared to wild type. Previous studies have revealed that cysteine oxidation with subsequent formation of intramolecular disulfide bond is necessary for Pap1 nuclear localization and subsequent DNA binding [72–74]. We therefore wanted to investigate redox state of Pap1 cysteines in *cbf11Δ* cells. For this purpose a novel method had to be introduced to our laboratory. The protocol from [137, 138] has been taken and optimized (see Materials and methods).

Following chapter contains rather very preliminary, unreliable, and incomplete data from which no conclusion can be made. Several imperfections can be observed, usually absence of sufficient controls. This chapter was included to the thesis namely as a documentation of an optimization process and its purpose is to serve as methodical guide for other co-workers that will be involved in this project in the future.

The principle of this method is based on the IAA ability to covalently bind reduced cysteine (S^-) residues. The presence of IAA-modified (reduced) cysteines (Cys-IAA) decreases protein mobility in polyacrylamide gel. Thus, bands with higher mobility contain oxidized proteins that were not modified with IAA (Fig. 29).

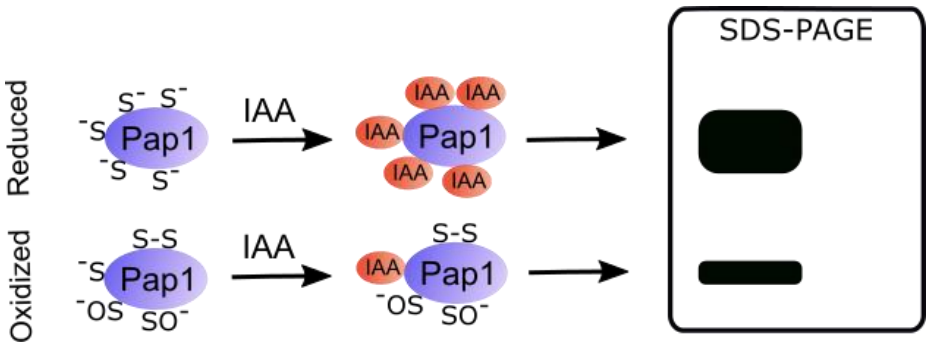

Fig. 29 – Scheme of modification of cysteine residues with IAA in Pap1. IAA covalently binds to reduced cysteine residues and causes mobility shift of modified proteins. Oxidized proteins therefore show higher mobility because fewer IAA molecules are attached to the protein.

Wild type, *pap1+(3Pk)* and *pap1+(3Pk) cbf11Δ* cells were cultured, harvested before or 30 min after the treatment with 0.5mM or 0.2mM hydrogen peroxide, and lysed. Lysates were subsequently treated with iodoacetamide and analyzed by non-reducing SDS-PAGE. Despite insufficient protein loading of negative control (see Cdc2 amount), the faint bands (marked with arrow) whose position resembles oxidized fraction of Pap1 [73] were detected. The specificity of anti Pk antibody was established several times earlier (Fig. 30C).

Next preliminary experiment was performed using wild type, *pap1+(3Pk)* and *pap1+(3Pk) cbf11Δ* cells exposed to 0.5mM hydrogen peroxide for 30 min or not. The exposition duration was prolonged to obtain higher signal which led to the full saturation of thick bands that represent reduced forms of Pap1. This over-exposition was, however, used also in the original studies [137, 138] or in [73]. Issues with wild type loading reappeared again, but clear fraction of possibly oxidized Pap1 was successfully visualized (Fig 30B).

Because 0.5mM might be considered as high H_2O_2 concentration for Pap1 activation, we decided to test also 0.2mM hydrogen peroxide in the third experiment, for this concentration was applied previously [137, 138] for investigation of Pap1 redox state. This experiment should therefore reveal whether our experimental system is consistent with already published data. Oxidized and reduced fractions of Pap1 were not separated sufficiently enough in previous experiment (Fig. 30B). To get better resolution, the protein separation trail length of non-reducing SDS-PAGE was prolonged. As a drawback, our loading control Cdc2 migrated out of the gel. Therefore, polyacrylamide gel stained with Coomasie Briliant Blue was used as loading control. Fig. 30D shows that longer separation step results in well distinguishable Pap1 fractions. On the other hand, it is impossible to read any pattern in Pap1 redox state in diverse strains and conditions due to different protein content of each loaded sample. Experiment was repeated several times, but for this reason it was hard to make any conclusion. It is therefore possible that method for measuring protein concentration (Protein DC^{TM} Assay; Bio-Rad) is not fully compatible with IAA treated samples. Protein-reagent interaction gives colored product and assay derives protein concentration from the absorbance of the sample. It is therefore possible that IAA treatment might affect either protein-reagent interaction or colorometry. Protein concentration can be measured with different method in the future.

We failed to generate reliable consistent data and experiment therefore did not answer to our questions. We cannot afford other independent experiments because of limited time. Novel tool for investigation of cysteine oxidation in Pap1 has been at least partially introduced to our laboratory for further studies though.

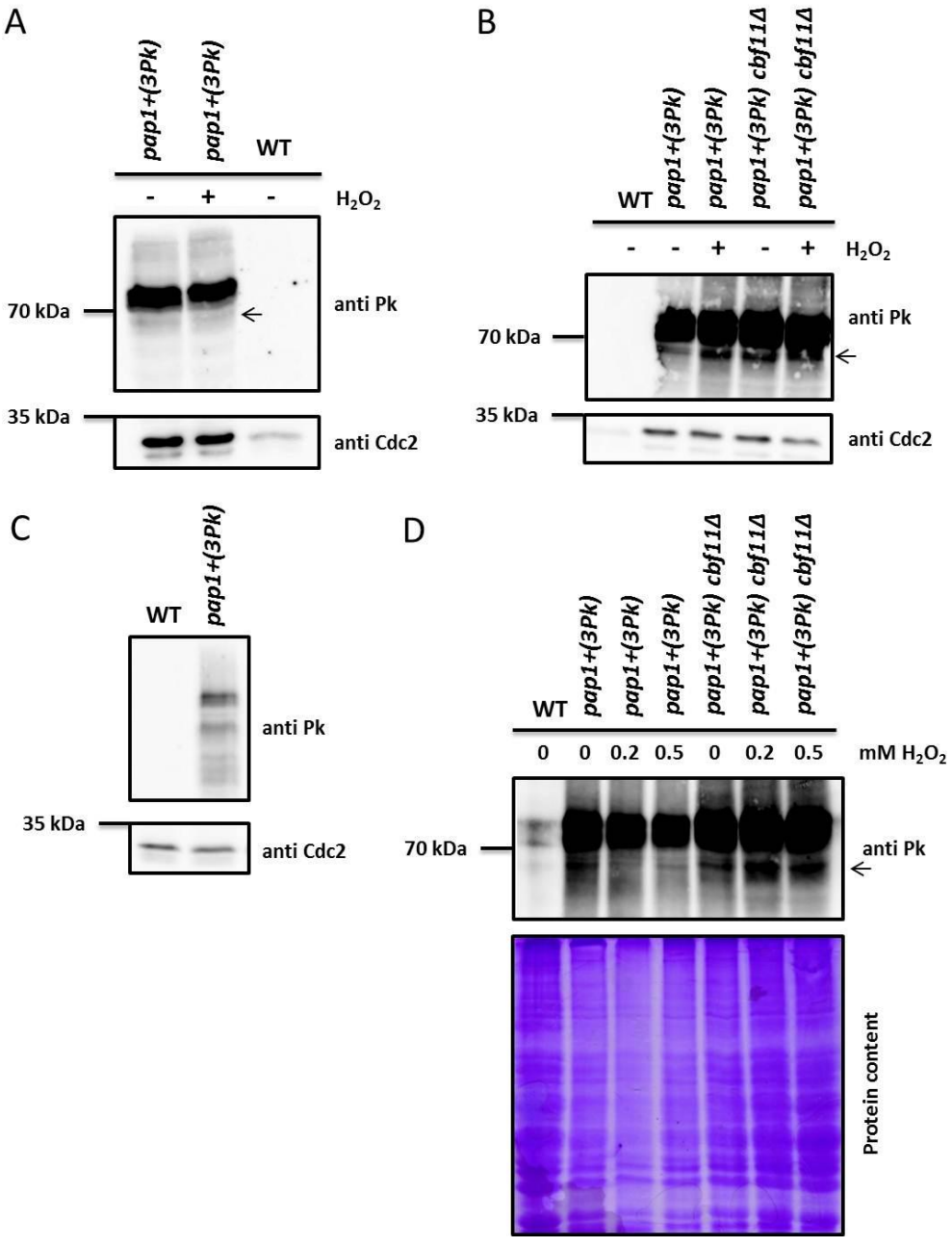

Fig. 30 – Optimization of method for investigation of cysteine redox state within Pap1 transcription factor. Wild type, *pap1+(3Pk)* and *pap1+(3Pk) cbf11Δ* cells were harvested before and after the 30 min long exposition to 0.5mM H_2O_2, lysed, treated with IAA, separated by non-reducing SDS-PAGE, and blotted. Pap1 was detected with anti Pk tag antibody. Cdc2, the cyclin-dependent protein kinase, was detected with commercially accessible anti Cdc2 antibody (PSTAIRE) as a loading control (**A**, **B**). Protein lysates from untagged cells and strain comprising 3Pk-tagged Pap1 were separated by SDS-PAGE and 3Pk-tagged Pap1 was immunodetected to test specificity of anti Pk antibody. The abundance of Cdc2 was used as loading control. Depicted figure is representative of two independent experiments (**C**). Wild type, *pap1+(3Pk)* and *pap1+(3Pk) cbf11Δ* cells were harvested before and after the 30 min exposition to 0.5mM or 0.2mM H_2O_2, lysed, treated with IAA, separated by non-reducing SDS-PAGE, and tagged Pap1 was visualized by immuodetection. Pap1 was detected with anti Pk tag antibody. Proteins in polyacrylamide gel were stained with Coomasie Briliant Blue and used as loading control (**D**).Oxidized fraction of Pap1 is marked with arrow.

6. DISCUSSION

CSL transcription factors have been studied entirely in the context of metazoan signaling pathway Notch for decades. The presence of conserved CSL proteins in fungi [129] shows that CSL family is relatively ancient and was likely present in the common ancestor of fungi and metazoa. Since Notch pathway is considered as a metazoan hallmark, there is high probability that CSL transcription factors should be able to operate Notch-independently. Indeed, several publications identified Notch-independent functions of CSL in metazoans [130–132]. Additionally, profound phenotypes have been observed in *Schizosaccharomyces pombe* deletion mutants of CSL coding genes including growth rate retardation, cell division issues, and adhesion changes [126]. Notch signaling networks are not completely understood yet. It has been shown that outcomes of Notch signaling are tissue and cell-type dependent and can be significantly distinct even in different signaling contexts [115]. The discovery of original role of CSL proteins would allow researchers to understand regulatory mechanisms of these important transcription factors in wider context and complexity.

Very pronounced phenotype, observed in deletion mutant of one of the two *S. pombe* CSL paralogs – Cbf11, was resistance to oxidative stress (Fig. 6). Preliminary data (Fig. 7) additionally demonstrate that important antioxidants (*ctt1* and *gst2*) are upregulated in *cbf11Δ* as well as components of the Atf1/Sty1 pathway (namely *atf1* and *pyp2*), which is triggered by various stress stimuli. Additionally, ChIP-seq performed by Dr. Převorovský (Fig. 8), revealed putative binding sites of Cbf11 in promoters of these genes. Thus, the role of CSL proteins in response to oxidative stress in *S. pombe* has been explored in this work.

6.1. Deciphering of the relationship between Cbf11 and Cbf12

The antagonistic function of these two paralogs has been described earlier. The deletion of *cbf11* causes very similar phenotypes as overexpression of *cbf12* [126]. Dr. Převorovský observed this phenomenon also at molecular level in dataset from his transcriptome analysis of different CSL mutants in *S. pombe* (Fig. 32), where either deletion of *cbf11* or *cbf12* overexpression resulted in the similar expression change.

Consistently, this work for the first time shows that *cbf12* mRNA level is increased in *cbf11Δ* cells (Fig. 13E), but this type of regulation is not reciprocal as deletion of *cbf12*

has only negligible effect on *cbf11* transcript level (Fig. 13F). Physiological concentration of Cbf12 seems to have only very little, if any effect on transcript level of oxidative stress responsive genes *ctt1*, *gst2*, *pyp2*, and *atf1* as expression of these genes is very similar in exponentially growing wild type and *cbf12Δ* cells (Fig. 13). Overexpression of *cbf12*, in contrast, resulted in increased mRNA levels of stress related transcription factors *atf1* and, potentially, *hsr1*, and phosphatase *pyp2* (Fig. 32), indicating Cbf12 is able to positively regulate stress response. Since Cbf11 seems to be rather negative regulator of the stress response (its deletion resulted in upregulation of *ctt1*, *gst2*, *pyp2*, and *atf1* genes; see Fig. 13), regulation of certain genes involved in stress response signaling is another example of previously observed functional antagonism of these two paralogs [126].

Because human genome contains more CSL paralogs, principles of intricate reciprocal regulation between different CSL transcription factors has to be unraveled for full understanding of their Notch-independent functions, but this goal is far beyond the purpose of this work. Anyway, to gain insight into the exact molecular mechanism of mutual regulatory relationships among different CSL paralogs, it should be determined whether observed changes in mRNA levels of *cbf12* in *cbf11Δ* cells are result of increased/decreased transcription or rather mRNA stability (Cbf12 has been already described to be regulated by Zfs1-mediated mRNA decay [146]), whether upregulation of *cbf12* causes reduction of transcript and protein levels of *cbf11*, whether the overexpression of *cbf12* in *cbf11Δ* strain will further augment gene derepression (in other words, if changes in gene expression caused by *cbf11* deletion and *cbf12* overexpression, depicted in Fig. 32, are result of direct functional antagonism of these two paralogs or rather result two independent regulatory events), whether Cbf12 can physically interact with Cbf11, or how deletion of one paralog influences cellular localization of the other.

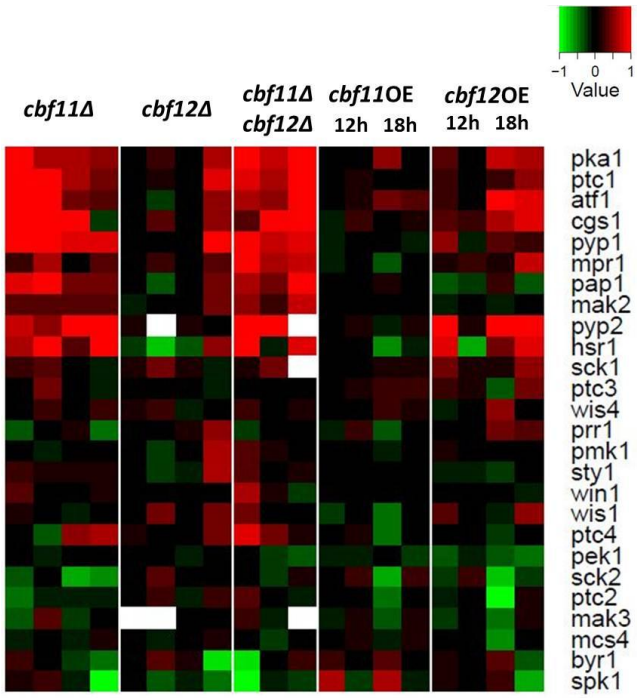

Fig. 32 – Expression analysis of selected regulatory genes in cells with deleted or overexpressed CSL proteins. Dr. Převorovský performed experiment and compiled data to depicted heat map. Heat map demonstrates fold-transcript level change of selected genes in various CSL mutants (*cbf11Δ* – column 1; *cbf12Δ* – column 2; *cbf11Δ cbf12Δ* – column 3; *cbf11* and *cbf12* overexpression – column 4 and 5, the fourth and the fifth columns are composed of two independent experiments analyzed in dedicated time after *cbf12* overexpression induction from inducible *nmt1* promoter) compared to wild type. Gene list contains selection of *S. pombe* MAPK with relevant regulators and effectors, namely kinases (*pka1* and its regulation subunit *cgs1*, *sck1*, *sck2*, *sck3*, *pmk1*, *sty1*, *pek1*, *spk1*, *byr1*), upstream activators of Sty1 (*mpr1*, *mcs4*, *mak2*, *win1*, *wis4*), phosphatases (*pyp1*, *pyp2*, *ptc1*, *ptc2*, *ptc3*, *ptc4*) and transcription factors (*atf1*, *hsr1*, *prr1*). Depicted genes were selected with intension to briefly visualize and explore influence of CSL transcription factors on *S. pombe* MAPK pathways. Data are depicted in log2 scale.

6.2. Cbf11 is probably negative regulator of *ctt1*, *gst2*, *pyp2* and *atf1* genes in cells

Our preliminary data implied CSL transcription factors might be involved in response to oxidative stress in *S. pombe*, for cells lacking transcription factor *cbf11* have been found to be resistant to high concentration of hydrogen peroxide (Fig. 8). On the basis of ChIP-seq (Fig. 6) and expression profiling data (Fig. 32) we predicted several genes connected to oxidative stress response that might be involved in resistance of *cbf11Δ* strain to hydrogen peroxide. RT-qPCR results actually revealed *cbf11Δ* cells contain enhanced

amount of *ctt1*, *gst2*, *pyp2* and *atf1* transcripts compared to wild type (Fig. 13), which led us to the conclusion that Cbf11 might act as a negative regulator of investigated genes. Hence, the mechanism of Cbf11-mediated repression of *ctt1*, *gst2*, *pyp2* and *atf1* has been investigated.

6.2.1. Different patterns of the *ctt1*, *gst2*, *pyp2*, and *atf1* upregulation in *cbf11Δ* cells

Interestingly, we observed two distinct patterns of gene expression (RT-qPCR dataset) during oxidative stress in in *cbf11Δ*. Transcripts of *ctt1* (Fig. 13A), *pyp2* (Fig. 13C), and *atf1* (Fig. 13D) are ~5-fold more abundant in untreated *cbf11Δ* compared to wild type. When exposed to hydrogen peroxide, expression of these genes in *cbf11* deficient cells further rises and culminates 30 min after the treatment with subsequent decline in transcript concentration to, or beneath the wild type level in given time points. The expression pattern of *gst2*, in contrast, appears to be completely different. Transcript level of *gst2* is enhanced ~80-fold in unstressed *cbf11Δ* cells compared to wild type. As the oxidative stress proceeds, the mRNA level of *gst2* in *cbf11Δ* cells slowly raises and peaks 60 min after the treatment, while the level of *gst2* transcript was intensively increasing in wild type cells. Unlike *ctt1*, *pyp2*, or *atf1*, only slight decline of *gst2* mRNA concentration has been detected during longer H_2O_2 exposition in either wild type or *cbf11Δ* strain (Fig. 13B), which is consistent with previous survey [144]. This observation, together with our finding that Cbf11 probably do not bind its predicted binding sites (Fig. 8) within promoters of *ctt1*, *gst2*, *pyp2*, and *atf1* (Fig. 15), suggests Cbf11 probably repress investigated genes indirectly through the modulation of at least two distinct pathways.

Spot tests performed by Mgr. Jarmila Tvarůžková discovered that catalase is key enzyme that mediates resistance to H_2O_2 in *cbf11Δ* cells. Despite *gst2* did not shown to be as important as *ctt1* (spot test performed by Mgr. Jarmila Tvarůžková), its excessive upregulation in unstressed *cbf11* deficient cells is worth further exploration, because clarification of cause of such a remarkable enhancement of gene expression might help to uncover the mode of Cbf11 action in the physiology of the cell. To keep discussion straightforward, regulatory mechanism that leads to derepression of *ctt1* and *gst2* in *cbf11Δ* cells will be elaborated separately.

6.2.2. Pap1-dependent upregulation of gst2 in cbf11Δ cells

Several authors have independently shown *gst2* is induced predominantly by transcription factor Pap1 [69, 76, 144], for which Pap1 became our promising candidate regulator that might be responsible for *gst2* upregulation in *cbf11Δ* cells. Thus, genetic interactions of *pap1*, its activity, and DNA binding properties have been studied in wild type and *cbf11Δ* cells.

A substantial decrease of *gst2* transcript level (Fig. 20B) was observed in treated and untreated *pap1Δ* cells compared to wild type, confirming previous studies [69, 76, 144, 147] which identified Pap1 as a key positive regulator of *gst2*. Furthermore, deletion of *pap1* in *cbf11Δ* cells prevented elevation of *gst2* transcript level (observed in single deletion mutant *cbf11*) and decreased it to the similar amount that has been measured in *pap1Δ* cells (Fig. 20B); suggesting Pap1 and Cbf11 operate via same signaling pathway. Because Cbf11 appears to suppress expression of *gst2*, it is likely that Cbf11 inhibits Pap1 signaling. Pap1 activity was therefore established using reporter vector pMP127 (Fig. 21C). Results of β-galactosidase assay consistently showed Pap1 activity is ~2.7 fold higher in *cbf11Δ* cells compared to wild type (Fig. 22).

To further explore Pap1 binding to *gst2* promoter, the chromatin immunoprecipitation was performed. We anticipated higher Pap1 binding to *gst2* promoter in unstressed *cbf11Δ* cells compared to wild type but results were quite unexpected. No remarkable difference in Pap1 binding to *gst2* promoter was observed between unstressed wild type and *cbf11Δ* cells. Pap1 occupancy at *gst2* promoter decreased when wild type cells were exposed to hydrogen peroxide for 30 min, probably as a consequence of oxidative inactivation of Pap1 (described in Fig. 2). If this is true, the enhancement of *gst2* mRNA level in wild type cells should be interrupted after 30 min of exposition to hydrogen peroxide, but it is rather gradually growing (Fig. 13B). On the other hand, Pap1 binding to *gst2* promoter in *cbf11Δ* cells was approximately constant before or after hydrogen peroxide treatment, implicating the loss of *cbf11* might somehow abrogate Pap1 inactivation.

Despite Pap1 should be excluded from the nucleus in unstressed cells [72], its enrichment at the *gst2* promoter was relatively high (compared to negative controls). This binding is probably responsible for basal expression of *gst2* in unstressed wild type cells (Fig. 13B) that was significantly lowered when *pap1* was deleted (Fig. 20B).

ChIP results are obviously not consistent with previous transcription analysis and β-galactosidase assay and our results might differ for several reasons. First, predicted potential Pap1 binding sites in gene promoters do not exactly match with consensual binding sequence that was cloned into pMP127 and it is possible that Pap1 has different affinity to diverse binding sequences. Nonetheless, this option can only explain inconsistencies between results obtained with ChIP and β-galactosidase assay but derepression of *gst2* in *cbf11Δ* cells (which is, according to the Fig. 20B, Pap1-dependent) remains unresolved. Additionally, results of β-galactosidase assay could be compromised by experimental setting. Reporter vector pMP127 carries selection marker *LEU2* for which we were forced to cultivate cells in defined EMM medium depleted of leucine instead of YES medium. Phenotypes that are typical for *cbf11Δ* cells are considerably diminished in EMM medium (personal communication with Dr. Převorovský); thus our results could be artificially decreased, implying inconsistency between ChIP and β-galactosidase assay might be even more pronounced. Second, Pap1-dependent upregulation of *gst2* in *cbf11Δ* cells might be caused by Pap1 indirectly. Third, results might be affected by the fact that all measured values are population averages. Population of *cbf11* deletion mutants is very heterogenic and contains different cells expressing broad range of different phenotypes (personal communication with Dr. Převorovský). Thus, excessive upregulation of *gst2* in sufficiently large fraction of the population can significantly increase *gst2* transcript concentration in whole culture when compared to wild type. Since ChIP quantifies gDNA bound by Pap1, the same fraction of population cannot increase an average signal to the extent measured by RT-qPCR (given cell might produce thousands of *gst2* mRNA copies but Pap1 can bind only one *gst2* promoter).

6.2.3. The crosstalk between Pap1 and Sty1/Atf1 pathways in *gst2* regulation

We have also observed previously described [65, 66] corroboration between Sty1/Atf1 and Pap1 pathways in *gst2* regulation. Continuous expression of *gst2* was impaired in *sty1Δ* or *atf1Δ* cells (Fig. 16B and 17B) during oxidative stress. This observation is not surprising, because Sty1/Atf1 signaling was identified as key inductor of *srx1*, which is responsible for Pap1 reactivation during late phases of oxidative stress [65, 66]. In contrast, deletion of *atf1* in *cbf11Δ* cells did not profoundly change *gst2* expression profile in this strain (Fig. 17B). Our data therefore demonstrate that functional Sty1/Atf1 pathway is, consistently with literature, needed for proper *gst2* expression during

oxidative stress in wild type cells while in cells with *cbf11* deletion *atf1* seems to be dispensable for *gst2* upregulation.

Additionally, deletion of *sty1* in both wild type and *cbf11Δ* cells interestingly increased basal *gst2* expression (Fig. 16B) via unknown mechanism that is likely Atf1-independent for no Atf1 binding has been detected in gst2 promoter [94].

6.2.4. Proposed mechanism of Cbf11-mediated regulation of *gst2*

It is probable that *gst2* is in *cbf11Δ* upregulated via transcription factor Pap1, whose nuclear fraction might be enlarged as Pap1 exerted higher activity in strain deficient in *cbf11*. Since Cbf11 is nuclear protein [126], its absence could potentially impair proper nuclear export of Pap1. Because oxidation of Pap1 cysteines is the sole process that has been shown to inhibit Crm1-mediated nuclear export of Pap1 [72] and only oxidized Pap1 might regulate gene expression [134], it is possible that Cbf11 could modulate redox state of nuclear Pap1 pool. This hypothesis is supported by the finding that Cbf11 physically interacts with Pap1 [148]. To explore this possibility, a novel method for investigation of redox state of cysteines in Pap1 was introduced to our laboratory (Fig. 30) but we failed to get reproducible data. This tool will be therefore used for Pap1 redox state investigation in the future.

Another possible explanation for hyperactivation of Pap1 in *cbf11Δ* cells is that Cbf11 might negatively regulate interaction between Pap1 and transcription factor Prr1 (constitutively nuclear transcription factor which interacts with oxidized Pap1 and mediates its sequence-specific association with DNA [134]), for physical interaction between Prr1 and Cbf11 has been also published [148]. Furthermore, *gst2* is also regulated by Sty1 kinase that is important for *gst2* upregulation especially during later phases of oxidative stress in *cbf11Δ* cells. Sty1-dependent continuous *gst2* expression might be mediated by sulfiredoxin Srx1. This is supported by spot test performed by Mgr. Jarmila Tvarůžková which revealed Srx1 is important for the resistance of *cbf11Δ* strain to oxidative stress. Dr. Převorovský moreover found *srx1* transcript is 7.8 times more abundant in unstressed *cbf11Δ* cells compared to wild type. Interestingly, Atf1, the major substrate of Sty1 kinase, which is essential for *srx1* upregulation in wild type cells as well, is probably not important for *gst2* expression when *cbf11* is lost. These conclusions are visualized in Fig. 33.

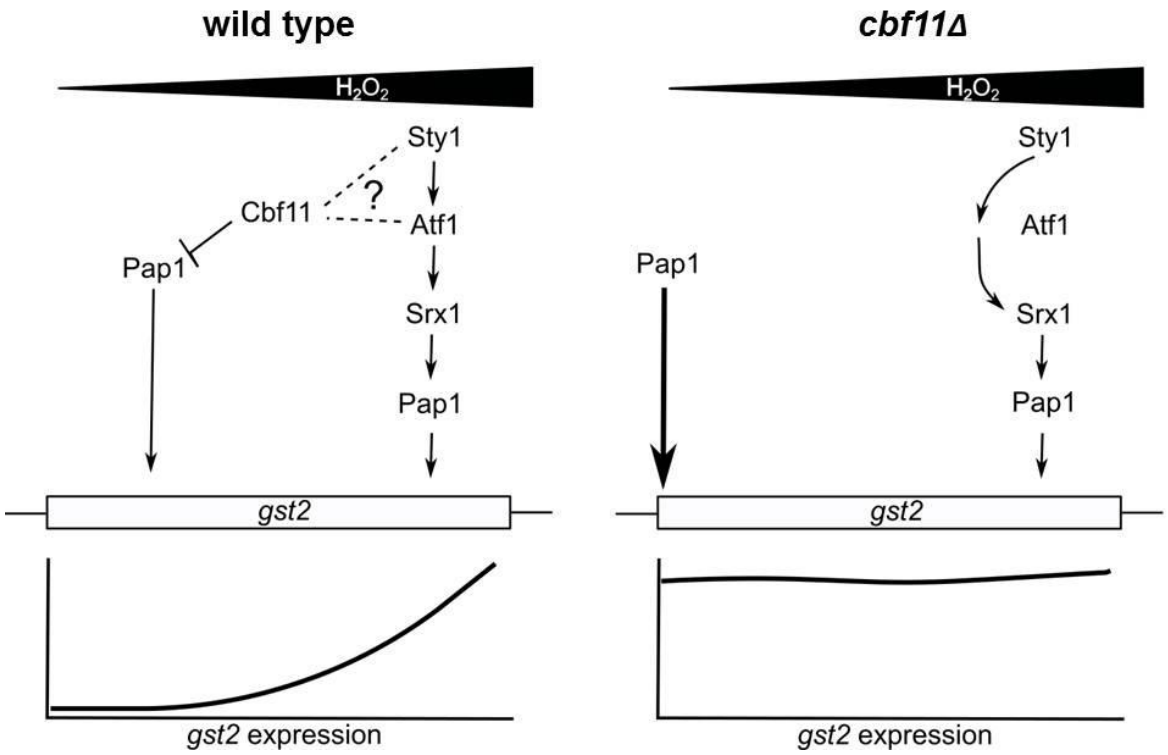

Fig. 33 – Proposed model of Cbf11 influence on the expression of *gst2* gene. The picture visualizes summarization of our data and their interpretation. Cbf11 appears to be negative regulator of transcription factor Pap1 and consequently also of *gst2* gene. Cbf11 probably helps to keep Pap1 inactive in unstressed wild type cells. During oxidative stress, Pap1 is activated and induces *gst2* expression that is sustained by Sty1/Atf1-dependent induction of Srx1 which enables reactivation of Pap1 during prolonged or intense oxidative stress. In *cbf11Δ* cells, Pap1 is active even before hydrogen peroxide treatment and augments *gst2* expression. This augmentation is also dependent on Sty1 kinase, however, Atf1 does not appear to be necessary for Srx1 induction, suggesting loss of Cbf11 alters also Sty1/Atf1 pathway.

6.2.5. Pap1-dependent upregulation of *ctt1* in *cbf11Δ* cells

It has been previously shown that transcription factor Pap1 might be employed in transcriptional activation not only of *gst2* but also of *ctt1* gene during minor oxidative stress [69, 134] (and during moderate or intense oxidative stress through Sty1/Atf1-dependent activation of Srx1 that indirectly reconstitutes the Pap1 activity [65, 66]). Hence, we analyzed influence of transcription factor Pap1 on *ctt1* gene, whose expression pattern (Fig. 13A) pronouncedly differs from the expression pattern of *gst2* (Fig. 13B) in *cbf11Δ* cells.

6.2.5.1. The employment of Pap1 in *ctt1* regulation

Our data, consistently with literature [69, 134], provided an evidence that Pap1 is actually important also for *ctt1* upregulation. Catalase expression was remarkably decreased after the treatment with H_2O_2 in *pap1Δ* cells compared to wild type. Nonetheless, its basal expression was in *pap1Δ* cells (when compared to wild type) unchanged, indicating Pap1 is required for intense catalase upregulation during oxidative stress but does not, in contrast to *gst2* regulation, affect basal expression of *ctt1* (Fig. 20A). This statement is supported by ChIP results that detected only poor Pap1 enrichment in CP2 region (locus containing three predicted potential Pap1 binding sites; see Fig. 23A) of *ctt1* promoter in unstressed cells. Pap1 was significantly enriched in CP2 region only when cells were exposed to hydrogen peroxide (Fig. 26). Our observation is consistent with [134] and in accordance with widely accepted regulatory mechanism of Pap1 (Fig. 2) that allows its DNA binding only after ROS-mediated nuclear accumulation [73, 74, 134]. The question why is Pap1 able to sustain basal expression of *gst2* (Fig. 20B and Fig. 27) but not *ctt1* in unstimulated cells remains unresolved. It is possible that Pap1 is recruited to different promoters with different affinity. This is supported by the fact that sequences of predicted Pap1 binding sites in CP2 and GP3 regions (Fig. 23A) are not identical. Additionally, Pap1 binding to DNA might be affected by hypothetically different composition and the abundance of DNA-binding-protein complexes localized within promoter regions of *ctt1* and *gst2*.

6.2.5.2. The mechanism of Pap1-dependent upregulation of *ctt1* in *cbf11Δ* cells

Since Pap1 seems to act as an important inductor of *ctt1* gene in response to oxidative stress (Fig. 20A and Fig. 26) [69, 134] and Cbf11 has been identified as potential negative regulator of Pap1 signaling pathway (Fig. 20 and Fig. 22), Cbf11 should be involved in Pap1 signaling also in the case of *ctt1* regulation, and Cbf11 absence should positively influence expression of *ctt1* in Pap1-dependent manner. Performed experiments confirmed this hypothesis with the discovery that the pattern of *ctt1* stress-related expression was similarly decreased in *pap1Δ* and *pap1Δ cbf11Δ* cells (Fig. 20A), suggesting that Cbf11 and Pap1 indeed operate within the same pathway in the regulation of both *ctt1* and *gst2* genes; the stress-induced upregulation of *ctt1* in *cbf11Δ* cells was furthermore Pap1 dependent for deletion of *pap1* in treated *cbf11Δ* cells resulted in profound decline of *ctt1* transcript levels (Fig. 20A).

Similarly to wild type cells, ChIP does not show any augmented enrichment of Pap1 in the *ctt1* promoter in unstressed *cbf11Δ* (Fig. 26) despite the increased activity of Pap1 that has been detected in unstressed *cbf11* deficient cells (Fig. 22). Pap1 therefore seems to bind *ctt1* promoter for some reason only after hydrogen peroxide treatment in both *cbf11Δ* and wild type cells. Importantly, Pap1 occupancy at *ctt1* promoter was significantly higher in treated *cbf11Δ* strain (Fig. 26), supporting our hypothesis that activity of transcription factor Pap1 is increased in *cbf11Δ* cells. Although, it is good to keep in mind that ChIP results might be potentially compromised by several artifacts discussed above (see chapter 6.2.2.).

These data (summarized in Fig. 34) together suggest oxidative stress-related upregulation of *ctt1* in *cbf11Δ* cells is partially mediated by transcription factor Pap1. However, derepression of basal *ctt1* activity observed in *cbf11Δ* was not completely abrogated in *pap1Δ cbf11Δ* cells and limited but substantial upregulation of *ctt1* was measured during early phases of oxidative stress in *pap1Δ cbf11Δ* strain. This phenomenon is probably caused by another regulator that should be also influenced by Cbf11 loss.

6.2.5.3. Sty1-dependent upregulation of *ctt1* in *cbf11Δ* cells

Interestingly, *ctt1* has been shown to be regulated by either Pap1 or Atf1 transcription factors [69, 149]. Together with our previous discovery that Sty1/Atf1 signaling is altered in *cbf11* deficient cells (Fig. 33 and Fig. 34) it is therefore possible that the upregulation of *ctt1* in *cbf11Δ* cells might be directly mediated via Sty1/Atf1 pathway. Thus, the influence of Sty1/Atf1 signaling on *ctt1* expression in wild type and *cbf11Δ* cells has been explored.

Large body of evidence declares catalase belongs to the CESR genes and its transcription is beside Pap1 also induced via heterodimer Atf1/Pcr1 and its upstream activator kinase Sty1 in response to environmental stress [42, 69, 89, 94, 95, 140]. In agreement with literature [80, 149], mRNA levels of *ctt1* were profoundly reduced in unstimulated *sty1Δ* cells compared to wild type. Gentle elevation of catalase transcript was observed in stressed *sty1Δ* cells, but it was circa 100-times less abundant than wild type *ctt1* mRNA pool (Fig. 16A). Certain level of catalase transcription might be probably maintained by Pap1 during oxidative stress (Fig.20A and Fig. 26). Expression profile of *ctt1* in H_2O_2-treated *atf1Δ* cells strongly resembled catalase induction in *sty1* deficient strain (Fig. 17A). Thus, Sty1 activates catalase, in accordance with literature [89], via its

downstream target - transcription factor Atf1. Basal and stress-induced upregulation of catalase in *cbf11Δ* cells was abolished in double deletion mutant *sty1Δ cbf11Δ*, whose *ctt1* expression profile was very similar to single *sty1Δ* cells (Fig. 16A), suggesting Cbf11 and Sty1 are employed in the same pathway. Intriguingly, deletion of *atf1* in *cbf11Δ* cells caused relatively small decrease in *ctt1* mRNA level (Fig. 17A).

These data together indicate that contribution of Sty1 and Atf1 to the *ctt1* induction is equal in wild type, which is (similarly to *gst2* regulation; chapter 6.2.4., Fig. 17B and Fig. 33) not true in *cbf11Δ* cells, where upregulation of catalase is Sty1-dependent but Atf1 is not required anymore. Our conclusions are graphically depicted in Fig. 34.

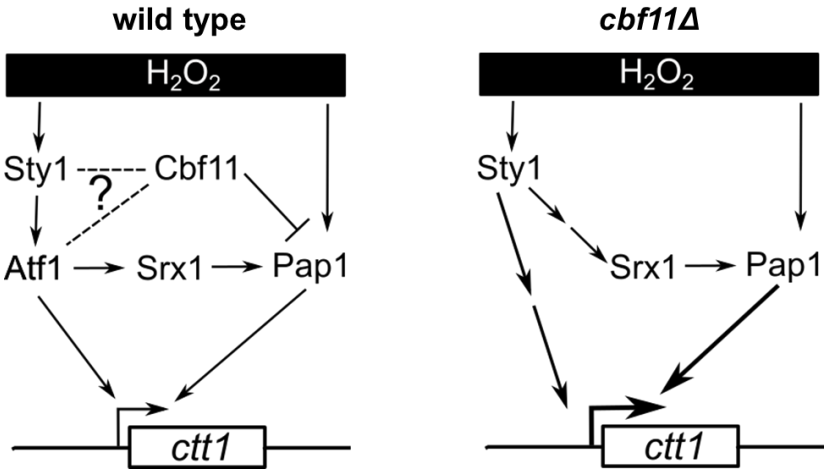

Fig. 34 – Pap1-dependent and Sty1-dependent regulation of *ctt1* gene in wild type and *cbf11Δ* cells. The presence of hydrogen peroxide activates transcription factor Pap1 that induces catalase expression in wild type cells. If stressor is not eliminated, Pap1 is oxidatively inactivated and CESR genes, including catalase and Srx1, are induced through Sty1/Atf1 pathway to cope with the stressor. Srx1 subsequently reactivates Pap1 which corroborates with Atf1 in induction of *ctt1* transcription. In unstressed *cbf11Δ* cells, however, Sty1 appears to increase basal expression of *ctt1* Atf1-independently. This mechanism might also lead to the induction of Srx1 (expression data of Dr. Převorovský). Activity of Pap1 should be enhanced in untreated *cbf11Δ* but it has, according to our data, only negligible effect on *ctt1* expression. In the presence of hydrogen peroxide, both pathways are activated, inducing together expression of catalase that is profoundly higher in *cbf11Δ* cells when compared to wild type. Cbf11 therefore seems to be negative regulator of both Pap1 and Sty1 signaling.

6.3. Alterations in Sty1/Atf1 pathway caused by the *cbf11* loss

We have revealed Sty1 is essential for upregulation of *ctt1* in wild type and *cbf11Δ* cells (Fig. 16A), which is not surprising since Sty1 is known and thoroughly studied inductor of CESR genes [42]. Genes *atf1* and *pyp2* belong to the CESR gene group [42] and are, according to our present knowledge, almost exclusively regulated by SAPK pathway [42, 69, 86, 88, 89, 90, 91, 94]. Thus, their expression should be regulated via Sty1 in *cbf11Δ* cells as well. We therefore assumed upregulation of these genes (Fig. 13) can be caused by increased activity of Sty1 in *cbf11Δ* cells. Additionally, we have found interesting alteration of signal transduction within Sty1/Atf1 pathway when Cbf11 was absent (Fig. 33 and Fig. 34). In order to explain these phenomena, we have assessed the amount and the activity of Sty1 in wild type and *cbf11* deficient cells and explored genetic interactions of important SAPK regulators and effectors (*sty1*, *atf1*, and *pyp2*).

6.3.1. The phosphorylation state of Sty1 kinase

Total amounts of Sty1 and its phosphorylated fraction Sty1-P were examined in wild type and *cbf11Δ* cells. Because Sty1 is crucial positive regulator of stress response in *S. pombe* [42, 69, 94], unphosphorable mutants of Sty1 are as sensitive to stress as *sty1Δ* cells are [88], *cbf11Δ* cells exert Sty1-dependent upregulation of stress responsive genes (Fig. 16), and *cbf11*-deficient cells are resistant to oxidative stress (Fig. 6), we expected that Sty1 would be rather constitutively hyperphosphorylated and active in *cbf11Δ* cells. In strong contrast to our expectations, activatory hyperphosphorylation of Sty1 seems to be prohibited in strains with deleted *cbf11Δ* (Fig. 19A, B). More detailed analysis provided evidence that hydrogen peroxide treatment actually leads to the Sty1-P accumulation in both wild type and *cbf11Δ* cells, but phosphorylation of Sty1 in *cbf11Δ* cells is rather transient (Fig. 19C). Cells with deletion of *cbf11* comprise enhanced mRNA levels of phosphatases *pyp2*, *pyp1*, and *ptc1* (Fig. 32) that have been reported to dephosphorylate Sty1 [85]–[87]. Thus, the most straightforward and simple explanation for decreased Sty1-P levels in *cbf11Δ* cells is that increased activity of these phosphatases quenches Sty1 activation. Sty1, the upstream activator of *ctt1*, *gst2*, *pyp2*, and *atf1* genes, is apparently not more active in *cbf11Δ* than in wild type. Therefore mechanism through which *ctt1*, *gst2*, *pyp2*, and *atf1* are Sty1-dependently induced in *cbf11Δ* is unknown.

6.3.2. Negative feedback loop of Sty1/Atf1 pathway

Unexpectedly, obtained data suggest there might be increased activity of phosphatases Pyp2, Pyp1, and Ptc1 (Fig. 13C, Fig. 19, and Fig. 32), which are responsible for quenching of Sty1 signal [85–87], rather than predicted accumulation of active Sty1-P in *cbf11Δ* cells. Hence, the negative feedback loop of Sty1/Atf1 pathway, represented predominantly by phosphatase Pyp2, has been researched in detail. We have described expression profiles of *pyp2* in stress and non-stress conditions, investigated the dependence of *pyp2* expression on its upstream regulators Sty1 and Atf1, and proposed model how Pyp2 affects gene expression in *cbf11Δ* strain.

6.3.2.1. Expression pattern of *pyp2* in wild type and *cbf11Δ*

Deletion of *cbf11* resulted in upregulation of *pyp2* (Fig. 13C). Cbf11 furthermore seems to regulate *pyp2* via Sty1/Atf1 signaling pathway for expression of *pyp2* during oxidative stress is similarly decreased in both single deletion mutants *sty1Δ* and *atf1Δ* compared to double deletion mutants *sty1Δ cbf11Δ* and *atf1Δ cbf11Δ* (Fig. 16C and Fig. 17C). Sty1 and Atf1 are therefore essential for induction of *pyp2* when both wild type and *cbf11Δ* cells are exposed to hydrogen peroxide. Basal *pyp2* transcript concentration remained in *sty1Δ* and *sty1Δ cbf11Δ* strains unchanged (approximately at the wild type level), suggesting *pyp2* is induced only in stress conditions, which has been postulated by Millar *et al.* [85] before. However, increased basal activity of *pyp2* was detected not only in *cbf11Δ* strain. Deletion of *atf1* surprisingly increased basal expression of *pyp2* compared to wild type cells as well. It has been shown earlier that Atf1 might rarely repress expression of certain genes, probably via chromatin remodeling [42, 98, 99]. In the case of *pyp2*, which is being activated only during stress conditions, Atf1 might inhibit its activation till it receives activatory phosphorylation from Sty1. Double deletion mutant *atf1Δ cbf11Δ* exerts very similar *pyp2* basal activity to *cbf11Δ* cells. Thus, deletion of *cbf11* results in upregulation of *pyp2*, but Sty1 and Atf1 are dominant and essential regulators of its stress-induced expression.

6.3.2.2. The influence of phosphatase Pyp2 on the expression of Sty1-dependent genes in *cbf11Δ* cells

Additionally, as Pyp2 phosphatase is responsible for attenuation and accurate termination of Sty1-mediated stress response [86], the observed reduction of *ctt1* and *pyp2*

mRNA levels detected 60 min posterior the treatment in *cbf11Δ* cells (compared to wild type) (Fig. 13) can be explained if Sty1/Atf1 signaling participates in the upregulation of *ctt1* and *pyp2*. Wild type amount of Pyp2 has been shown to abolish Sty1 signaling in about 30 min upon the stress stimulus; when expression of *pyp2* simultaneously reaches its peak [85, 86, 88]. This pattern of *pyp2* expression can be observed in Fig. 13C as well. We assumed that augmented levels of *pyp2* mRNA (Fig. 13B) should lead to the increased Pyp2 production in *cbf11Δ* cells. Thus, potential reinforcement of Pyp2 phosphatase activity (and potential increase of activity of phosphatase Pyp1 – Fig. 32) in the *cbf11* deficient cells might accelerate signal annulment and subsequently contribute to the profound loss of *ctt1* and *pyp2* transcript levels during late phases of oxidative stress (60 and 120 min after the treatment) (Fig. 13A, C).

6.3.3. The role of Atf1 in *ctt1* and *pyp2* upregulation in *cbf11Δ* cells

Despite the fact that Sty1 exerted rather decreased level of activatory phosphorylation in *cbf11Δ* cells (Fig. 19), the observed upregulation of CESR genes *ctt1* and *pyp2* might be caused by upregulated *atf1* (Fig. 13D) in this strain. Upregulation of Atf1 mediated by Sty1-dependent stabilization of *atf1* transcript has been already described [139]. Because Cbf11 probably do not bind promoter of *atf1* (Fig. 15), the stabilization of *atf1* mRNA might be the cause of its derepression in *cbf11Δ* cells. The ability of Atf1 to trigger transcription of either *ctt1* and *pyp2* (and whole CESR group of genes) in response to stress stimuli [42, 94], suggests higher concentration of Atf1 in *cbf11Δ* cells might result in derepression of large subset of genes. Furthermore, upregulation of all investigated genes (*ctt1*, *gst2*, *pyp2*, and *atf1*) was, consistently with [139], Sty1-dependent (Fig. 16) in both wild type and *cbf11* deficient strain. On the other hand, gene derepression in *cbf11Δ* cells shown striking Atf1-independence (except *pyp2*) for which is the hypothesis described above falsified and the mechanism of Cbf11 function in Sty1/Atf1 pathwayis still unknown.

Interestingly, deletion of *sty1* had a pronounced effect on the *atf1* expression. Not only *atf1* induction was impaired in *sty1 Δ* cells, but even reduction in its total mRNA pool has been detected after the treatment with hydrogen peroxide (Fig. 16D). This *atf1* transcript level reduction might be caused by hydrogen peroxide induced mRNA decay that is in wild type cells prevented by oxidized Sty1 and its cooperation with RNA-binding protein Csx1 [139, 150].

6.4. Proposed models of Cbf11 mechanism of action

Taken all data together, we have identified transcription factor Cbf11 as indirect negative regulator of *ctt1*, *gst2*, *pyp2* and *atf1* genes. The observation that Cbf11 repress these genes indirectly is surprising since CSL transcription factors suppress transcription of target genes directly in metazoa [117, 123, 151]. Two signaling stress responsive pathways – Pap1 and Sty1/Atf1 seem to be functionally connected to Cbf11. These two pathways are essential for upregulation of catalase, enzyme that executes H_2O_2 detoxification and is responsible for resistance of *cbf11Δ* cells to this compound. While Pap1 activity might be increased in *cbf11Δ* cells, the relationship between Sty1/Atf1 pathway and Cbf11 is much more complicated. Sty1 is a key molecule for upregulation of all investigated genes, but it is probably not more active in *cbf11Δ* cells and Atf1 is not important (except for *pyp2*) for upregulation of *ctt1* and *gst2* in *cbf11Δ* cells. Sty1 might therefore, hypothetically, utilize distinct substrate in induction of these genes in *cbf11Δ*. But it is not known which protein is directly affected by Cbf11 loss, or conversely, what is the exact function of Cbf11 in wild type cells. Investigated and proposed relationships between Cbf11 and relevant components of stress response signaling are illustrated in Fig. 35.

Observed activation of oxidative stress response pathways might also suggest *cbf11Δ* cells suffer some kind of metabolic imperfection that elevates endogenous ROS concentration, triggering stress response in this manner. This hypothesis is being investigated by other co-workers and is supported by the discovery that pretreatment with H_2O_2 increases resistance of cells to oxidative stress [152]. However, the upregulation of studied genes in *cbf11Δ* cells is Atf1-independent (except *pyp2*) and therefore probably not caused by higher endogenous ROS production, because signal from H_2O_2 sensors (Mak2, Mak3) should be transduced to target genes via canonical signaling (through Atf1) in this case [79].

Alternatively, there is also another explanation for observed phenomena. Expression of stress-responsive genes in *Saccharomyces cerevisiae* is widely influenced by their mRNA stability [153]. Pathways of stress response signaling are conserved in *S. pombe* and *S. cerevisiae* [2] and it is therefore possible that Cbf11 facilitates specific mRNA degradation. Thus, deletion of *cbf11* and consequent augmentation of specific transcript might be wrongly interpreted as enhanced transcription. Transcriptome analysis and mathematical modeling suggest that mRNA decay is employed in gene expression

regulation in *S. pombe*, but the Atf1-dependent genes are regulated predominantly at the transcriptional level [154]. Since Atf1 does not appear to be involved in *cbf11Δ* cells resistance to oxidative stress, regulation via mRNA stability is also possible.

These explanations should be definitely investigated in the future to provide complex view on the role of transcription factor Cbf11 in the fission yeast physiology.

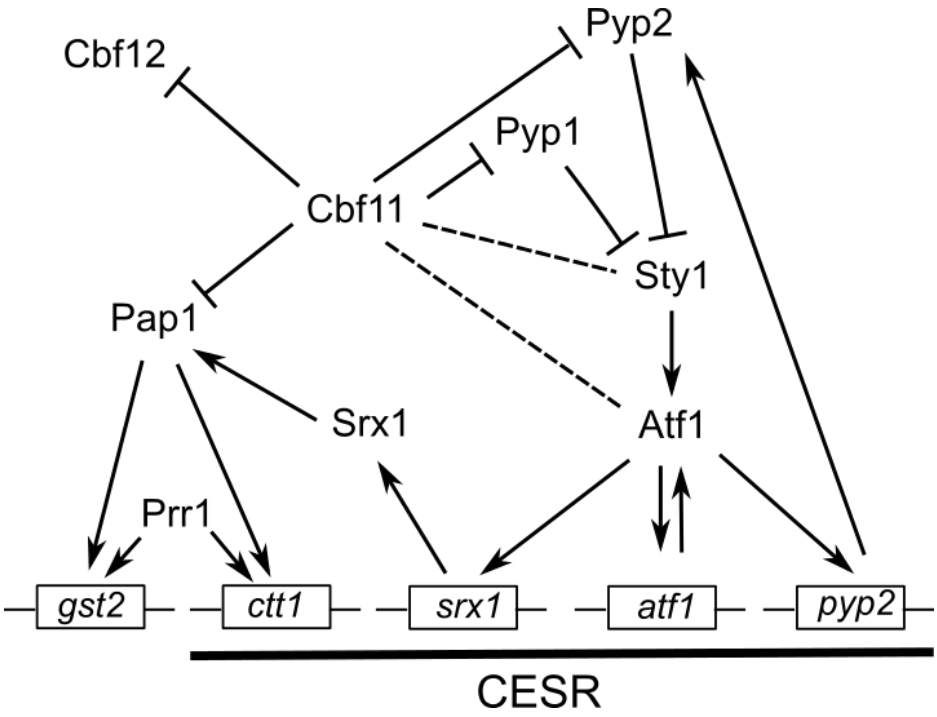

Fig. 35 – Schematic illustration depicting regulatory relationships between Cbf11 and signaling pathways of oxidative stress response. Proposed scheme depicts relationships between Cbf11, Cbf12 and regulators of stress response in general. It does not reflect physical interactions of proteins or exact mechanisms of their action. Our data suggest Cbf11 acts as negative regulator of its paralog Cbf12 (which does not appears to be important for response to oxidative stress in *S. pombe*) and Pap1 pathway. Additionally, Cbf11 probably regulate expression of phosphatases Pyp1 and Pyp2 that are negative regulators of Sty1/Atf1 pathway. We have produced an evidence for Cbf11 employment in Sty1/Atf1 signaling, but its particular contribution for this pathway remains unknown. According to RT-qPCR data, depicted genes are upregulated in *cbf11Δ* cells in Sty1-dependent manner, which seems to be contradictory to negative influence of Cbf11 on Pyp2 and Pyp1. Thus, it is complicated to deduce mechanistic model of Cbf11 function in Sty1/Atf1 pathway from available data. This intricate regulatory circuit should be subjected to further research in the future. In general, overall activity of Cbf11 towards response to oxidative stress can be probably described as inhibitory.

7. CONCLUSIONS

- The transcript levels of *ctt1*, *gst2*, *pyp2*, *atf1*, *cbf11*, and *cbf12* were established in wild type, *cbf11Δ*, and *cbf12Δ* cells in normal conditions and during oxidative stress of moderate intensity. Results of this analysis showed transcription factor Cbf11 acts as a negative regulator of investigated genes while Cbf12 probably does not affect their mRNA levels.
- On the basis of previously performed ChIP-seq (Dr. Převorovský), putative Cbf11 binding sites in the promoters of *ctt1*, *gst2*, *pyp2*, and *atf1* were predicted. Chromatin immunoprecipitation for TAP-tagged Cbf11, however, did not show any relevant enrichment of this transcription factor in predicted genes. It has been therefore concluded that Cbf11 modulates response to oxidative stress in *S. pombe* rather indirectly.
- Four novel strains – *sty1Δ cbf11Δ*, *atf1Δ cbf11Δ*, *pap1+(3Pk) cbf11Δ*, and *pap1Δ* – were prepared for analysis of Cbf11 influence on Sty1 and Pap1 signaling.
- RT-qPCR provided evidence that observed upregulation of *ctt1*, *gst2*, *pyp2*, and *atf1* in *cbf11Δ* strain is Sty1-dependent and upregulation of *ctt1* and *gst2* is, additionally, Pap1-dependent in *cbf11Δ* cells. Moreover, it has been shown that Cbf11 is functionally connected with Pap1 and Sty1/Atf1 signaling.
- Reporter vector pMP127 for Pap1 activity measurement was constructed.
- β-galactosidase expressed from pMP127 showed increased activity of Pap1 in unstressed in *cbf11Δ* cells, suggesting Cbf11 might negatively regulate transcription factor Pap1.
- Pap1 binding sites in the promoter regions of *ctt1*, *gst2*, were obtained from available literature or predicted by computational analysis. In contrast to previous results, chromatin immunoprecipitation for Pk-tagged Pap1 detected increased Pap1 enrichment in predicted binding sites only during oxidative stress in *cbf11Δ* cells compared to wild type.
- Novel method for investigation of Pap1 cysteines redox state was introduced to our laboratory for further exploration of Cbf11 influence on Pap1 activity and redox state.
- The activity of Sty1 was investigated by western blotting. Interestingly, the level of phosphorylated Sty1 is profoundly decreased in stressed *cbf11Δ* cells compared to

wild type. However, loss of Cbf11 does not prevent Sty1 activation; it rather appears to alter signaling dynamics, probably through Atf1-dependent upregulation of phosphatase *pyp2*. Cbf11 might be therefore important for fine-tuning of Sty1 signaling in wild type cells.

8. REFERENCES

[1] W. Dröge, "Free Radicals in the Physiological Control of Cell Function.," *Physiol. Rev.*, vol. 82, pp. 47–95, 2002.

[2] M. A. Papadakis, C. T. Workman, "Oxidative Stress Response Pathways: Fission Yeast as Archetype.," *Crit. Rev. Microbiol.*, vol. 7828, pp. 1–16, 2014.

[3] M. Kamarehei, R. Yazdanparast, "Modulation of Notch Signaling Pathway to Prevent H2O2/Menadione-Induced SK-N-MC Cells Death by EUK134.," *Cell. Mol. Neurobiol.*, vol. 34, pp. 1037–45, 2014.

[4] F. Xie, W. Cai, Y. Liu, Y. Li, B. Du, L. Feng, L. Qiu, "Vaccarin Attenuates the Human EA.hy926 Endothelial Cell Oxidative Stress Injury Through Inhibition of Notch Signaling.," *Int. J. Mol. Med.*, vol. 35, pp. 135–42, 2015.

[5] E. Cadenas, K. J. Davies, "Mitochondrial Free Radical Generation, Oxidative Stress, and Aging.," *Free Radic. Biol. Med.*, vol. 29, pp. 222–30, 2000.

[6] J. F. Turrens, "Mitochondrial Formation of Reactive Oxygen Species.," *J. Physiol.*, vol. 552, pp. 335–44, 2003.

[7] A. Perner, L. Andresen, G. Pedersen, J. Rask-Madsen, "Superoxide Production and Expression of NAD(P)H Oxidases by Transformed and Primary Human Colonic Epithelial Cells.," *Gut*, vol. 52, pp. 231–6, 2003.

[8] A. F. Miller, "Superoxide Dismutases: Active Sites that Save, But a Protein that Kills.," *Curr. Opin. Chem. Biol.*, vol. 8, pp. 162–8, 2004.

[9] B. Chance, H. Sies, A. Boveris, "Hydroperoxide Metabolism in Mammalian Organs.," *Physiol. Rev.*, vol. 59, pp. 527–605, 1979.

[10] T. G. Gabig, B. M. Babior, "The O2(-) -Forming Oxidase Responsible for the Respiratory Burst in Human Neutrophils. Properties of the Solubilized Enzyme.," *J. Biol. Chem.*, vol. 254, pp. 9070–4, 1979.

[11] N. Kaul, H. J. Forman, "Activation of NF kappa B by the Respiratory Burst of Macrophages.," *Free Radic. Biol. Med.*, vol. 21, pp. 401–5, 1996.

[12] M. F. Neurath, C. Becker, K. Barbulescu, "Role of NF-kappa B in Immune and Inflammatory Responses in the Gut," *Gut*, vol. 43, pp. 856–860, 1998.

[13] Z. Sun, R. Andersson, "NF-kappaB Activation and Inhibition: A Review.," *Shock*, vol. 18, pp. 99–106, 2002.

[14] C. C. Winterbourn, M. B. Hampton, J. H. Livesey, A. J. Kettle, "Modeling the Reactions of Superoxide and Myeloperoxidase in the Neutrophil Phagosome: Implications for Microbial Killing.," *J. Biol. Chem.*, vol. 281, pp. 39860–9, 2006.

[15] A. Levine, R. Tenhaken, R. Dixon, C. Lamb, “H2O2 from the Oxidative Burst Orchestrates the Plant Hypersensitive Disease Resistance Response.,” *Cell*, vol. 79, pp. 583–93, 1994.

[16] P. D. Ray, B. W. Huang, Y. Tsuji, “Reactive Oxygen Species (ROS) Homeostasis and Redox Regulation in Cellular Signaling.,” *Cell. Signal.*, vol. 24, pp. 981–90, 2012.

[17] M. Sundaresan, Z. X. Yu, V. J. Ferrans, K. Irani, T. Finkel, “Requirement for Generation of H2O2 for Platelet-Derived Growth Factor Signal Transduction.,” *Science*, vol. 270, pp. 296–9, 1995.

[18] T. Meng, T. Fukada, N. K. Tonks, “Reversible Oxidation and Inactivation of Protein Tyrosine Phosphatases *in vivo*.,” *Mol. Cell*, vol. 9, pp. 387–99, 2002.

[19] J. H. Seo, Y. Ahn, S. Lee, C. Yeol Yeo, K. Chung Hur, “The Major Target of the Endogenously Generated Reactive Oxygen Species in Response to Insulin Stimulation is Phosphatase and Tensin Homolog and not Phosphoinositide-3 Kinase (PI-3 kinase) in the PI-3 Kinase/Akt Pathway.,” *Mol. Biol. Cell*, vol. 16, pp. 348–57, 2005.

[20] S. R. Lee, K. S. Yang, J. Kwon, C. Lee, W. Jeong, S. G. Rhee, “Reversible Inactivation of the Tumor Suppressor PTEN by H2O2.,” *J. Biol. Chem.*, vol. 277, pp. 20336–42, 2002.

[21] C. C. Winterbourn, M. B. Hampton, “Thiol Chemistry and Specificity in Redox Signaling.,” *Free Radic. Biol. Med.*, vol. 45, pp. 549–61, 2008.

[22] C. R. Reczek, N. S. Chandel, “ROS-Dependent Signal Transduction.,” *Curr. Opin. Cell Biol.*, vol. 33C, pp. 8–13, 2014.

[23] Y. M. W. Janssen-Heininger, B. T. Mossman, N. H. Heintz, H. J. Forman, B. Kalyanaraman, T. Finkel, J. S. Stamler, S. G. Rhee, A. Van der Vliet, “Redox-Based Regulation of Signal Transduction: Principles, Pitfalls, and Promises.,” *Free Radic. Biol. Med.*, vol. 45, pp. 1–17, 2008.

[24] M. S. Cooke, M. D. Evans, M. Dizdaroglu, J. Lunec, “Oxidative DNA Damage: Mechanisms, Mutation, and Disease.,” *FASEB J.*, vol. 17, pp. 1195–214, 2003.

[25] A. Acharya, I. Das, D. Chandhok, T. Saha, “Redox Regulation in Cancer: A Double-Edged Sword with Therapeutic Potential.,” *Oxid. Med. Cell. Longev.*, vol. 3, pp. 23–34, 2010.

[26] J. Styskal, H. Van Remmen, A. Richardson, A. B. Salmon, “Oxidative Stress and Diabetes: What Can We Learn About Insulin Resistance from Antioxidant Mutant Mouse Models?,” *Free Radic. Biol. Med.*, vol. 52, pp. 46–58, 2012.

[27] B. Halliwell, “Oxidative Stress and Neurodegeneration: Where Are We Now?,” *J. Neurochem.*, vol. 97, pp. 1634–58, 2006.

[28] R. Dumitrascu, J. Heitmann, W. Seeger, N. Weissmann, R. Schulz, “Obstructive Sleep Apnea, Oxidative Stress and Cardiovascular Disease: Lessons from Animal Studies.,” *Oxid. Med. Cell. Longev.*, vol. 2013, p. 234631, 2013.

[29] M. Dizdaroglu, P. Jaruga, “Mechanisms of Free Radical-Induced Damage to DNA.,” *Free Radic. Res.*, vol. 46, pp. 382–419, 2012.

[30] J. Cadet, J. L. Ravanat, M. TavernaPorro, H. Menoni, D. Angelov, “Oxidatively Generated Complex DNA Damage: Tandem and Clustered Lesions.,” *Cancer Lett.*, vol. 327, pp. 5–15, 2012.

[31] B. S. Berlett, E. R. Stadtman, “Protein Oxidation in Aging, Disease, and Oxidative Stress.,” *J. Biol. Chem.*, vol. 272, pp. 20313–6, 1997.

[32] T. Jung, T. Grune, “The Proteasome and Its Role in the Degradation of Oxidized Proteins.,” *IUBMB Life*, vol. 60, pp. 743–52, 2008.

[33] C. A. Ross, M. A. Poirier, “Protein Aggregation and Neurodegenerative Disease.,” *Nat. Med.*, vol. 10, pp. S10–7, 2004.

[34] T. Pohle, T. Brzozowski, J. C. Becker, I. R. Van der Voort, A. Markmann, S. J. Konturek, A. Moniczewski, W. Domschke, J. W. Konturek, “Role of Reactive Oxygen Metabolites in Aspirin-Induced Gastric Damage in Humans: Gastroprotection by Vitamin C.,” *Aliment. Pharmacol. Ther.*, vol. 15, pp. 677–87, 2001.

[35] B. Halliwell, S. Chirico, “Lipid Peroxidation: Its Mechanism, Measurement, and Significance.,” *Am. J. Clin. Nutr.*, vol. 57, pp. 715S–724S, 1993.

[36] A. W. Girotti, “Lipid Hydroperoxide Generation, Turnover, and Effector Action in Biological Systems.,” *J. Lipid Res.*, vol. 39, pp. 1529–42, 1998.

[37] A. Ayala, M. F. Muñoz, S. Argüelles, “Lipid Peroxidation: Production, Metabolism, and Signaling Mechanisms of Malondialdehyde and 4-hydroxy-2-nonenal.,” *Oxid. Med. Cell. Longev.*, vol. 2014, p. 360438, 2014.

[38] J. Heuvingh, S. Bonneau, “Asymmetric Oxidation of Giant Vesicles Triggers Curvature-Associated Shape Transition and Permeabilization.,” *Biophys. J.*, vol. 97, pp. 2904–12, 2009.

[39] J. W. Borst, N. V. Visser, O. Kouptsova, A. J. Visser, “Oxidation of Unsaturated Phospholipids in Membrane Bilayer Mixtures is Accompanied by Membrane Fluidity Changes.,” *Biochim. Biophys. Acta*, vol. 1487, pp. 61–73, 2000.

[40] M. C. Howland, A. N. Parikh, “Model Studies of Membrane Disruption by Photogenerated Oxidative Assault.,” *J. Phys. Chem. B*, vol. 114, pp. 6377–85, 2010.

[41] S. L. Forsburg, “The Art and Design of Genetic Screens: Yeast.,” *Nat. Rev. Genet.*, vol. 2, pp. 659–68, 2001.

[42] D. Chen, W. M. Toone, J. Mata, R. Lyne, G. Burns, K. Kivinen, A. Brazma, N. Jones, J. Bähler, "Global Transcriptional Responses of Fission Yeast to Environmental Stress.," *Mol. Biol. Cell*, vol. 14, pp. 214–29, 2003.

[43] K. Shiozaki, P. Russell, "Cell-Cycle Control Linked to Extracellular Environment by MAP Kinase Pathway in Fission Yeast.," *Nature*, vol. 378, pp. 739–43, 1995.

[44] K. Shiozaki, P. Russell, "Stress-Activated Protein Kinase Pathway in Cell Cycle Control of Fission Yeast.," *Methods Enzymol.*, vol. 283, pp. 506–20, 1997.

[45] E. Herrero, J. Ros, G. Bellí, E. Cabiscol, "Redox Control and Oxidative Stress in Yeast Cells.," *Biochim. Biophys. Acta*, vol. 1780, pp. 1217–35, 2008.

[46] N. Mutoh, C. W. Nakagawa, K. Yamada, "Characterization of Cu, Zn-Superoxide Dismutase-Deficient Mutant of Fission Yeast *Schizosaccharomyces pombe*.," *Curr. Genet.*, vol. 41, pp. 82–8, 2002.

[47] J. H. Jeong, E. S. Kwon, J. H. Roe, "Characterization of the Manganese-Containing Superoxide Dismutase and Its Gene Regulation in Stress Response of *Schizosaccharomyces pombe*.," *Biochem. Biophys. Res. Commun.*, vol. 283, pp. 908–14, 2001.

[48] K. Watanabe, S. Shibuya, Y. Ozawa, H. Nojiri, N. Izuo, K. Yokote, T. Shimizu, "Superoxide Dismutase 1 Loss Disturbs Intracellular Redox Signaling, Resulting in Global Age-Related Pathological Changes.," *Biomed Res. Int.*, vol. 2014, p. 140165, 2014.

[49] C. W. Nakagawa, N. Mutoh, Y. Hayashi, "Transcriptional Regulation of Catalase Gene in the Fission Yeast *Schizosaccharomyces pombe*: Molecular Cloning of the Catalase Gene and Northern Blot Analyses of the Transcript.," *J. Biochem.*, vol. 118, pp. 109–16, 1995.

[50] Y. S. Ho, Y. Xiong, W. Ma, A. Spector, D. S. Ho, "Mice Lacking Catalase Develop Normally But Show Differential Sensitivity to Oxidant Tissue Injury.," *J. Biol. Chem.*, vol. 279, pp. 32804–12, 2004.

[51] N. Mutoh, C. W. Nakagawa, K. Yamada, "The Role of Catalase in Hydrogen Peroxide Resistance in Fission Yeast *Schizosaccharomyces pombe*.," *Can. J. Microbiol.*, vol. 45, pp. 125–9, 1999.

[52] E. Paulo, S. García-Santamarina, I. A. Calvo, M. Carmona, S. Boronat, A. Domènech, J. Ayté, E. Hidalgo, "A Genetic Approach to Study H2O2 Scavenging in Fission Yeast--Distinct Roles of Peroxiredoxin and Catalase.," *Mol. Microbiol.*, vol. 92, pp. 246–57, 2014.

[53] V. Wood, M. A. Harris, M. D. McDowall, K. Rutherford, B. W. Vaughan, D. M. Staines, M. Aslett, A. Lock, J. Bähler, P. J. Kersey, S. G. Oliver, "PomBase: A Comprehensive Online Resource for Fission Yeast.," *Nucleic Acids Res.*, vol. 40, pp. D695–9, 2012.

[54] J. Y. Song, J. H. Roe, “The Role and Regulation of Trxl, a Cytosolic Thioredoxin in *Schizosaccharomyces pombe*.,” *J. Microbiol.*, vol. 46, pp. 408–14, 2008.

[55] J. Y. Song, J. Cha, J. Lee, J. H. Roe, “Glutathione Reductase and a Mitochondrial Thioredoxin Play Overlapping Roles in Maintaining Iron-Sulfur Enzymes in Fission Yeast.,” *Eukaryot. Cell*, vol. 5, pp. 1857–65, 2006.

[56] A. Holmgren, C. Johansson, C. Berndt, M. E. Lönn, C. Hudemann, C. H. Lillig, “Thiol Redox Control via Thioredoxin and Glutaredoxin Systems.,” *Biochem. Soc. Trans.*, vol. 33, pp. 1375–7, 2005.

[57] Y. Wei, M. a Funk, L. A. Rosado, J. Baek, C. L. Drennan, J. Stubbe, “The Class III Ribonucleotide Reductase from *Neisseria bacilliformis* Can Utilize Thioredoxin as a Reductant.,” *Proc. Natl. Acad. Sci. U. S. A.*, vol. 111, pp. E3756–65, 2014.

[58] C. H. Williams, L. D. Arscott, S. Müller, B. W. Lennon, M. L. Ludwig, P. F. Wang, D. M. Veine, K. Becker, R. H. Schirmer, “Thioredoxin Reductase Two Modes of Catalysis Have Evolved.,” *Eur. J. Biochem.*, vol. 267, pp. 6110–7, 2000.

[59] S. Y. Lee, J. Y. Song, E. S. Kwon, J. H. Roe, “Gpx1 Is a Stationary Phase-Specific Thioredoxin Peroxidase in Fission Yeast.,” *Biochem. Biophys. Res. Commun.*, vol. 367, pp. 67–71, 2008.

[60] S. García-Santamarina, S. Boronat, I. A. Calvo, M. Rodríguez-Gabriel, J. Ayté, H. Molina, E. Hidalgo, “Is Oxidized Thioredoxin a Major Trigger for Cysteine Oxidation? Clues From a Redox Proteomics Approach.,” *Antioxid. Redox Signal.*, vol. 18, pp. 1549–56, 2013.

[61] A. M. Day, J. D. Brown, S. R. Taylor, J. D. Rand, B. A. Morgan, E. A. Veal, “Inactivation of a Peroxiredoxin by hydrogen Peroxide Is Critical for Thioredoxin-Mediated Repair of Oxidized Proteins and Cell Survival.,” *Mol. Cell*, vol. 45, pp. 398–408, 2012.

[62] E. M. Hanschmann, J. R. Godoy, C. Berndt, C. Hudemann, C. H. Lillig, “Thioredoxins, Glutaredoxins, and Peroxiredoxins--Molecular Mechanisms and Health Significance: from Cofactors to Antioxidants to Redox Signaling.,” *Antioxid. Redox Signal.*, vol. 19, pp. 1539–605, 2013.

[63] A. Hall, P. A. Karplus, L. B. Poole, “Typical 2-Cys Peroxiredoxins--Structures, Mechanisms and Functions.,” *FEBS J.*, vol. 276, pp. 2469–77, 2009.

[64] P. A. Karplus, L. B. Poole, “Peroxiredoxins as Molecular Triage Agents, Sacrificing Themselves to Enhance Cell Survival During a Peroxide Attack.,” *Mol. Cell*, vol. 45, pp. 275–8, 2012.

[65] A. P. Vivancos, E. A. Castillo, B. Biteau, C. Nicot, J. Ayté, M. B. Toledano, E. Hidalgo, “A Cysteine-Sulfinic Acid in Peroxiredoxin Regulates H2O2-Sensing by the Antioxidant Pap1 Pathway.,” *Proc. Natl. Acad. Sci. U. S. A.*, vol. 102, pp. 8875–80, 2005.

[66] S. M. Bozonet, V. J. Findlay, A. M. Day, J. Cameron, E. A. Veal, B. A. Morgan, "Oxidation of a Eukaryotic 2-Cys Peroxiredoxin Is a Molecular Switch Controlling the Transcriptional Response to Increasing Levels of Hydrogen Peroxide.," *J. Biol. Chem.*, vol. 280, pp. 23319–27, 2005.

[67] D. Sheehan, G. Meade, V. M. Foley, C. A. Dowd, "Structure, Function and Evolution of Glutathione Transferases: Implications for Classification of Non-Mammalian Members of an Ancient Enzyme Superfamily.," *Biochem. J.*, vol. 360, pp. 1–16, 2001.

[68] E. A. Veal, W. M. Toone, N. Jones, B. A. Morgan, "Distinct Roles for Glutathione S-Transferases in the Oxidative Stress Response in *Schizosaccharomyces pombe*.," *J. Biol. Chem.*, vol. 277, pp. 35523–31, 2002.

[69] D. Chen, C. R. M. Wilkinson, S. Watt, C. J. Penkett, W. M. Toone, N. Jones, J. Bähler, "Multiple Pathways Differentially Regulate Global Oxidative Stress Responses in Fission Yeast.," *Mol. Biol. Cell*, vol. 19, pp. 308–17, 2008.

[70] T. Toda, M. Shimanuki, M. Yanagida, "Fission Yeast Genes that Confer Resistance to staurosporine Encode an AP-1-Like Transcription Factor and a Protein Kinase Related to the Mammalian ERK1/MAP2 and Budding Yeast FUS3 and KSS1 kinases.," *Genes Dev.*, vol. 5, pp. 60–73, 1991.

[71] J. N. Glover, S. C. Harrison, "Crystal Structure of the Heterodimeric bZIP Transcription Factor c-Fos-c-Jun Bound to DNA.," *Nature*, vol. 373, pp. 257–61, 1995.

[72] N. Kudo, H. Taoka, T. Toda, M. Yoshida, S. Horinouchi, "A Novel Nuclear Export Signal Sensitive to Oxidative Stress in the Fission Yeast Transcription Factor Pap1.," *J. Biol. Chem.*, vol. 274, pp. 15151–8, 1999.

[73] A. P. Vivancos, E. A. Castillo, N. Jones, J. Ayté, E. Hidalgo, "Activation of the Redox Sensor Pap1 by Hydrogen Peroxide Requires Modulation of the Intracellular Oxidant Concentration.," *Mol. Microbiol.*, vol. 52, pp. 1427–35, 2004.

[74] E. A. Castillo, J. Ayté, C. Chiva, A. Moldón, M. Carrascal, J. Abián, N. Jones, E. Hidalgo, "Diethylmaleate Activates the Transcription Factor Pap1 by Covalent Modification of Critical Cysteine Residues.," *Mol. Microbiol.*, vol. 45, pp. 243–54, 2002.

[75] H. G. Kim, B. C. Kim, K. Kim, E. Park, C. Lim, "Transcriptional Regulation of the *Schizosaccharomyces pombe* Gene Encoding Glutathione S-Transferase I by a Transcription Factor Pap1.," *J. Microbiol.*, vol. 42, pp. 353–6, 2004.

[76] C. J. Lim, Y. Cho, J. Sa, H. W. Lim, H. G. Kim, S. Kim, E. Park, "Pap1-Dependent Regulation of the GSTII Gene From the Fission Yeast.," *Mol. Cells*, vol. 14, pp. 431–6, 2002.

[77] Y. Y. Lei, W. J. Wang, J. H. Mei, and C. L. Wang, "Mitogen-Activated Protein Kinase Signal Transduction in Solid Tumors.," *Asian Pacific J. Cancer Prev.*, vol. 15, pp. 8539–48, 2014.

[78] T. Takeda, T. Toda, K. Kominami, A. Kohnosu, M. Yanagida, N. Jones, "*Schizosaccharomyces pombe* atf1+ encodes a Transcription Factor Required for Sexual Development and Entry into Stationary Phase.," *EMBO J.*, vol. 14, pp. 6193–208, 1995.

[79] V. Buck, J. Quinn, T. Soto Pino, H. Martin, J. Saldanha, K. Makino, B. A. Morgan, J. B. Millar, "Peroxide Sensors for the Fission Yeast Stress-Activated Mitogen-Activated Protein Kinase Pathway.," *Mol. Biol. Cell*, vol. 12, pp. 407–19, 2001.

[80] A. N. Nguyen, A. Lee, W. Place, K. Shiozaki, "Multistep Phosphorelay Proteins Transmit Oxidative Stress Signals to the fission Yeast Stress-Activated Protein Kinase.," *Mol. Biol. Cell*, vol. 11, pp. 1169–81, 2000.

[81] S. Morigasaki, K. Shimada, A. Ikner, M. Yanagida, K. Shiozaki, "Glycolytic Enzyme GAPDH Promotes Peroxide Stress Signaling through Multistep Phosphorelay to a MAPK Cascade.," *Mol. Cell*, vol. 30, pp. 108–13, 2008.

[82] K. Shiozaki, M. Shiozaki, P. Russell, "Mcs4 Mitotic Catastrophe Suppressor Regulates the Fission Yeast Cell Cycle Through the Wik1-Wis1-Spc1 Kinase Cascade.," *Mol. Biol. Cell*, vol. 8, pp. 409–19, 1997.

[83] S. Morigasaki, A. Ikner, H. Tatebe, K. Shiozaki, "Response Regulator-Mediated MAPKKK Heteromer Promotes Stress Signaling to the Spc1 MAPK in Fission Yeast.," *Mol. Biol. Cell*, vol. 24, pp. 1083–92, 2013.

[84] I. Samejima, S. Mackie, P. A. Fantes, "Multiple Modes of Activation of the Stress-Responsive MAP Kinase Pathway in Fission Yeast.," *EMBO J.*, vol. 16, pp. 6162–70, 1997.

[85] J. B. Millar, V. Buck, M. G. Wilkinson, "Pyp1 and Pyp2 PTPases Dephosphorylate an Osmosensing MAP Kinase Controlling Cell Size at Division in Fission Yeast.," *Genes Dev.*, vol. 9, pp. 2117–30, 1995.

[86] G. Degols, K. Shiozaki, P. Russell, "Activation and Regulation of the Spc1 Stress-Activated Protein Kinase in *Schizosaccharomyces pombe*.," *Mol. Cell. Biol.*, vol. 16, pp. 2870–7, 1996.

[87] A. N. Nguyen, K. Shiozaki, "Heat-Shock-Induced Activation of Stress MAP Kinase is Regulated by Threonine- and Tyrosine-Specific Phosphatases.," *Genes Dev.*, vol. 13, pp. 1653–63, 1999.

[88] F. Gaits, G. Degols, K. Shiozaki, P. Russell, "Phosphorylation and Association with the Transcription Factor Atf1 Regulate Localization of Spc1/Sty1 Stress-Activated Kinase in Fission Yeast.," *Genes Dev.*, vol. 12, pp. 1464–73, 1998.

[89] M. G. Wilkinson, M. Samuels, T. Takeda, W. M. Toone, J. C. Shieh, T. Toda, J. B. Millar, N. Jones, "The Atf1 Transcription Factor is a Target for the Sty1 Stress-Activated MAP Kinase Pathway in Fission Yeast.," *Genes Dev.*, vol. 10, pp. 2289–301, 1996.

[90] K. Shiozaki, P. Russell, "Conjugation, Meiosis, and the Osmotic Stress Response Are Regulated by Spc1 Kinase through Atf1 Transcription Factor in Fission Yeast.," *Genes Dev.*, vol. 10, pp. 2276–88, 1996.

[91] K. Shiozaki, M. Shiozaki, P. Russell, "Heat Stress Activates Fission Yeast Spc1/StyI MAPK by a MEKK-Independent Mechanism.," *Mol. Biol. Cell*, vol. 9, pp. 1339–49, 1998.

[92] X. Zhou, Y. Ma, R. Sugiura, D. Kobayashi, M. Suzuki, L. Deng, T. Kuno, "MAP Kinase Kinase Kinase (MAPKKK)-Dependent and -Independent Activation of Sty1 Stress MAPK in Fission Yeast.," *J. Biol. Chem.*, vol. 285, pp. 32818–23, 2010.

[93] K. M. Kowalczyk, S. Hartmuth, D. Perera, P. Stansfield, J. Petersen, "Control of Sty1 MAPK Activity through Stabilisation of the Pyp2 MAPK Phosphatase.," *J. Cell Sci.*, vol. 126, pp. 3324–32, 2013.

[94] M. Eshaghi, J. H. Lee, L. Zhu, S. Y. Poon, J. Li, K. H. Cho, Z. Chu, R. K. M. Karuturi, J. Liu, "Genomic Binding Profiling of the Fission Yeast Stress-Activated MAPK Sty1 and the bZIP Transcriptional Activator Atf1 in Response to H2O2.," *PLoS One*, vol. 5, p. e11620, 2010.

[95] M. Sansó, M. Gogol, J. Ayté, C. Seidel, E. Hidalgo, "Transcription Factors Pcr1 and Atf1 Have Distinct Roles in Stress- and Sty1-Dependent Gene Regulation.," *Eukaryot. Cell*, vol. 7, pp. 826–35, 2008.

[96] C. L. Lawrence, H. Maekawa, J. L. Worthington, W. Reiter, C. R. M. Wilkinson, N. Jones, "Regulation of *Schizosaccharomyces pombe* Atf1 Protein Levels by Sty1-Mediated Phosphorylation and Heterodimerization With Pcr1.," *J. Biol. Chem.*, vol. 282, pp. 5160–70, 2007.

[97] X. Zhou, Y. Ma, T. Kato, T. Kuno, "A Measurable Activation of the bZIP Transcription Factor Atf1 in a Fission Yeast Strain Devoid of Stress-Activated and Cell Integrity Mitogen-Activated Protein Kinase (MAPK) Activities.," *J. Biol. Chem.*, vol. 287, pp. 23434–9, 2012.

[98] K. J. Woolcock, R. Stunnenberg, D. Gaidatzis, H. R. Hotz, S. Emmerth, P. Barraud, M. Bühler, "RNAi Keeps Atf1-Bound Stress Response Genes in Check at Nuclear Pores.," *Genes Dev.*, vol. 26, pp. 683–92, 2012.

[99] J. Gao, J. L. Wagnon, R. M. Protacio, G. V. Glazko, M. Beggs, V. Raj, M. K. Davidson, W. P. Wahls, "A Stress-Activated, p38 Mitogen-Activated Protein Kinase-ATF/CREB Pathway Regulates Posttranscriptional, Sequence-Dependent Decay of Target RNAs.," *Mol. Cell. Biol.*, vol. 33, pp. 3026–35, 2013.

[100] P. García, E. Paulo, J. Gao, W. P. Wahls, J. Ayté, E. Lowy, E. Hidalgo, "Binding of the Transcription Factor Atf1 to Promoters Serves as a Barrier to Phase Nucleosome Arrays and Avoid Cryptic Transcription.," *Nucleic Acids Res.*, vol. 42, pp. 10351–9, 2014.

[101] R. Kopan, M. X. G. Ilagan, "The Canonical Notch Signaling Pathway: Unfolding the Activation Mechanism.," *Cell*, vol. 137, pp. 216–33, 2009.

[102] S. E. Pursglove, J. P. Mackay, "CSL: A Notch Above the Rest.," *Int. J. Biochem. Cell Biol.*, vol. 37, pp. 2472–7, 2005.

[103] D. Maier, H. Praxenthaler, A. Schulz, A. Preiss, "Gain of Function Notch Phenotypes Associated With Ectopic Expression of the Su(H) C-Terminal Domain Illustrate Separability of Notch and Hairless-Mediated Activities.," *PLoS One*, vol. 8, p. e81578, 2013.

[104] V. Morel, F. Schweisguth, "Repression by Suppressor of Hairless and Activation by Notch Are Required to Define a Single Row of Single-Minded Expressing Cells in the *Drosophila* Embryo.," *Genes Dev.*, vol. 14, pp. 377–88, 2000.

[105] S. Bray, M. Furriols, "Notch Pathway: Making Sense of Suppressor of Hairless.," *Curr. Biol.*, vol. 11, pp. 217–21, 2001.

[106] S. Jarriault, C. Brou, F. Logeat, E. H. Schroeter, R. Kopan, A. Israel, "Signalling Downstream of Activated Mammalian Notch.," *Nature*, vol. 377, pp. 355–8, 1995.

[107] I. Greenwald, "LIN-12/Notch Signaling: Lessons From Worms and Flies.," *Genes Dev.*, vol. 12, pp. 1751–62, 1998.

[108] A. L. Penton, L. D. Leonard, N. B. Spinner, "Notch Signaling in Human Development and Disease.," *Semin. Cell Dev. Biol.*, vol. 23, pp. 450–7, 2012.

[109] Y. Y. Hu, M. H. Zheng, R. Zhang, Y. M. Liang, H. Han, "Notch Signaling Pathway and Cancer Metastasis.," *Adv. Exp. Med. Biol.*, vol. 727, pp. 186–98, 2012.

[110] E. Ben-Shushan, E. Feldman, B. E. Reubinoff, "Notch Signaling Regulates Motor Neuron Differentiation of Human Embryonic Stem Cells.," *Stem Cells*, vol. 33, pp. 403–15, 2015.

[111] J. S. Mumm, R. Kopan, "Notch Signaling: From the Outside in.," *Dev. Biol.*, vol. 228, pp. 151–65, 2000.

[112] J. E. Treisman, "Retinal Differentiation in *Drosophila*.," *Wiley Interdiscip. Rev. Dev. Biol.*, vol. 2, pp. 545–57, 2013.

[113] M. Kaspar, T. Klein, "Functional Analysis of Murine CBF1 During *Drosophila* Development.," *Dev. Dyn.*, vol. 235, pp. 918–27, 2006.

[114] K. M. Bhat, “Notch Signaling Acts Before Cell Division to Promote Asymmetric Cleavage and Cell Fate of Neural Precursor Cells.,” *Sci. Signal.*, vol. 7, p. ra101, 2014.

[115] R. J. Fleming, “Structural Conservation of Notch Receptors and Ligands.,” *Semin. Cell Dev. Biol.*, vol. 9, pp. 599–607, 1998.

[116] V. C. Luca, K. M. Jude, N. W. Pierce, M. V Nachury, S. Fischer, K. C. Garcia, “Structural Biology. Structural Basis for Notch1 Engagement of Delta-Like 4.,” *Science*, vol. 347, pp. 847–53, 2015.

[117] R. A: Kovall, W. A. Hendrickson, “Crystal Structure of the Nuclear Effector of Notch Signaling, CSL, Bound to DNA.,” *EMBO J.*, vol. 23, pp. 3441–51, 2004.

[118] T. Tun, Y. Hamaguchi, N. Matsunami, T. Furukawa, T. Honjo, M. Kawaichi, “Recognition Sequence of a Highly Conserved DNA Binding Protein RBP-J kappa.,” *Nucleic Acids Res.*, vol. 22, pp. 965–71, 1994.

[119] S. Dou, X. Zeng, P. Cortes, H. Erdjument-Bromage, P. Tempst, T. Honjo, L. D. Vales, “The Recombination Signal Sequence-Binding Protein RBP-2N Functions as a Transcriptional Repressor.,” *Mol. Cell. Biol.*, vol. 14, pp. 3310–9, 1994.

[120] B. Castro, S. Barolo, A. M. Bailey, J. W. Posakony, “Lateral Inhibition in Proneural Clusters: *cis*-Regulatory Logic and Default Repression by Suppressor of Hairless.,” *Development*, vol. 132, pp. 3333–44, 2005.

[121] S. Zhou, M. Fujimuro, J. J. D. Hsieh, L. Chen, A. Miyamoto, G. Weinmaster, S. D. Hayward, “SKIP, a CBF1-Associated Protein, Interacts With the Ankyrin Repeat Domain of NotchIC To Facilitate NotchIC Function.,” *Mol. Cell. Biol.*, vol. 20, pp. 2400–10, 2000.

[122] E. C. Lai, “Keeping a Good Pathway Down: Transcriptional Repression of Notch Pathway Target Genes by CSL proteins.,” *EMBO Rep.*, vol. 3, pp. 840–5, 2002.

[123] J. J. Wilson, R. Kovall, “Crystal Structure of the CSL-Notch-Mastermind Ternary Complex Bound to DNA.,” *Cell*, vol. 124, pp. 985–96, 2006.

[124] F. Oswald, B. Täuber, T. Dobner, S. Bourteele, U. Kostezka, G. Adler, S. Liptay, R. M. Schmid, “p300 Acts as a Transcriptional Coactivator for Mammalian Notch-1.,” *Mol. Cell. Biol.*, vol. 21, pp. 7761–74, 2001.

[125] C. Oka, T. Nakano, A. Wakeham, J. L. de la Pompa, C. Mori, T. Sakai, S. Okazaki, M. Kawaichi, K. Shiota, T. W. Mak, T. Honjo, “Disruption of the Mouse RBP-J kappa Gene Results in Early Embryonic Death.,” *Development*, vol. 121, pp. 3291–301, 1995.

[126] M. Převorovský, T. Grousl, J. Stanurová, J. Rynes, W. Nellen, F. Půta, P. Folk, “Cbf11 and Cbf12, the Fission Yeast CSL Proteins, Play Opposing Roles in Cell Adhesion and Coordination of Cell and Nuclear Division.,” *Exp. Cell Res.*, vol. 315, pp. 1533–47, 2009.

[127] M. Převorovský, S. R. Atkinson, M. Ptáčková, J. R. McLean, K. Gould, P. Folk, F. Půta, J. Bähler, "N-Termini of Fungal CSL Transcription Factors Are Disordered, Enriched in Regulatory Motifs and Inhibit DNA Binding in Fission Yeast.," *PLoS One*, vol. 6, p. e23650, 2011.

[128] M. Oravcová, M. Teska, F. Půta, P. Folk, M. Převorovský, "Fission Yeast CSL Proteins Function as Transcription Factors.," *PLoS One*, vol. 8, p. e59435, 2013.

[129] M. Převorovský, F. Půta, P. Folk, "Fungal CSL Transcription Factors.," *BMC Genomics*, vol. 8, p. 233, 2007.

[130] S. Koelzer, "A Notch-Independent Function of Suppressor of Hairless During the Development of the Bristle Sensory Organ Precursor Cell of *Drosophila*.," *Development*, vol. 130, pp. 1973–88, 2003.

[131] T. M. Beres, T. Masui, G. H. Swift, L. Shi, R. M. Henke, R. J. MacDonald, "PTF1 is an Organ-Specific and Notch-Independent Basic Helix-Loop-Helix Complex Containing the Mammalian Suppressor of Hairless (RBP-J) or its Paralogue, RBP-L.," *Mol. Cell. Biol.*, vol. 26, pp. 117–30, 2006.

[132] S. Barolo, R. G. Walker, A. D. Polyanovsky, G. Freschi, T. Keil, J. W. Posakony, "A Notch-Independent Activity of Suppressor of Hairless is Required for Normal Mechanoreceptor Physiology.," *Cell*, vol. 103, pp. 957–69, 2000.

[133] A. Neves, J. R. Priess, "The REF-1 Family of bHLH Transcription Factors Pattern *C. elegans* Embryos Through Notch-Dependent and Notch-Independent Pathways.," *Dev. Cell*, vol. 8, pp. 867–79, 2005.

[134] I. A. Calvo, P. García, J. Ayté, E. Hidalgo, "The Transcription Factors Pap1 and Prr1 Collaborate to Activate Antioxidant, But Not Drug Tolerance, Genes in response to H2O2.," *Nucleic Acids Res.*, vol. 40, pp. 4816–24, 2012.

[135] R. H. Jones, S. Moreno, P. Nurse, N. C. Jones, "Expression of the SV40 Promoter in Fission Yeast: Identification and Characterization of an AP-1-Like Factor.," *Cell*, vol. 53, pp. 659–67, 1988.

[136] M. Převorovský, "pREPORT: A Multi-Readout Transcription Reporter Vector for Fission Yeast.," *Yeast*, vol. 32, pp. 327–34, 2015.

[137] J. D. Brown, A. M. Day, S. R. Taylor, L. E. Tomalin, B. A. Morgan, E. A. Veal, "A Peroxiredoxin Promotes H2O2 Signaling and Oxidative Stress Resistance by Oxidizing a Thioredoxin Family Protein.," *Cell Rep.*, vol. 5, pp. 1425–35, 2013.

[138] A. Delaunay, D. Pflieger, M. B. Barrault, J. Vinh, M. B. Toledano, "A Thiol Peroxidase Is an H2O2 Receptor and Redox-Transducer in Gene Activation.," *Cell*, vol. 111, pp. 471–81, 2002.

[139] A. M. Day, E. A. Veal, "Hydrogen Peroxide-Sensitive Cysteines in the Sty1 MAPK Regulate the Transcriptional Response to Oxidative Stress.," *J. Biol. Chem.*, vol. 285, pp. 7505–16, 2010.

[140] G. Degols, P. Russell, “Discrete Roles of the Spc1 Kinase and the Atf1 Transcription Factor in the UV Response of *Schizosaccharomyces pombe*.,” *Mol. Cell. Biol.*, vol. 17, pp. 3356–63, 1997.

[141] C. W. Nakagawa, K. Yamada, N. Mutoh, “Role of Atf1 and Pap1 in the Induction of the Catalase Gene of Fission Yeast *Schizosaccharomyces pombe*.,” *J. Biochem.*, vol. 127, pp. 233–38, 2000.

[142] J. Gregan, P. K. Rabitsch, C. Rumpf, M. Novatchkova, A. Schleiffer, K. Nasmyth, “High-Throughput Knockout Screen in Fission Yeast.,” *Nat. Protoc.*, vol. 1, pp. 2457–64, 2006.

[143] E. A. Veal, V. J. Findlay, A. M. Day, S. M. Bozonet, J. M. Evans, J. Quinn, B. A. Morgan, “A 2-Cys Peroxiredoxin Regulates Peroxide-Induced Oxidation and Activation of a Stress-Activated MAP Kinase.,” *Mol. Cell*, vol. 15, pp. 129–39, 2004.

[144] H. G. Kim, B. Kim, E. Park, K. Ahn, C. Lim, “Differential Regulation of Three Genes Encoding Glutathione S-transferases in *Schizosaccharomyces pombe*.,” *Mol. Cells*, vol. 18, pp. 332–9, 2004.

[145] P. Angel, M. Imagawa, R. Chiu, B. Stein, R. J. Imbra, H. J. Rahmsdorf, C. Jonat, P. Herrlich, M. Karin, “Phorbol Ester-Inducible Genes Contain a Common *cis* Element Recognized by a TPA-Modulated *trans*-Acting Factor.,” *Cell*, vol. 49, pp. 729–39, 1987.

[146] M. L. Wells, W. Huang, L. Li, K. E. Gerrish, D. C. Fargo, F. Ozsolak, P. J. Blackshear, “Posttranscriptional Regulation of Cell-Cell Interaction Protein-Encoding Transcripts by Zfs1p in *Schizosaccharomyces pombe*.,” *Mol. Cell. Biol.*, vol. 32, pp. 4206–14, 2012.

[147] K. Takács, Z. Gazdag, P. Raspor, M. Pesti, “Gene Expressions and Enzyme Analyses in the *Schizosaccharomyces pombe* Deltapap1 Transcription Factor Mutant Exposed to Cd(2+).,” *J. Basic Microbiol.*, vol. 47, pp. 74–83, 2007.

[148] V. Pancaldi, O. S. Saraç, C. Rallis, J. R. McLean, M. Převorovský, K. Gould, A. Beyer, J. Bähler, “Predicting the Fission Yeast Protein Interaction Network.,” *G3 (Bethesda).*, vol. 2, pp. 453–67, 2012.

[149] W. M. Toone, S. Kuge, M. Samuels, B. A. Morgan, T. Toda, N. Jones, “Regulation of the Fission Yeast Transcription Factor Pap1 by Oxidative Stress: Requirement for the Nuclear Export Factor Crm1 (Exportin) and the Stress-Activated MAP Kinase Sty1/Spc1.,” *Genes Dev.*, vol. 12, pp. 1453–63, 1998.

[150] M. A. Rodríguez-Gabriel, G. Burns, W. H. McDonald, V. Martín, J. R. Yates, J. Bähler, P. Russell, “RNA-Binding Protein Csx1 Mediates Global Control of Gene Expression in Response to Oxidative Stress.,” *EMBO J.*, vol. 22, pp. 6256–66, 2003.

[151] R. A. Kovall, “Structures of CSL, Notch and Mastermind Proteins: Piecing Together an Active Transcription Complex.,” *Curr. Opin. Struct. Biol.*, vol. 17, pp. 117–27, 2007.

[152] J. Quinn, V. J. Findlay, K. Dawson, J. B. A. Millar, N. Jones, B. A. Morgan, W. M. Toone, “Distinct Regulatory Proteins Control the Graded Transcriptional Response to Increasing H(2)O(2) Levels in Fission Yeast *Schizosaccharomyces pombe*.,” *Mol. Biol. Cell*, vol. 13, pp. 805–16, 2002.

[153] O. Shalem, O. Dahan, M. Levo, M. R. Martinez, I. Furman, E. Segal, Y. Pilpel, “Transient Transcriptional Responses to Stress Are Generated by Opposing Effects of mRNA Production and Degradation.,” *Mol. Syst. Biol.*, vol. 4, p. 223, 2008.

[154] S. Marguerat, K. Lawler, A. Brazma, J. Bähler, “Contributions of Transcription and mRNA Decay to Gene Expression Dynamics of Fission Yeast in Response to Oxidative Stress.,” *RNA Biol.*, vol. 11, pp. 702–14, 2014.